A scaling methodology for axial buckling of sandwich composite cylindrical shells

Uriol Balbin, Ines

DOI
10.4233/uuid:63254d10-9a39-44b0-bfe3-4e4bbc455c74

Publication date
2025

Document Version
Final published version

Citation (APA)
Uriol Balbin, I. (2025). *A scaling methodology for axial buckling of sandwich composite cylindrical shells*. [Dissertation (TU Delft), Delft University of Technology]. https://doi.org/10.4233/uuid:63254d10-9a39-44b0-bfe3-4e4bbc455c74

Important note
To cite this publication, please use the final published version (if applicable).
Please check the document version above.

A scaling methodology for axial buckling of sandwich composite cylindrical shells

Ines Uriol Balbin

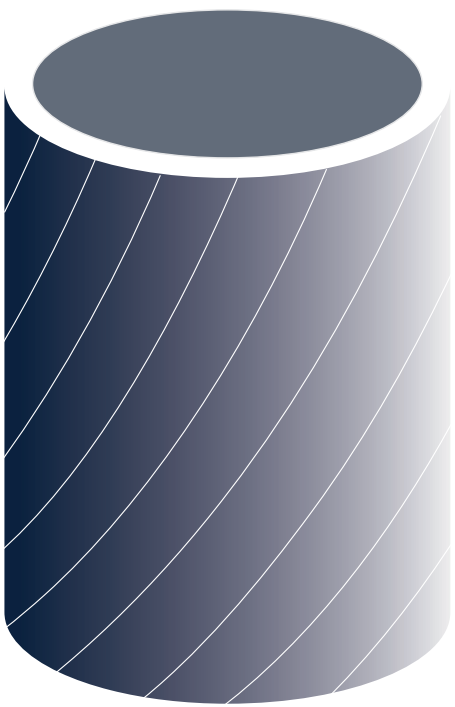

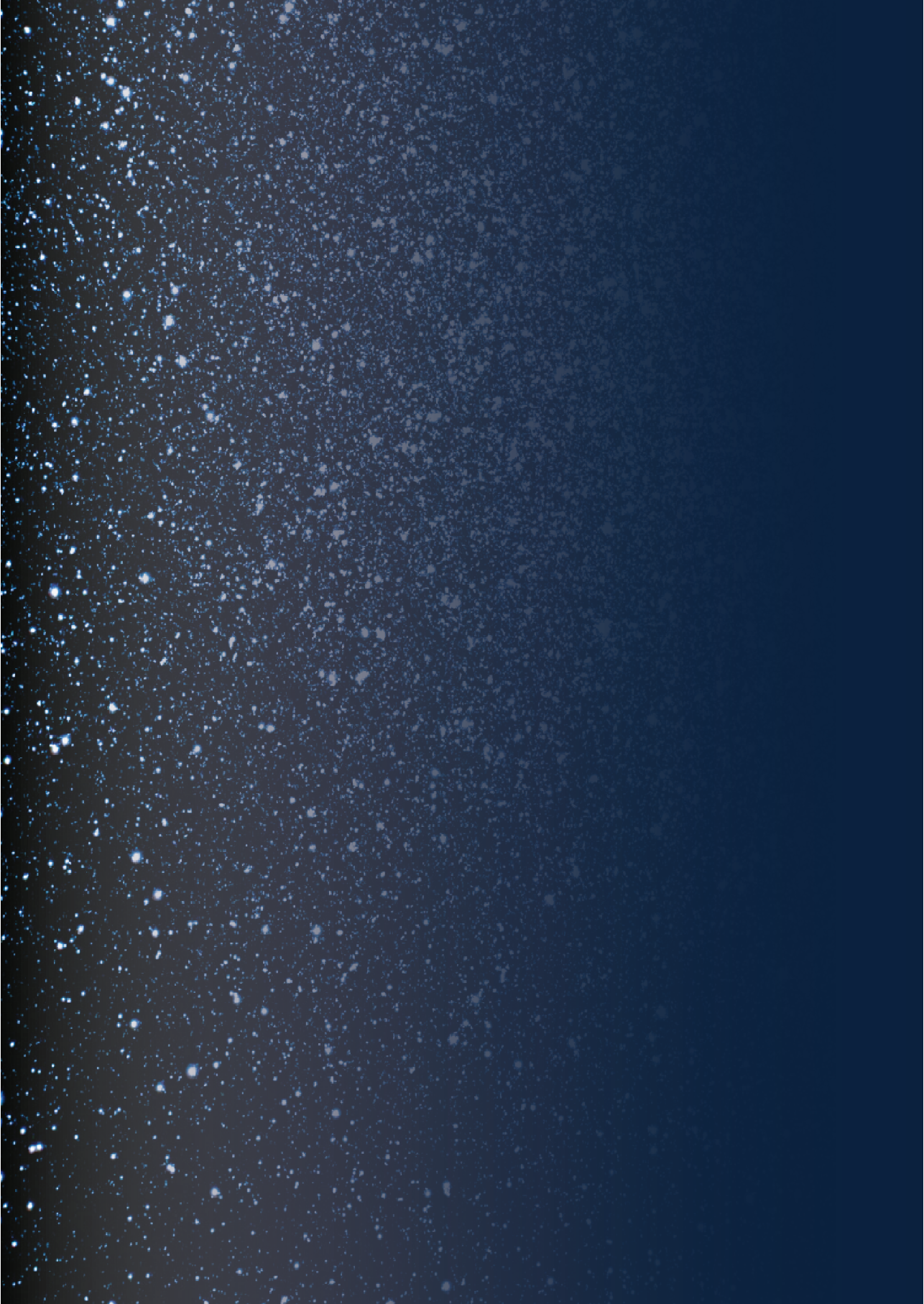

A SCALING METHODOLOGY FOR AXIAL BUCKLING OF SANDWICH COMPOSITE CYLINDRICAL SHELLS

Dissertation

for the purpose of obtaining the degree of doctor
at Delft University of Technology
by the authority of the Rector Magnificus Prof. dr. ir. T.H.J.J. van der Hagen,
chair of the Board of Doctorates,
to be defended publicly on
Thursday 19th, June 2025 at 15.00 o'clock

by

Ines URIOL BALBIN

Master of Science in Aerospace Engineering,
Universitat Politecnica de Valencia, Valencia, Spain,

This dissertation has been approved by the promotors.

Composition of the doctoral committee:

Rector Magnificus,	chairperson
Prof.dr. C. Bisagni,	Delft University of Technology, *promotor*
Prof.dr.ir. R. De Breuker,	Delft University of Technology, *promotor*
Independent members:	
Prof.dr.-Ing. B. Kriegesmann,	Technische Universität Hamburg, Germany
Prof.dr. A. Pirrera,	University of Bristol, United Kingdom
Prof. C.A. Dransfeld,	Delft University of Technology
Dr.-Ing. S.G.P. Castro,	Delft University of Technology
Prof.dr.ir. R. Benedictus,	Delft University of Technology, *reserve member*

Keywords: Buckling, Scaling, Sandwich composite

Printed by: Ipskamp

Front & Back: Cover by Ines Uriol Balbin and Luca Flessati

ISBN 978-94-6518-065-6

An electronic version of this dissertation is available at
http://repository.tudelft.nl/.

It is OK

CONTENTS

Summary ix

Samenvatting xi

Nomenclature xiii

1 Introduction 1

1.1 Background and Motivation 1

1.2 Research Questions 4

1.3 Methodology 5

1.4 Overview of the Thesis 6

2 Literature Review 9

2.1 Buckling of Shells 9

2.1.1 Analytical Models for Predicting Shell Buckling Behaviour 11

2.1.2 Simulation Tools for Predicting Shell Buckling Behaviour 13

2.2 Scaling Methods 17

2.2.1 Dimensional Analysis 18

2.2.2 Similarity between Governing Equations. 19

2.2.3 Similarity between Nondimensional Governing Equations. 20

3 Nondimensional Buckling Formulation Including Transverse Shear Effects 23

3.1 Model Assumptions and Coordinate System 24

3.2 Equilibrium and Compatibility Equations 27

3.2.1 Strain-Displacement Equations 27

3.2.2 Constitutive Equations 30

3.2.3 Equilibrium equations 35

3.2.4 Compatibility equations 37

3.3 Linearized Buckling Equations 37

3.4 Design Space Analysis via Nondimensional Parameters 41

3.5 Finite element verification 47

3.6 Conclusions 49

4 Imperfections in the Nondimensional Buckling Formulation 51

4.1 Modeling of Imperfections 52

4.2 Equilibrium and Compatibility Equations 53

4.3 Nonlinear Deformations of Imperfect Cylindrical Shells 54

4.4 Influence of Nondimensional Parameters in the Imperfection Sensitivity of Cylindrical Shells 56

4.5 Conclusions 66

5 Scaling Methodology 67

5.1 Baseline Structures 68

5.2 Scaling Strategies 70

5.2.1 Scaling Strategy 1 71

5.2.2 Scaling Strategy 2 81

5.3 Sensitivity Study of the Geometrical Parameters . . . 91
5.4 Conclusions . . . 93

6 Numerical Analysis and Comparison with Available Data 95

6.1 Numerical Analysis . . . 97
6.1.1 Linear Analysis . . . 98
6.1.2 Non-linear Analysis . . . 100
6.2 Comparison with Available Test Data . . . 106
6.3 Conclusions . . . 110

7 Conclusion 111

7.1 Key Findings and Contributions . . . 111
7.1.1 Shear Transverse Effects Influence . . . 112
7.1.2 Imperfection Sensitivity . . . 112
7.1.3 Analysis-Based Methodology . . . 113
7.1.4 Predictions in different scales . . . 114
7.1.5 Contributions . . . 115
7.2 Recommendations for Future Research . . . 115

Bibliography 117

Acknowledgements 129

A Scaled structures 131

A.1 Baseline 2 . . . 131
A.1.1 Strategy 1 . . . 132
A.1.2 Strategy 2 . . . 133

A.2 Baseline 3 135

A.2.1 Strategy 1 135

A.2.2 Strategy 2 137

A.3 Baseline 4 139

A.3.1 Strategy 1 139

A.3.2 Strategy 2 141

Curriculum Vitæ **143**

List of Publications **145**

SUMMARY

This thesis investigates the buckling behavior of sandwich composite cylindrical shells, which can be part of the primary structure of launch vehicles. The work focuses on developing a scaling methodology using nondimensional parameters, aiming to create a reliable framework for scaling down large composite structures to manageable laboratory sizes, while preserving their buckling response.

The thesis first reviews the state-of-the-art approaches for studying shell buckling, including analytical, numerical, and experimental techniques. Furthermore, different scaling methodologies utilized in structural analysis are reviewed. Inspired by the literature, the proposed scaling method starts from the redefinition of buckling equations in their nondimensional form allowing to naturally derive the scaling laws from their components. However, a limitation of this approach is the necessity of a comprehensive nondimensional formulation of the problem.

The need for a comprehensive nondimensional formulation leads to the first two research questions. The first question, addressed in the third chapter is, *To what extent do the shear transverse effects influence the buckling response in sandwich composite structures of different scales?* To answer this question, the study first extends the nondimensional buckling equations to include transverse shear effects. The second question, addressed in the fourth chapter, is, *What is the theoretical influence of imperfection sensitivity in the buckling response of sandwich composite shells of different scales?* To answer this question, the nondimensional formulation is extended to account for imperfections, by including a trigonometric function approach.

Once the nondimensional formulation is defined, the work moves to the task of using it to define a systematic scaling methodology. The third question deals with this specific aspect of the work and is, *How can a systematic methodology be designed to scale down composite cylindrical shells while preserving their buckling response?* To answer this third question, the thesis proposes a novel scaling methodology, presenting two distinct scaling strategies. The first strategy involves scaling sandwich composite shells while retaining similar structural properties. This approach faces challenges due to manufacturing constraints, particularly in scaling down thicknesses. The second strategy scales from sandwich composite shells to equivalent composite laminate shells, which are easier to manufacture but introduce new challenges when comparing the two structural types. Both strategies offer trade-offs: while the first one provides more accurate scaling, the second one is more feasible for laboratory-scale testing.

Finally, the fourth question is *What are the discrepancies between analytical predictions and experimental observations of buckling behavior in different scales of composite shell structures produced with the systematic methodology?* To tackle the fourth question, analytical and numerical results are compared with the available large scale and laboratory tests, these latter designed by following the second scaling strategy. A key challenge identified in the research is the discrepancy between analytical predictions and experimental results. Although the theoretical model predicts an 8% error in the nondimensional load between full-scale and laboratory-scale models, experimental results reveal a larger 22% error. The gap between theoretical predictions and experimental observations highlights the need for further refinement of the scaling methodology and, in particular, of the modeling of imperfections.

The thesis concludes with an overview of the research questions and recommendations for future research, suggesting more extensive testing, in particular of laboratory-scale sandwich composite structures. Additionally, the incorporation of more detailed models of imperfections into the nondimensional framework is recommended to improve the alignment between theoretical and experimental results. Overall, this research provides significant contributions to scaling methods and offers a solid foundation for future improvements in the scaled testing of large-scale sandwich composite shells.

SAMENVATTING

Dit proefschrift onderzoekt het knikgedrag van sandwich-composiet cilinders, die deel kunnen uitmaken van de primaire structuur van draagraketten. Het werk richt zich op het ontwikkelen van een schaalmethodologie met behulp van dimensieloze parameters, met als doel een betrouwbaar kader te creëren om grote composietstructuren terug te schalen naar beheersbare laboratoriumafmetingen, terwijl hun knikgedrag behouden blijft.

Het proefschrift begint met een overzicht van de meest geavanceerde benaderingen voor het bestuderen van knikgedrag van schalen, waaronder analytische, numerieke en experimentele technieken. Bovendien worden verschillende schaalmethodologieën die in structurele analyses worden gebruikt, besproken. Geïnspireerd door de literatuur begint de voorgestelde schaalmethode met het herdefiniëren van de knikvergelijkingen in hun dimensieloze vorm, waardoor de schaalwetten op natuurlijke wijze uit hun componenten kunnen worden afgeleid. Een beperking van deze benadering is echter de noodzaak van een uitgebreide dimensieloze formulering van het probleem.

De noodzaak van een uitgebreide dimensieloze formulering leidt tot de eerste twee onderzoeksvragen. De eerste vraag, behandeld in hoofdstuk drie, is: *In hoeverre beïnvloeden de schuiftransversale effecten de knikrespons in sandwich-composietstructuren op verschillende schalen?* Om deze vraag te beantwoorden breidt de studie eerst de dimensieloze knikvergelijkingen uit om schuiftransversale effecten mee te nemen. De tweede vraag, behandeld in hoofdstuk vier, is: *Wat is de theoretische invloed van imperfectiegevoeligheid op de knikrespons van sandwich-composietschalen op verschillende schalen?* Om deze vraag te beantwoorden wordt de dimensieloze formulering uitgebreid om imperfecties mee te nemen door middel van een benadering met trigonometrische functies.

Zodra de dimensieloze formulering is gedefinieerd, richt het werk zich op het gebruik hiervan om een systematische schaalmethodologie te definiëren. De derde vraag gaat specifiek in op dit aspect van het werk en luidt: *Hoe kan een systematische methodologie worden ontworpen om composiet cilinders te verkleinen terwijl hun knikgedrag behouden blijft?* Om deze derde vraag te beantwoorden stelt de proefschrift een nieuwe schaalmethodologie voor, waarbij twee verschillende schaalstrategieën worden gepresenteerd. De eerste strategie omvat het schalen van sandwich-composietschalen met behoud van vergelijkbare structurele eigenschappen. Deze aanpak stuit op uitdagingen vanwege fabricagebeperkingen, met name bij het verkleinen van diktes. De tweede strategie schaalt van een sandwich-composietschalen naar een equivalente composiet-

laminaatschalen, die makkelijker te maken zijn, maar ook nieuwe uitdagingen opleveren bij het vergelijken van beide typen. Beide strategieën bieden afwegingen: terwijl de eerste strategie nauwkeurigere schaalresultaten oplevert, is de tweede beter haalbaar voor testen op laboratoriumschaal.

Tot slot is de vierde vraag: *Wat zijn de discrepanties tussen analytische en numerieke voorspellingen en experimentele waarnemingen van knikgedrag op verschillende schalen van composiet schaalstructuren geproduceerd met de systematische methodologie?* Om de vierde vraag aan te pakken, worden analytische en numerieke resultaten vergeleken met beschikbare tests op grote schaal en op laboratoriumschaal, waarbij deze laatste zijn ontworpen volgens de tweede schaalstrategie. Een belangrijke uitdaging die in het onderzoek wordt geïdentificeerd, is de discrepantie tussen analytische voorspellingen en experimentele resultaten. Hoewel het theoretische model een fout van 8% in de dimensieloze belasting voorspelt tussen volledige en laboratoriumschaalmodellen, onthullen experimentele resultaten een grotere fout van 22%. De kloof tussen theoretische voorspellingen en experimentele waarnemingen benadrukt de noodzaak van verdere verfijning van de schaalmethodologie en met name van het modelleren van imperfecties.

De proefschrift sluit af met een overzicht van de onderzoeksvragen en aanbevelingen voor toekomstig onderzoek, waarbij meer uitgebreide tests worden voorgesteld, met name van sandwich-composietstructuren op laboratoriumschaal. Daarnaast wordt aanbevolen om meer gedetailleerde modellen van imperfecties in het dimensieloze raamwerk op te nemen om de overeenstemming tussen theoretische en experimentele resultaten te verbeteren. Dit onderzoek levert een significante bijdrage aan de ontwikkeling van schaalmethoden en biedt een solide fundament voor toekomstige optimalisaties in het geschaalde testen van grootschalige sandwich-composietschalen

NOMENCLATURE

ABBREVIATIONS

Abbreviation	Definition
DESICOS	DESign guideline for Imperfection sensitive COmposite launcher Structures
DIC	Digital Image Correlation
FEA	Finite Element Analysis
FSDT	First-order Shear Deformation Theory
IS	Imperfection Sensitivity
ISS	International Space Station
KDF	KnockDown Factor
NESC	NASA Engineering and Safety Center
SBKF	Shell Buckling Knockdown Factor
SLS	Space Launch System
SPLA	Single Perturbation Load Approach

SYMBOLS

Symbol	Definition	Unit
a_{ij}	Components of the compliance matrix	[N/mm]
$b1_0, b1_1, b2_0, b2_1$	Median surface slope amplitudes	[-]
B_1, B_2	Normalized components of the change of slope of the normal to the undeformed mid-surface	[-]
$\bar{B_1}, \bar{B_2}$	Prebuckling normalized components of the change of slope of the normal to the undeformed mid-surface	[-]
$\hat{B_1}, \hat{B_2}$	Small perturbation at buckling of the normalized components of the change of slope of the normal to the undeformed mid-surface	[-]
D_{ij}	Components of the bending stiffness matrix	[N mm]
E_x, E_y	Lamina Young's Moduli	[MPa]
E_{11}, E_{22}	Nondimensional strains	[-]

Symbol	Definition	Unit
E^0_{11}, E^0_{22}	Nondimensional strains at the reference surface	[-]
F	Nondimensional stress function	[-]
$\bar{F}$	Nondimensional prebuckling stress function	[-]
$\hat{F}$	Small perturbation at buckling of the nondimensional stress function	[-]
F_p	Particular solution of the stress function	[-]
F_h	Homogeneous solution of the stress function	[-]
$\mathscr{F}$	Nondimensional buckling load with transverse shear	[-]
$\mathscr{F}_0$	Nondimensional buckling load without transverse shear	[-]
$\mathscr{F}_i$	Nondimensional buckling load including imperfections	[-]
G_x,G_y	Core Shear moduli	[MPa]
G_{xy}	Lamina Shear Modulus	[MPa]
h	Distance between the midsurface of the inner and outer facesheets	[mm]
$H(z_1, z_2)$	Function dependent on the solution and the imposed imperfection	[-]
k_1, k_2	Coefficients of the homogeneous solution that satisfy the boundary conditions	[-]
L	Length of the shell	[mm]
m	Half-waves in the longitudinal direction	[-]
M_x, M_y, M_{xy}	Moment per unit length resultants	[N]
$\mathscr{M}_{11}$,$\mathscr{M}_{22}$, $\mathscr{M}_{12}$	Nondimensional moment resultants	[-]
n	Number of waves in the circumferential direction	[-]
N_x, N_y, N_{xy}	Force per unit length resultants	[N/mm]
$\mathscr{N}_{11}, \mathscr{N}_{22}, \mathscr{N}_{12}$	Nondimensional force resultants	[-]
P	Axial buckling load including transverse shear	[kN]
P_0	Axial buckling load without including transverse shear	[kN]
P_i	Axial buckling load including imperfections	[kN]
Q_x, Q_y	Transverse shear stress resultants	[N/mm]
$\mathscr{Q}_{11}, \mathscr{Q}_{22}$	Nondimensional transverse shear resultants	[-]
R	Radius of the shell middle surface	[mm]
r	Number of stacking repetitions	[-]
t_f	Facesheet thickness	[mm]
t_c	Core thickness	[mm]
u	Axial displacement	[mm]
U	Nondimensional axial displacement	[-]
v	Circumferential displacement	[mm]
V	Nondimensional circumferential displacement	[-]
w	Radial displacement	[mm]
w_I	Nondimensional amplitude of the imperfection	[-]

Symbol	Definition	Unit
w_0, w_1	Radial displacement amplitudes	[-]
W	Nondimensional radial displacement	[-]
$\bar{W}$	Nondimensional prebuckling radial displacement	[-]
$\hat{W}$	Small perturbation at buckling of the radial displacement	[-]
W_I	Deviations in the shell reference surface	[-]
W_{total}	Sum of the radial displacement field and the deviations	[-]
x	Axial direction	[mm]
y	Circumferential direction	[mm]
z	Radial direction	[mm]
z_1	Nondimensional axial direction	[-]
z_2	Nondimensional circumferential direction	[-]
z_3	Nondimensional radial direction	[-]
α_m	In-plane stiffness weighted geometry parameter	[-]
α_b	Out-of-plane stiffness weighted geometry parameter	[-]
β	Flexural orthotropy parameter	[-]
β_x, β_y	Components of the change of slope of the normal to the undeformed mid-surface	[-]
$\gamma_{xy}, \gamma_{yz}, \gamma_{xz}$	Strains components	[-]
γ^0_{xy}	Strain component at the reference surface	[-]
$\Gamma_{12}, \Gamma_{23}, \Gamma_{13}$	Nondimensional strains	[-]
Γ^0_{12}	Nondimensional strain component at the reference surface	[-]
δ	Average shortening	[mm]
Δ	Nondimensional average shortening	[-]
ϵ_x, ϵ_y	Strains components	[-]
$\epsilon^0_x, \epsilon^0_y$	Strains components at the reference surface	[-]
θ	Facesheet angle	[^{o}]
μ	Membrane orthotropy parameter	[-]
ν_{xy}	Lamina poisson ratio	[-]
ν_m	Membrane poisson ratio	[-]
ν_b	Flexural poisson ratio	[-]
ϕ	Transverse ratio	[-]
χ_1, χ_2	Nondimensional transverse shear parameters	[-]
ω_I	Imperfection amplitude	[mm]

1

INTRODUCTION

Non est ad astra mollis e terris via

Seneca

1.1. BACKGROUND AND MOTIVATION

THE importance of space technology in modern society cannot be overstated, particularly for applications such as Earth observation, which are both essential to our daily lives and profitable. For example, the Copernicus program, a European Earth observation initiative, is projected to generate profits 10 times higher than its costs [1]. This highlights the incredible potential of space technology, both to provide meaningful insights into our environment and to be a source of economic prosperity.

Every space mission begins with a launch, which is one of the most delicate and cost-intensive parts of the process. Failure to launch has severe consequences, including the cost of the payload and relaunch, an investigation of the failure, and subsequent mitigation measures [2]. Furthermore, the launch vehicle imposes restrictions on the maximum mass and volume of any spacecraft, necessitating sophisticated structures in space.

For these reasons, the primary structures of launch vehicles have traditionally been designed conservatively [3]. The emergence of reusable launch vehicles, the reduction of

launch costs, and the rapid development of the field are forcing launch vehicle companies to reconsider this approach [4]. The reduction in weight of the primary structure can lower launch costs and/or increase the payload, making the launch vehicle more competitive. The current and developing European launchers (Fig. 1.1) are rapidly adapting to this new paradigm. This shift in design methodology has led to technological advances in materials and the use of new methods for structural analysis.

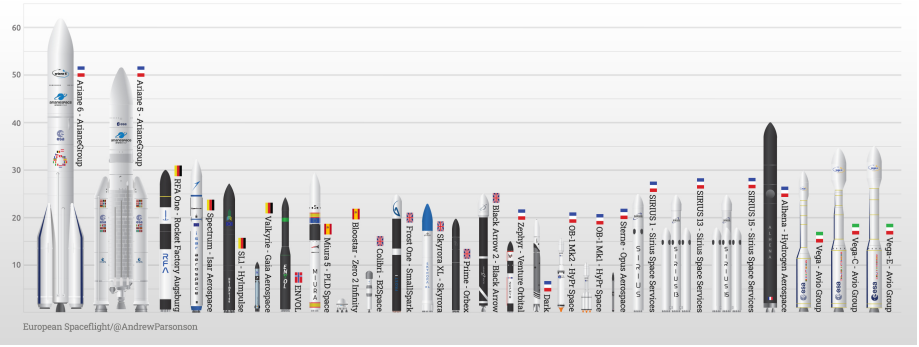

Figure 1.1: European launchers in operation and development in 2022 [1]

In the process of designing the primary structures of launch vehicles, a significant amount of focus has been placed on the design of cylindrical because these shells are an essential component in many different types of lightweight structures. However, cylindrical shells, especially those found in launch vehicle structures, are buckling-critical structures. Therefore, the critical axial buckling load is a critical design consideration, and understanding the buckling behavior is key for modern high performance applications. In particular, shell buckling under compression loads is of significant interest. For this reason, understanding the buckling behavior of cylindrical shells is critical in designing the primary structures of launch vehicles that are lightweight yet strong enough to withstand high compression loads.

Over the past decades, there have been considerable research efforts to analyze and improve the buckling strength of cylindrical shells under compression loads. One of the best-known programs is the NASA Shell Buckling Knockdown Factor (SBKF) program financed by NASA Engineering and Safety Center (NESC), which aimed to develop and validate methods for predicting the ultimate strength of thin-walled structural components under axial compression loads. The program involved a series of full-scale tests on cylindrical shells like the one seen in Fig. 1.2 of different geometries, materials, and fabrication methods. The results of the tests were used to calibrate and validate numerical models and to establish design criteria and safety factors for shell structures used in aerospace applications [5]. The SBKF program has greatly contributed to the development of more reliable and efficient structural designs for space launch vehicles as well as other aerospace applications. The data collected from the SBKF program, as well as the

[1] https://europeanspaceflight.com/european-rocket-index/

resulting knockdown factors [6], will also have a big impact on non-aerospace engineering projects that require thin-walled structures to safely withstand compressive loads. [7, 8]

Figure 1.2: Shell Buckling Knockdown Factor test article [2]

One of the materials tested during the SBKF [9, 10] was the sandwich composite material. In sandwich composite materials, as seen Fig. 1.3, two rigid facesheets are separated by a strong and lightweight core material, such as a honeycomb structure or foam. This arrangement results in a high stiffness-to-weight ratio, which makes sandwich composites useful for lightweight constructions. Sandwich composites are utilized extensively in the space sector due to their superior mechanical qualities, which include high specific strength and stiffness. Compared to other similar technical solutions, honeycomb sandwich composite constructions were shown by Sleight et al. [11] to have the best mass, cost, technological maturity, damage tolerance, and ability to be constructed, repaired, and inspected.

In the context of space launch vehicles, the use of sandwich composites in the principal components permits a substantial weight and cost reduction while preserving the requisite structural performance. Sandwich composite structures and composite laminate structures are the principal types of structures utilized in the construction of the most recent generation of space launchers, such as Ariane 6 and Space Launch System (SLS) [12].

When it comes to the design of cylindrical shells for launch vehicles, conducting extensive testing campaigns on the scale of the one that was carried out by the SBKF program has been standard practice [13]. In addition, testing is an extremely valuable

[2] https://www.nasa.gov/offices/nesc/home/FeatureShellBucklingTest.html

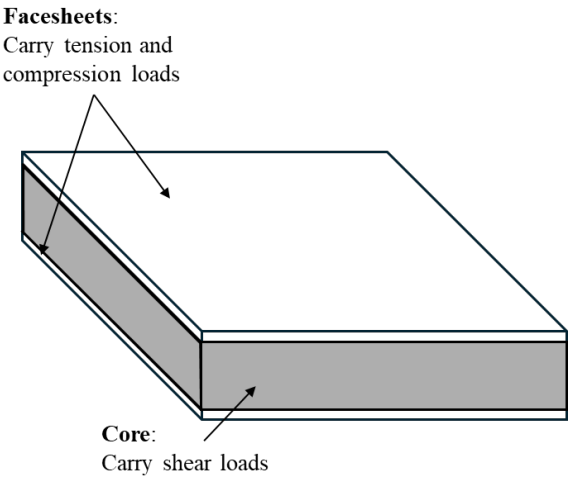

Figure 1.3: Sandwich composite configuration.

resource for those who are researching the buckling of cylindrical sandwich composite shells. This is because testing validates the numerical and analytical methods that are utilized by design professionals [14]. However, full-scale testing of large cylindrical sandwich shells has two major limitations that limit its usefulness. In the first place, the outcomes of the tests are extremely reliant on the characteristics of the manufacturing process and the imperfection signature of the shell [15]. Secondly, the cost of testing is high not only due to the high number of tests that are required but also due to the large scale of the structures that are taken into consideration [16]. Despite these drawbacks, testing is still a vital tool for validating the performance of cylindrical sandwich shells.

In this context, this thesis aims to develop a scaling methodology to replicate large-scale cylindrical shell buckling in standard laboratory testing size. Shell buckling behavior is an important requirement in the design of primary structures for launch vehicles, and the use of a scaling methodology offers a promising alternative to the challenges associated with full-scale testing.

1.2. RESEARCH QUESTIONS

THE thesis topic is the study of instability of cylindrical sandwich composite shells, typical of space components. Within this large topic, **the objective is to characterize the buckling response of these large shells through an analytically scaled down model, that can be verified computationally and finally tested in a laboratory scale, where the results are applicable to the large structure**.

The challenges and expected contributions of this thesis can be summarized by the

following four research questions.

RQ1 To what extent do the shear transverse effects influence the buckling response in sandwich composite structures of different scales?

By adding transverse shear effects into the nondimensional formulation, this study improves our knowledge of the design space in the buckling behavior of sandwich composite shells. The addition of transverse shear in the nondimensional formulation for buckling was previously unexplored, hence this study makes an important contribution to the discipline.

RQ2 What is the theoretical influence of imperfection sensitivity in the buckling response of sandwich composite shells of different scales?

Addressing the impact of imperfection sensitivity in the buckling response is a critical and challenging aspect of designing of sandwich composite cylindrical shells. This is a well researched issue, and the current state of the art will be presented in Chapter 2. Creating a theoretical framework inside the nondimensional formulation to account for imperfections at various scales, results in useful insights into the buckling response of both full-scale and scaled-down models.

RQ3 How can a systematic methodology be designed to scale down composite cylindrical shells while preserving their buckling response?

This research question addresses the main contribution of this dissertation: the establishment of a systematic scaling approach for sandwich composite cylindrical shells using a nondimensional theoretical framework. This offers two theoretical strategies for developing reduced-scale models that replicate the buckling behavior of full-scale sandwich composite structures.

RQ4 What are the discrepancies between analytical predictions and experimental observations of buckling behaviour in different scales of composite shell structures produced with the systematic methodology?

The study reveals some inconsistencies between the proposed theoretical models, and the experimental findings of scaled-down composite shells. The methodology established in this research offers a theoretical framework for scaling; nevertheless, more experimental validation is required to fully understand and tackle these discrepancies. This work's novelty is in recognizing these gaps and suggesting directions for future study, especially on improvements of the scaling approach and the better alignment of theoretical predictions with empirical behavior.

1.3. METHODOLOGY

THE thesis addresses the outlined questions using a combination of analytical and numerical techniques. This enables the development of a comprehensive understanding of the structure's behavior and the identification of the primary influencing factors in the scaling strategies.

Broadly speaking, the following four-step methodology was utilized to answer the outlined research questions:

Nondimensionalization: The first step is to use a systematic nondimensionalization procedure to make a mathematical model of the structure. The model is based on the governing equations and accounts for the structure's geometry, material, and loading factors. The nondimensionalization approach makes it easier to analyze the structure and identify the major elements that impact its buckling behavior.

Development of Scaling Strategies: The second step is to create two scaling strategies by used the nondimensional factors identified in step one. On the basis of a physical understanding of the baseline structures, scaling laws are utilized to establish the characteristics of the scaled models. Two scaling strategies are developed and examined to find the best approach for the specific structures under consideration.

Finite Element Analysis: In the third step, finite element analysis (FEA) is used to verify the mathematical model created in the first step and the scaling strategies developed in the second. The FEA is performed using the commercial software Abaqus. The outcomes of the FEA are compared to those of the mathematical model to ensure their accuracy and identify any issues.

Data Analysis: The final step in the methodology is to analyze the data obtained from the mathematical model, FEA, and external experimental testing. The analysis involves identifying the key factors that affect the behavior of the structure and quantifying their effects. The results of the analysis will be used to assess the effectiveness of the scaling strategy.

1.4. OVERVIEW OF THE THESIS

THE work is organized into 7 chapters, as shown in Fig. 1.4. The figure shows the research question addressed in each chapter as well as the methodologies used.

In this **first chapter**, a brief background on the topic is presented, as well as the thesis objective, research questions and methodology. **Chapter 2** expands on the relevant background and contains a review of the relevant literature in the two key topics of this thesis: Shell Buckling and Scaling Methodologies.

Chapter 3 contains a detailed description of the analytical formulation for sandwich cylindrical shells in the nondimensional form. The formulation described here is valid for sandwich cylinders with composite faces with a shear-deformable core under axial compression. **Chapter 4** expands the analytical formulation for the same sandwich shells to include initial geometrical imperfections.

The scaling methodology is presented in **Chapter 5**. Two different scaling strategies are presented and the sensitivity to the different geometrical parameters is discussed.

In **Chapter 6** the numerical verification of the structures is discussed as well as the comparison with experimental results. Two tests of different scales are compared using the scaling methodology proposed. Finally, **Chapter 7** reflects on the results as well as the research questions formulated, presents the conclusions of the thesis, and introduces some future research recommendation.

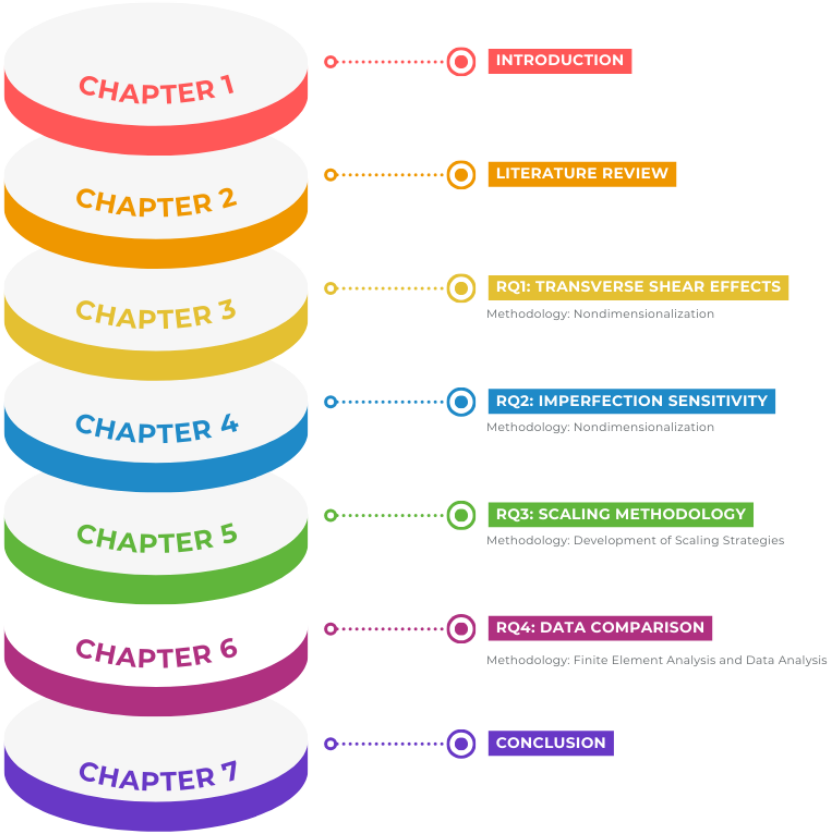

Figure 1.4: Thesis Outline.

2

LITERATURE REVIEW

Las experiencias de hoy
son el recuerdo de mañana

Isabel Allende

This chapter describes the literature relevant to the challenges described in the introduction. It is divided into two separate but connected sections, each of which is necessary to understand the research questions outlined. In the first part, shell buckling is discussed by looking at analytical models and simulation tools previously used to characterize the phenomenon. Since this is a broad topic, extensively studied in the literature, the focus is on the shell buckling under axial compression in sandwich composite cylinders. The second part moves the discussion to the scaling methods, including dimensional analysis and similarities between governing equations. Collectively, these parts constitute the fundamental basis for the study and provide a framework to understand the novel scaling method proposed in this thesis.

2.1. BUCKLING OF SHELLS

SHELL buckling is a highly non-linear phenomenon, where manufacturing imperfections significantly reduce the buckling load. This reduction is typically considered in design through the use of buckling knockdown factors, which are derived from experimental data. A key source for these factors is the recently updated NASA SP-8007 [6],

which provides knockdown factors for various shell types, including orthotropic shells and sandwich shells with isotropic facing sheets.

The 2020 update to SP-8007 was made under the Shell Buckling Knockdown Factor Program [17], addressing limitations in the original 1968 standard. One significant limitation was the overly conservative design approach, which considered the worst possible imperfection. Furthermore, in 1968, limited data were available for composite shells. In 2012, Takano [18] compiled test data on composite cylindrical shells, which formed the basis for new statistically-derived knockdown factors for composite cylinders.

Even with these updated design guidelines, shell buckling requires a combination of experimental, analytical, and numerical approaches to obtain accurate solutions [19]. The challenge with using newer analysis methods is that they require detailed knowledge of the initial geometric imperfections, which is rarely available. For prototypes, imperfections can be measured experimentally (as seen in Fig. 2.1) and incorporated into the theoretical analysis to accurately predict the buckling load. However, this approach is impractical for mass-produced shells, and still does not address the challenge of designing the shell before the prototype is produced.

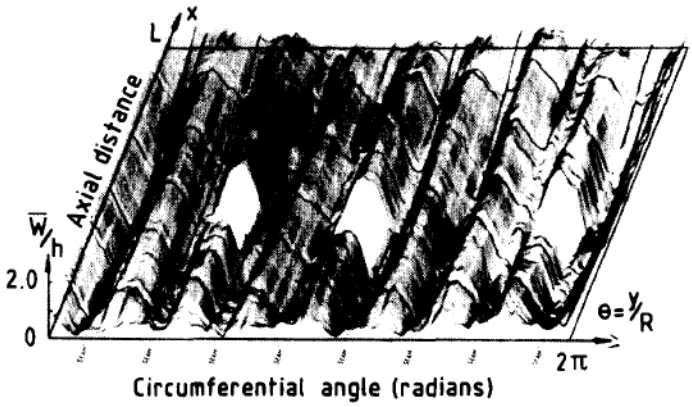

Figure 2.1: Measured initial shape of the ARIANE shell AR23-1. [20]

Due to the critical importance of this type of structure and the limitations of the knockdown factors, axially loaded cylindrical shells have been thoroughly investigated through analysis, simulation, testing, and a combination of all of them. The relevant literature referring to each of them is detailed in the following sections.

2.1.1. ANALYTICAL MODELS FOR PREDICTING SHELL BUCKLING BEHAVIOUR

Analytical models are the first tool designers use to predict the buckling behavior of the structure. Analytical calculations are faster and more flexible to dimension and/or material changes [21]. However, making the right assumptions and choosing the appropriate analytical model is a prerequisite to getting acceptable results.

The buckling behavior of sandwich shells in general and composite sandwich shells in particular have been studied by several authors [22, 23]. Two particular aspects of the analytical model have a significant influence on the accuracy of the analytical results for sandwich composite shells [24]. The first is the modeling of the shear-deformable core and the second is the inclusion of the imperfection sensitivity characteristic of shell buckling in general.

The first aspect is modeling the shear deformable core. This is important since the facesheets of the sandwich are generally thin compared to the total thickness of the sandwich structure. Therefore, modelling of the facesheets using the two-dimensional classical laminate theory (i.e. without accounting for the transverse shear behaviour) is considered sufficiently accurate for buckling purposes. In cases where delamination problems [25] or thermal dynamic behavior [26, 27] want to be studied, the authors have used shear deformation modelling for the laminate composite shells as well.

Modelling the core without considering the transverse normal stress can be done for cases with a metallic honeycomb core, where the core is very stiff in the through-the-thickness direction. However, in most cases, the core has a low transverse shear modulus, and modeling it with the two-dimensional classical laminate theory is inadequate and will result in a very stiff formulation [28, 29].

Several solutions for modeling the shear-deformable core of the buckling of sandwich plates and shells are available in the literature [30] and are briefly discussed here. These modeling approaches can be divided into categories depending on the variation of the displacement components through the thickness. The two approaches are order First-order shear deformation theory and higher order theory. The difference in the deformation pattern for sandwich structures is illustrated in Fig. 2.2. Choosing one or the other can be relevant depending on the specific case. For instance, Szekrenyes [28] clearly lustrates how the mayor modeling approaches result in diverse results for the case of a delaminated sandwich shell.

Most analytical modeling approaches are based on a first order shear deformation theory (FSDT) [31, 32]. In the FSDT, the core cross section, normal to the mid-surface of the undeformed state, remains flat but not normal in the deformed state. For sandwich structures, the first order shear deformation plate theory has been used with thin and soft core layers [33]. A correction factor must be used to adjust the transverse shear stiffness [34, 35, 36]. The correction factor ensures that the shear strain energy calculated using FSDT matches the actual shear strain energy [37].

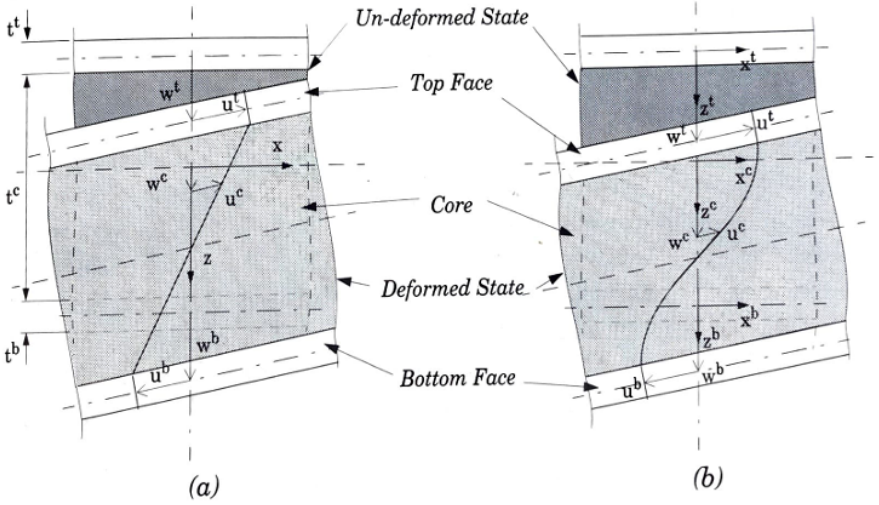

Figure 2.2: Deformation pattern through the thickness of the sandwich shell: (a) First-order shear deformation theory. (b) High-order theory. [24]

Other models are based on a higher-order theory [38]. Higher-order, in this case, does not refer to the order of the final system of differential equations but to the number of terms in the power series expansion of the displacements. Higher-order theories account for shear rotations and parabolic variation of the shear stresses, which have the advantage of eliminating the need for shear correction factors [39].Finally, other authors have proposed more complex formulations such as incorporating the kinematics of first-order shear deformation theory with zigzag layer functions [40] or a sublaminate formulation [41].

Modeling the imperfection sensitivity is not exclusive to sandwich cylindrical shells, since this is an intrinsic part of the shell buckling behavior. Imperfection sensitivity is widely acknowledged to be the main cause of discrepancy between the experimental data and analytical prediction [42]. This was acknowledged early on, and a series of theories were developed to explain the roots of difference [43, 44].

Koiter [45] was the first to propose the concept of imperfection sensitivity and to develop an analysis method for shells under buckling. Koiter demonstrated that the imperfection sensitivity of shell structures is closely linked to their initial postbuckling behavior. Specifically, interest lies in the variation of the loading parameter, A, in the vicinity of the bifurcation point, $A = A_c$, where A represents the loading parameter, and δ is the amplitude of the buckling mode, normalized by the wall thickness, t. If the shell exhibits a unique buckling mode associated with the lowest buckling load, its buckling and initial postbuckling behavior can be described accordingly.

Traditional defects are generally considered as the global or local initial imperfections of cylindrical shells due to an unsatisfactory manufacturing process or other external factors [46, 47]. It is generally believed that defects incurred during the manufacturing process or while in-service are the most important reasons for the reduction in load bearing capacity of cylindrical shells. Subsequently, various types of defects were investigated in the pursuit of the most unfavourable form of defects.

For example, Koiter et al. [48] used a trigonometric series expansion method and a small parameter perturbation method to study the influence of axisymmetric defects in the form of trigonometric functions on the buckling of cylindrical shells.

Coupling the Ritz or Galerkin method to a small parameter perturbation method are the most-used methods to introduce the imperfection sensitivity [49]. However, these methods have some limitations such as the solution assumed in the Galerkin and the Ritz method usually does not satisfy the simply supported boundary conditions [50], and the small parameter perturbation converges quite slowly for the buckling problem of cylindrical shells. Other alternative would be the use of the Hamilton system to elastic mechanics [51]. Following this approach, Liao [52] introduced the concept of homotopy in topology and differential geometry in the analytical approximation of differential equations for the buckling of isotropic cylindrical shells.

Regarding the type of defects, a distinction must be made between local defects (i.e. a localized thickness variation) with periodic defects (i.e. variation of the thickness at the mandrel joint) since local defects reduce the buckling load more substantially [53]. To introduce periodic defects, a trigonometric imperfection, partly inward and partly outward [54] is considered to be the easiest method to introduce the sensitivity to the imperfections. An asymptotic formula for buckling of cylindrical shells with uniform, axisymmetric and parabolic thickness defects has also been developed [55]. To study local defects, exponential functions are the most commonly used method [56]. Specific types of local defects such as structural cracks or corrosion defects [57, 58] lead to complex analytical solutions even in the case of isotropic shells.

2.1.2. SIMULATION TOOLS FOR PREDICTING SHELL BUCKLING BEHAVIOUR

Simulation tools are widely used to predict the buckling behaviour, including load and modes, of sandwich composite cylindrical shells [59, 60]. They present the advantage of allowing a greater detail in the design features such as the inclusion of cut-outs [61, 62] or cracks [63].

Therefore, in order to develop an accurate finite element model, a wider range of properties of the shell must be known. For instance, the imperfection signature plays an important role in the numerical study of shell buckling phenomena due to the high sensitivity of these structures to imperfections [64]. An imperfection signature is defined as the specific pattern and magnitude of deviations from the ideal geometry of a shell.

This imperfection signature is best derived from the physical specimen, but this strategy is very resource-consuming, because it requires the production of the specimen before running the simulation. Arbocz pioneered the use of measured imperfections in shell buckling simulations. A reference database of measured imperfection was created [65] such the data could be used in future simulations before having the specimen.

An incomplete imperfection signature of the test specimen can also be implemented in the finite element model with accurate results. In 2000, Bisagni used the measured imperfection signature of the central part of the shell [66]. The imperfection signature was completed for the areas without measurements with a linear interpolation up to the nominal geometry in the edges. These simulations, made with both Riks analysis and nonlinear dynamic analysis overestimated the buckling loads from the experiments. Wullschleger [67] also found in a different set of composite cylindrical shells that the numerical results with a partial imperfection signature overestimated the experimental results.

Pseudo-random imperfections can also be introduced into the wall geometry to carry out nonlinear analysis. Lincoln et al. [68], to examine the improved buckling response of shells manufactured via Continuous Tow Shearing introduced a pseudo-random variation in the radial node coordinate across the shell, with the size ranging from 0 to the wall thickness. This method was used across different cylinders to allow for a comparison and establish some guidelines.

In 2002, NASA Langley Research Center Hilburger [69], included in their simulation more types of imperfections: ply thickness variations, ply gaps, and fiber volume fraction. Moreover, they attempted to introduce uncertainty producing prediction ranges [70]. The best and worst cases were determined by combinatorial analysis. The results confirmed that a higher imperfection amplitude leads to a lower buckling load. The errors in the buckling predictions were under 10%. In this type of simulations, the numerically predicted loads were still overestimating the experimental results.

The inclusion of variances in fiber volume fraction (FVF) in the measured imperfection models was further studied by Broggi [71]. In this study, the measured variations in thickness were used to obtain the FVF, since changes in the percentage of resin were believed to account for most of the thickness variation. However, the FVF-variation-inclusive model predicted a buckling load less acurately than the model using with measured imperfections only. The influence of variations in ply gaps [72] was also considered. However, it was found that an accurate variation of the ply gaps in the imperfection models did not produce significantly different results.

Since these methods require a large amount of information about the shells, the Single Perturbation Load Approach (SPLA) [73] was developed to address this limitation. The errors between the test and the simulation were between 4% and 12% and resulted in less conservative estimates than the NASA SP-8007 guidelines. Recent studies have built upon this method in the context of large wind turbine towers which are also buckling-

sensitive structures [74].

The thickness imperfection may be calculated or measured [75]. In the first case, where the thickness is calculated, the outer surface measurements minus the inner surface measurements produce the shell thickness distribution. One technique to measure the inner and outer surface is structured light scanning [76]. In the second case, where the thickness is measured, direct ultrasonic measurement may be performed on test specimens [77].

This thickness imperfection can be directly introduced in the model via the node positions if solid or continuum shell elements are used. If conventional shell elements are used, the thickness variation can be input to the thickness of the core [76] in the case of sandwich constructions or just the composite layers in the case of a solid laminate [77].

Another aspect of the measured imperfections is that often the geometric imperfection measurement data points do not correspond precisely to the node coordinates of the shell finite element model [78]. To introduce the imperfection data into the mesh from the measurements, interpolation or curve fitting techniques are required. The method chosen has some influence on the accuracy of the results [79], but extensive comparisons have not been made in cylindrical sandwich composite shells.

Among the different types of interpolation used in the literature, the simplest one, linear interpolation, appears to be the most common [80, 81, 67]. However, more advanced interpolation methods, such as inverse distance-weighted interpolation, have also been used by some researchers [82, 83]. In this interpolation method, each point is the result of the weighted mean of the closest measured points. The weighted interpolation provides a smoother surface since it avoids one of the shortcommings of linear interpolation, which is the inclusion of measurement system noise. An example of the model with inverse distance-weighted interpolation can be seen in Fig. 2.3.

Curve fitting can also be used successfully [84]. For instance, Fourier analysis can be used to generate mean imperfection signatures. This can be particularly convenient to compare if some manufacturing techniques produce variations in the thickness amplitude at certain frequencies.

Modeling the test set-up to some extent can also influence the accuracy of the results. In some cases, only the potting used in the experiment to facilitate load introduction was included in the numerical model [85, 77]. In the experiments on the composite shells of the NASA Langley Shell Buckling Knockdown factor program [76], the full setup was included load orientation lines and assembly at the edges of the shell. The introduction of a more complete model reduced the difference between the simulation and test results. The remaining differences were attributed to an asymmetry in the load introduction of that specific test setup [77] or inaccurate material properties [76].

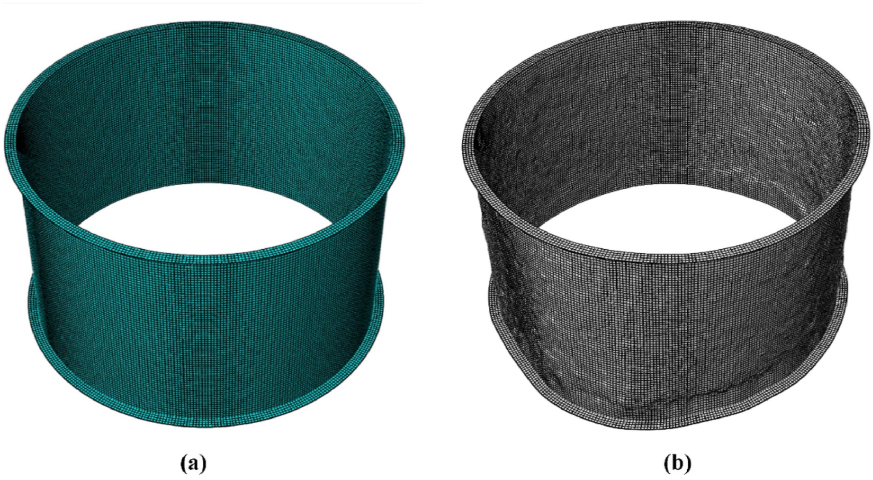

Figure 2.3: FE model of the test cylinder: (a) perfect model and (b) with actual surface morphology deviated from a perfect cylinder scaled by 50 times. [82]

Schillo [86] attempted to study in detail the influence of load asymmetry in the test setup in a series of simulations of filament-wound composite cylindrical shells that also included measured geometric imperfections. Furthermore, researchers used microscopy to measure the material properties instead of using the nominal material data. This study established the importance of loading imperfections on buckling behavior. The loading imperfections were found to have five times more influence on the buckling load than the measured imperfection. This study is noteworthy because it intentionally applied large loading imperfections, revealing that the NASA standard SP-8007 was not a conservative estimation in this case.

Another unusual result was found by Wu in 2013 [87], where the imperfect shells produced a higher buckling load than the one predicted by the perfect model. This study researched the buckling behavior of two variable-strength composite shells. In this type of composite shell, the manufacturing process (filament winding) introduces fiber tows that overlap, resulting in an intrinsic thickness difference. However, other studies with variable stiffness shells [85, 88] have found that the experimental buckling load was lower than the load of the perfect shell. These studies also produced simulations with a high degree of accuracy, provided that the measured geometric imperfections were included in the model.

Hartwich et al. [89] also found in a series of tests designed to analyze the influence of manufacturing on the imperfection sensitivity that the filament winding samples pose a more regular imperfection shape than the layered ones. The experimental results support the notion that more regular imperfection patterns, even those with higher imperfection amplitudes, reduce buckling load less than more irregular ones, such as those caused by fiber overlap.

Unlike many measured imperfection approach studies, Hilburger [69] produced a window of buckling behavior predictions rather than single predictions of combinations of imperfections. Combinatorial analysis was used to create high and low bounds for the ranges. In practice, this approach to characterizing uncertainty in model parameters could be applied to any combination of properties. The fact that different measurement systems in the work of Labans [88] produced different numerical buckling load predictions suggests that it may be useful to generate a range of predictions as Hilburger [69] did.

Another significant difference was highlighted by Friedrich and Schröder [90], when they studied numerically the discrepancy between boundary conditions and load introduction of full-scale built-in and sub-scale experimental shell structures. They aimed to study potential inaccuracies between launch vehicle structures, which are loaded in a load-controlled manner, and most lab buckling experiments, which are conducted in a displacement-controlled manner. Their study also produced results that indicated a high dependency of boundary conditions on the collapse loads.

Finally, Wagner et al. [91] introduced a comparison between geometric imperfection signatures, probabilistic and deterministic lower bound methods for differently manufactured shells under axial compression. Their findings indicate that the use of measured geometric imperfection is often unreliable for the analyzed shells, as the associated test buckling loads are frequently underestimated. The probabilistic analysis incorporating geometric and wall thickness imperfections was conducted; however, even at elevated reliability levels, this analysis yielded non-conservative estimations of buckling loads.

2.2. SCALING METHODS

THE study of the buckling behavior of large shell structures through full-size tests is complex and expensive. To the high cost of the shell itself, one must add the cost of the equipment necesary to perform test in large structures. For this reason, scaled structures are often preferred to evaluate the buckling behavior. For metallic structures, such scaled cylinders have already been proven effective for developing design guidelines [92]. However, scaling down representative large sandwich composite structures can be challenging because of the high number of parameters involved in the stiffness properties of the structure such as the thickness, the materials and the ply orientations. The design of a scaled structure needs to be considered carefully in order to obtain a comparable result. Moreover, the scale change should account for the manufacturing and facility constraints of the new scale.

It is important to distinguish between changes in scale and changes in size. A scale change, as defined by Simitses et al.[93], refers to the changes in the geometric dimensions or to the changes in the response to external causes such as the force. On the other hand, changes in size relate to the changes in material strength or stiffness. The changes in size are rarely considered [94], after all the material properties obtained from coupon

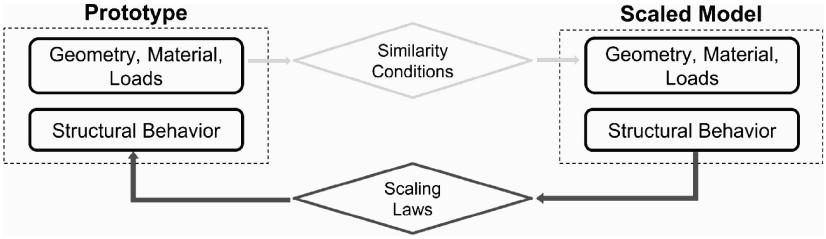

Figure 2.4: A schematic for predicting the structural behavior of an enlarged prototype using testing results from a scaled model. [98]

testing are regularly used for full structure calculations.

One scaling approach consists in considering each possible scaled configuration on a case-by-case basis. An European Union project with the goal of examining the imperfection sensitivity of large composite shell structures named DESICOS (New Robust DESign Guideline for Imperfection Sensitive COmposite Launcher Structures) utilized this approach. The scaled configurations were chosen by an iteration process where the focus was to keep some geometric relations (i.e. Radius to thickness, R/t and Length to Radius, L/R) and the lowest eigenvalue equal to the original structure [95].

More formal methodologies have also been developed [96] and this section describes different scaling methods that have been used in shells with several degrees of success. To have a correct scaling between two or more systems, similitude theory prescribes that the relations between the mathematical parameters that describe our systems must be enforced. If a relation between the mathematical parameters between different systems can be established, this is usually called a scaling law [97]. Via the scaling laws the parameters between the two structures can be converted. In this work, two scales are considered. The larger one will be named the baseline structure, and the smaller system will be named the scaled structure. A schematic for predicting the structural behavior of an large scale prototype using testing results from a scaled model is shown in Fig. 2.4.

When all the established scaling laws are obeyed, this is known as complete similarity. In some cases not all of them can be fulfilled at once. This can be due to an incompatibility between the defined scaling laws or practical problems such as manufacturing or laboratory constraints. In those cases only partial similarity can be achieved since one or more scaling laws have to be disregarded. The importance of all scaling laws is not equal in most cases [99]. Identifying and enforcing the scaling laws with the highest influence becomes critical to the success of the scaling process.

2.2.1. DIMENSIONAL ANALYSIS

The earliest formal scaling method is the use of dimensional analysis to design scaled structures [100]. This method is based on the Pi-Buckingham theorem and consists on

identifying all the system variables and from them produce a series of independent normalized parameters. These parameters are then treated as the scaling laws [101]. Structures are considered to have complete similarity between the baseline structure and its scaled structure when all the independent normalized parameters are equal in both configurations.

Parameter selection is of paramount importance, since some parameters are easier to measure and calculate, and others are easier to modify when searching for the scaled configuration. Consequently this method relies heavily on the experience and knowledge of the physical problem [102]. The main disadvantage of this methodology is the difficulty in identifying the scaling laws. Therefore, it is not commonly used for problems with a large number of design parameters.

Nevertheless, it has been heavily and successfully used to scale down and test structures from launch vehicles [103]. Saturn I [104] and Saturn V[105] vibrations characteristics were studied with scaled models obtained with this method. Scaled test to study the dynamic behavior were also made for the Space Shuttle [106] and the ISS (International Space Station)[107].

Dimensional analysis has also been applied to steel shells subjected to impact loading [108], where it was observed that small structures resist perforation better than large structures. In this case, it is understood that the size change (material properties: strain rate sensitivity and fracture) plays also an important role.

2.2.2. SIMILARITY BETWEEN GOVERNING EQUATIONS

If the governing equations of the phenomena are known, another formal method for scaling is based on similarity between governing equations. The principle of this method is that both the baseline structure and the scaled one are ruled by the same set of equations, which can be either the differential equations or the solution equation. Vibration problems are particularly amenable to this type of scaling [109].

This method is powerful in obtaining complete and partial similarity laws for the design of scaled structures, because it avoids the difficulty of identifying the normalized parameters. The main advantage of this method is that the scaling laws are deduced directly from each parameter in the governing equations. The difficulty is in simultaneously fulfilling all the scaling laws while remaining within the design and manufacturing constraints. The consequence is that in most cases the scaled model that is produced fulfills only partially the similarity laws. For these cases, the lack of complete similarity limits the applicability of the results. In case complete similitude is obtained, the scaling of both buckling load and the buckling mode shapes is realised [110].

This method was thoroughly used by Simitses [111, 112, 113], who studied extensively the case of scaling down laminated cylindrical shells. The method was applied to

vibration studies and buckling of shells under axial compression with and without imperfection. The scaling laws obtained do not allow for a large range of design freedom, therefore, the partial similarity and some distortion in the parameters were needed. The accuracy of the predictions was shown to vary depending not only in the amplitude of the distortion but also the parameters distorted. For instance, distortion of the number of plies or length still produced accurate results, whereas minimal distortion of the thickness or the radius resulted in inaccurate buckling predictions.

A variation of the method was developed in 2018 by Coutinho et al. [98]. This method tried to avoid the pitfall that scaling laws are considered for each individual application, which can be time consuming. In the method, a general approach, with less assumption is described. The method relies on three levels of a modular approach. There are six modules on the first level, which contain the scaling laws that correspond to the equations of the plate (strain-displacement, equations of motion...), kept with a minimal number of assumptions. These scaling laws are combined on the second level. If several bodies are considered in the structure, the third level allows for the interaction between them by imposing internal forces and displacements continuity at the interfaces. The method is applied successfully to a simply supported stiffened plate under uniform pressure, with good agreement between numerical results of both scales. This method could be extended to the scaling of other types of structures such as shells. Partial similitude could also be considered to enhance the method possibilities.

2.2.3. SIMILARITY BETWEEN NONDIMENSIONAL GOVERNING EQUATIONS

Finally, the use of nondimensional governing equations is also a scaling procedure. In this case the nondimensional parameters of the equations become the scaling laws. If the nondimensional parameters that conform the equations are equal in the baseline and scaled case, similarity can be obtained. The parameters depend on the nondimensionalisation procedure and some systems might be more suitable than others for different systems. The nondimensionalisation procedure is time consuming, but once the system is devised the determination of the scaling laws is straightforward.

Beyond their scaling applications, nondimensional parameters and equations are developed because they are extremely useful to navigate a large design space [114]. For instance, many different constructions may correspond to the same set of nondimensional parameters, and the relative magnitudes of the parameters can be used to identify special cases in which one or more parameters are negligible. From 2002-2008, Weaver et al. [115] made extensive use of nondimensionalisation procedures and parameters to gain insight into the behavior of laminated composite structures. In their study, to account for the effects of flexural-twist and extension-twist anisotropies on the buckling of compression-loaded cylindrical shells, correction factors derived from the nondimensionalisation procedures were calculated. In the field of the buckling of sandwich composite structures with shear deformable core, nondimensional parameters have been used to study and characterize plates [116].

In their investigation of the free vibration of stiffened shells, Tokamani et al. [117] made use of nondimensional parameters and equations for scaling purposes. In their scaling analysis the stiffeners were smeared, and the nondimensional frequency is obtained in terms of nondimensional parameters from nondimensional equations. The scaling laws were derived via substituting the parameters from the baseline in the nondimensional equation of the scaled shell. If the number of scaling laws is fewer than the number of variables, the process has a larger design freedom. This can be used to adapt to the manufacturing constraints obtaining the same accuracy at a reduced cost.

Other application where nondimensional parameters and equations were developed and successfully used for scaling is solar sail systems. Solar sails must be large by design, and the calculation of the deflection of the sail, modeled as a thin plate, and the deflection of the boom, modeled as a beam, is required. Nondimensional equations for this system, including the interactions, were proposed, and the parameters that conform them were established as scaling laws. Canfield et al.[118] used these nondimensional equations to use the results of a solar sail with a side length of 10 meters to propose larger designs (20 to 40 meters of side length).

Hilburger, et al. [119] also used the nondimensional equations based on Reissner-Mindlin plate theory to obtain scaling laws for sandwich composite plates subjected to combined loads. The main advantage of this method is that the results of the buckling equations are also in nondimensional form and can be compared with the different scales. This approach not only benefits from the use of scaling laws directly derived from the governing equations, but also provides the framework to evaluate the response.

However, even if the nondimensional parameters and equations provide an excellent scaling system and analysis framework, it should be noted that even in the cases of full similarity the results might diverge due to the simplifications applied in the governing equations. The user needs to make sure the equations describe account for phenomena that is relevant only in the scaled configurations or vice versa.

3

Nondimensional Buckling Formulation Including Transverse Shear Effects

Cuéntame un cuento de números,
háblame del dos y el tres
-del ocho que es al revés
igual que yo del derecho-.

Gloria Fuertes

This chapter aims to extend the existing nondimensionalisation formulation developed by Nemeth [121] to sandwich composite cylindrical shells with a shear deformable core under axial compression. This is done in order to later use the nondimensional equations as the basis for the scaling process.

To obtain the axial nondimensional buckling load, first, the problem and its assumptions are described. This includes the geometry and properties of the shell, as well as the nondimensional reference system and nondimensional displacements. Then, the fundamental relations are explained and derived both in the dimensional and nondimensional form: strain-displacement relations, constitutive equations, equilibrium equa-

This chapter has been published in Thin-Walled Structures **161**, 107393 (2021) [120].

tions and compatibility equations. The equilibrium and compatibility equations are linearized, possible solutions according to the boundary conditions are proposed, and the eigenvalue problem resultant is solved for the buckling load.

Finally, in order to illustrate the usefulness of the nondimensional equations and parameters, several shells are selected. The buckling response as well as the influence of the transverse shear of the core are among the differences that can be tracked via the nondimensional parameters.

3.1. MODEL ASSUMPTIONS AND COORDINATE SYSTEM

SANDWICH composite structures provide bending and in-plane extensional rigidity with composite facesheets separated by a low density core, which provides as well transverse shear rigidity to the construction. The laminated sandwich shells under consideration are composed of identical inner and outer facesheets and a core made of a shear deformable material. The facesheets are made of several laminae whose fibers can be oriented in any direction and any stacking sequence of the laminae is permissible.

The geometry of the shell is characterized by its length L, radius of the middle surface R, facesheet thickness t_f, and core thickness t_c as depicted in Figs. 3.1 and 3.2. Consistent with the shells formulation, the assumption that the shell thickness is small compared to the radius is made. The mid-surface of the sandwich construction is the reference surface. The distance between the mid-surfaces of the inner and outer facesheets, h, is also defined.

In this study, both facesheets are assumed to have equal thickness and are placed symmetrically with respect to the mid-surface of the sandwich construction. The normals of the laminate point outward, namely z and z_3 in Fig. 3.2, and thus the entire sandwich is geometrically symmetric, even if the layups of the facesheets differ. Each ply in both facesheets is modeled as orthotropic, linear elastic, and of constant thickness, resulting in a shell of constant overall thickness.

The transverse shear stiffness of the facesheets is neglected in this model, consistent with standard assumptions in sandwich structure analysis[122], where the facesheets are considered sufficiently thin and stiff compared to the much thicker and more compliant core. The core, which is orthotropic with one axis of orthotropy aligned with the shell axis, is linear elastic and of constant thickness. Its transverse shear stiffness is assumed to be dominant and is retained in the formulation. This assumption is applied consistently throughout the thesis.

The coordinate system x, y, z is measured with respect to the reference surface in the axial, circumferential and radial directions respectively as depicted in Fig. 3.2. The nondimensional or normalized coordinates, z_1, z_2 and z_3 are:

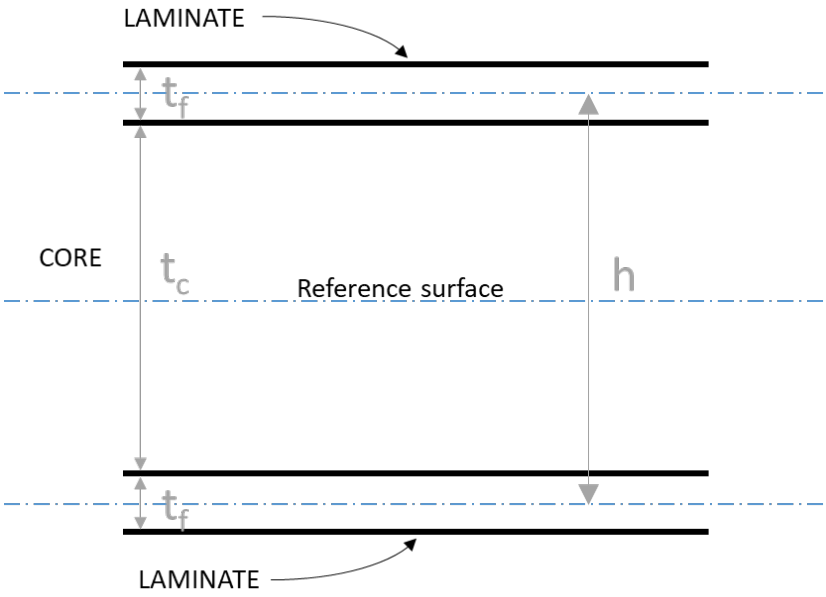

Figure 3.1: Cylindrical Sandwich Shell Section.

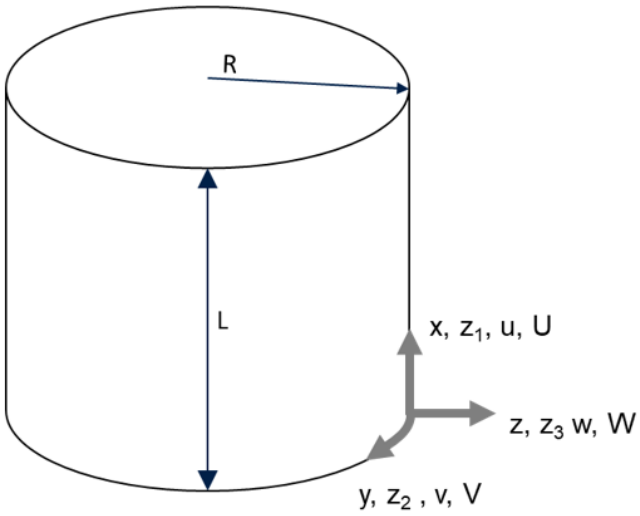

Figure 3.2: Cylindrical Shell Geometry and Coordinate System.

$$z_1 = \frac{x}{L} \tag{3.1}$$

$$z_2 = \frac{y}{R} \tag{3.2}$$

$$z_3 = \frac{z}{\sqrt{12}\sqrt[4]{a_{11}a_{22}D_{11}D_{22}}} \tag{3.3}$$

where the a_{ii} are membrane compliances and the D_{ii} are bending stiffnesses of the entire sandwich and are calculated using the classical laminate theory.

The denominator $\sqrt{12}\sqrt[4]{a_{11}a_{22}D_{11}D_{22}}$ of Eq. (3.3) represents the equivalent thickness of the sandwich structure. In the particular case where the structure is made of an isotropic material instead of a sandwich composite, the value of the equivalent thickness is the value of the exact thickness.

The components of displacement u, v and w of a point on the shell are the components in the x, y and z directions. The nondimensional displacements U, V, W are defined as:

$$U = \frac{L}{\sqrt{a_{11}a_{22}D_{11}D_{22}}}u \tag{3.4}$$

$$V = \frac{R}{\sqrt{a_{11}a_{22}D_{11}D_{22}}}v \tag{3.5}$$

$$W = \frac{1}{\sqrt[4]{a_{11}a_{22}D_{11}D_{22}}}w \tag{3.6}$$

The transverse shear stiffness is provided primarily by the core; therefore, only the transverse shear stiffness of the core is included in the formulation. The transverse shear stresses are assumed constant through the core thickness. To model the transverse shear stiffness the first-order shear deformation theory of Cheung and Tennyson [123] is adopted.

Unlike classical first-order shear deformation theories that require a shear correction factor, the formulation of Cheung and Tennyson [123] does not explicitly introduce such a factor. Instead, shear deformation is captured directly through kinematic assumptions and the definition of an effective displacement field across the core, using a geometrically defined distance h (seeFig. 3.1). Thus, no separate shear correction factor is required in this model. This theory satisfies the continuity of transverse shear stresses

at the facesheet-core interfaces and enforces zero shear stress on the free surfaces. As a result, a linear variation of the in-plane displacement components through the core thickness is obtained.

The shell is considered to have simply supported boundary conditions. Three assumptions are made in order to proceed with the analysis. First, no failure between the facesheet and the core is assumed. Second, in the laminate there is no slippage between plies, as well as no inter-cell buckling in the core. Finally, the normal stiffness of the core is considered very large, therefore instability associated with wrinkling of facesheets is not included.

The process to obtain the buckling load and mode of the shell follows the classical procedure [124]. First, the strains-displacement relations are established according to the proposed assumptions. Secondly, the equilibrium and compatibility equations are developed step by step and transformed into the nondimensional formulation. In order to obtain these equations, the strains-displacement relations are adapted to nondimensional form. The nondimensional linear buckling equations are obtained applying the adjacent equilibrium criterion [100] and a nondimensional axial buckling load solution is presented for the formulation with and without core transverse shear.

3.2. EQUILIBRIUM AND COMPATIBILITY EQUATIONS

THE equations used in the present study are relatively well known in their dimensional form [124]. The current nondimensionalisation keeps a similar format as the dimensional equations and it is here applied to axial compression. The formulation also can be used for other load cases.

First, the displacement field distribution and the strain displacement relations are presented. Then, the stress resultants and constitute equations are considered and the nonlinear equilibrium equations and the strain compatibility equations are obtained.

3.2.1. STRAIN-DISPLACEMENT EQUATIONS

Using the nonlinear strain-displacement relations, where the strains are considered to be small but the rotations are moderate, strains components $\epsilon_x, \epsilon_y, \gamma_{xy}, \gamma_{xz}$ and γ_{yz} can be expressed as:

$$\epsilon_x = \epsilon_x^0 - z\frac{\partial \beta_x}{\partial x} = \frac{\partial u}{\partial x} + \frac{1}{2}\left(\frac{\partial w}{\partial x}\right)^2 - z\frac{\partial \beta_x}{\partial x} \tag{3.7}$$

$$\epsilon_y = \epsilon_y^0 - z\frac{\partial \beta_y}{\partial y} = \frac{\partial v}{\partial y} + \frac{w}{R} + \frac{1}{2}\left(\frac{\partial w}{\partial y}\right)^2 - z\frac{\partial \beta_y}{\partial y} \tag{3.8}$$

$$\gamma_{xy} = {\gamma_{xy}}^0 - z\left(\frac{\partial \beta_y}{\partial y} + \frac{\partial \beta_x}{\partial y}\right) = \frac{\partial v}{\partial x} + \frac{\partial u}{\partial y} + \frac{\partial w}{\partial x}\frac{\partial w}{\partial y} - z\left(\frac{\partial \beta_y}{\partial x} + \frac{\partial \beta_x}{\partial y}\right) \tag{3.9}$$

$$\gamma_{xz} = \left(\frac{\partial w}{\partial y} - \beta_y\right) \tag{3.10}$$

$$\gamma_{yz} = \left(\frac{\partial w}{\partial x} - \beta_x\right) \tag{3.11}$$

where ϵ_y^0, ϵ_y^0 and ${\gamma_{xy}}^0$ are the components of the strains at the reference surface and β_x and β_y are the components of the change of slope of the normal to the undeformed mid-surface.

These components, β_x and β_y, are already nondimensional. However, for the purposes of this formulation, it is more convenient to create new nondimensional parameters that account for the geometry and material stiffness. Thus, two new nondimensional parameters, B_1 and B_2, are established:

$$B_1 = \frac{L}{\sqrt[4]{a_{11}a_{22}D_{11}D_{22}}}\beta_x \tag{3.12}$$

$$B_2 = \frac{R}{\sqrt[4]{a_{11}a_{22}D_{11}D_{22}}}\beta_y \tag{3.13}$$

The strain equations shown in Eqs. (3.7) to (3.11) can be also defined in terms of the nondimensional coordinates and displacements as can be seen in Eqs. (3.1) to (3.6), (3.12) and (3.13), where the nondimensional strains, E_{11}, E_{22}, Γ_{12}, Γ_{13} and Γ_{23} are expressed as:

$$E_{11} = \frac{L^2}{\sqrt{a_{11}a_{22}D_{11}D_{22}}}\epsilon_x = \frac{\partial U}{\partial z_1} + \frac{1}{2}\left(\frac{\partial W}{\partial z_1}\right)^2 - z_3\frac{\partial B_1}{\partial z_1} \tag{3.14}$$

$$E_{22} = \frac{R^2\epsilon_y}{\sqrt{a_{11}a_{22}D_{11}D_{22}}} = \frac{\partial V}{\partial z_2} + \frac{R}{\sqrt[4]{a_{11}a_{22}D_{11}D_{22}}}W + \frac{1}{2}\left(\frac{\partial W}{\partial z_2}\right)^2 - z_3\frac{\partial B_1}{\partial z_2} \tag{3.15}$$

$$\Gamma_{12} = \frac{LR}{\sqrt{a_{11}a_{22}D_{11}D_{22}}}\gamma_{xy} = \frac{\partial V}{\partial z_1} + \frac{\partial U}{\partial z_2} + \frac{\partial W}{\partial z_1}\frac{\partial W}{\partial z_2} - z_3\left(\frac{\partial B_2}{\partial z_1} + \frac{\partial B_1}{\partial z_2}\right) \tag{3.16}$$

$$\Gamma_{13} = \frac{R^2}{\sqrt{a_{11}a_{22}D_{11}D_{22}}}\gamma_{xz} = \frac{\partial W}{\partial z_2} - B_2 \tag{3.17}$$

$$\Gamma_{23} = \frac{L^2}{\sqrt{a_{11}a_{22}D_{11}D_{22}}}\gamma_{yz} = \frac{\partial W}{\partial z_1} - B_1 \tag{3.18}$$

Due to the chosen nondimensionalization procedure, as seen in Eqs. (3.10), (3.14), (3.16) and (3.18) most the equations in their nondimensional format only include the

derivations of nondimensional displacements U,V,W and the components of the change of slope of the normal B_1, B_2 with respect to the introduced nondimensional coordinates z_1, z_2.

However, in Eq. (3.15), there is also the term: $R/\sqrt[4]{a_{11}a_{22}D_{11}D_{22}}$. With few modifications this term can be expressed as Z, a nondimensional parameter known as the Batdorf-Stein parameter.

$$Z = \frac{R}{\sqrt{12}\sqrt[4]{a_{11}a_{22}D_{11}D_{22}}} \tag{3.19}$$

The Batdorf-Stein parameter, Z, formally introduced by Nemeth [125], relates the radius with the membrane compliances and bending stiffnesses. The Batdorf-Stein parameter is similar in character to a radius to thickness ratio R/t because it relates the shell radius R to an equivalent thickness $\sqrt{12}\sqrt[4]{a_{11}a_{22}D_{11}D_{22}}$. If an isotropic material were used this value would match the thickness exactly.

With the addition of the Batdorf-Stein parameter, the Eq. (3.15) results then as:

$$E_{22} = \frac{\partial V}{\partial z_2} + \sqrt{12}\,Z\,W + \frac{1}{2}\left(\frac{\partial W}{\partial z_2}\right)^2 - z_3\frac{\partial B_1}{\partial z_2} \tag{3.20}$$

From the Eqs. (3.14), (3.16) and (3.20), the nondimensional expressions of the reference surface strains can be obtained:

$$E^0_{11} = \frac{\partial U}{\partial z_1} + \frac{1}{2}\left(\frac{\partial W}{\partial z_1}\right)^2 \tag{3.21}$$

$$E^0_{22} = \frac{\partial V}{\partial z_2} + \sqrt{12}\,Z\,W + \frac{1}{2}\left(\frac{\partial W}{\partial z_2}\right)^2 \tag{3.22}$$

$$\Gamma^0_{12} = \frac{\partial V}{\partial z_1} + \frac{\partial U}{\partial z_2} + \frac{\partial W}{\partial z_1}\frac{\partial W}{\partial z_2} \tag{3.23}$$

In a similar way as the strains at any point of the shell are described in Eqs. (3.14), (3.16) and (3.20), the nondimensional values of the mid-surface strains E_{11}, E_{22} and Γ_{12} are thus expressed as:

$$E^0_{11} = \frac{L^2}{\sqrt{a_{11}a_{22}D_{11}D_{22}}}\epsilon^0_x \tag{3.24}$$

$$E^0_{22} = \frac{R^2}{\sqrt{a_{11}a_{22}D_{11}D_{22}}}\epsilon^0_y \tag{3.25}$$

$$\Gamma^0_{12} = \frac{LR}{\sqrt{a_{11}a_{22}D_{11}D_{22}}}\gamma^0_{xy} \tag{3.26}$$

3.2.2. CONSTITUTIVE EQUATIONS

In deriving a set of nondimensional constitutive equations, it is desirable to keep the number of parameters that characterize the material behavior to a minimum. Here, the semi-inverted constitutive equations are used, considering that the sandwich structure is symmetric, even if the laminates that conform the facesheets are not.

$$\epsilon_x^0 = a_{11}N_x + a_{12}N_y \tag{3.27}$$

$$\epsilon_y^0 = a_{12}N_x + a_{22}N_y \tag{3.28}$$

$$\gamma_{xy}^0 = a_{66}N_{xy} \tag{3.29}$$

where N_x, N_y and N_{xy} are the force components per unit length. The nondimensional components of these forces: $\mathcal{N}_{11}$, $\mathcal{N}_{22}$ and $\mathcal{N}_{12}$, can be defined as:

$$\mathcal{N}_{11} = \frac{R^2}{\sqrt{D_{11}D_{22}}}N_x \tag{3.30}$$

$$\mathcal{N}_{22} = \frac{L^2}{\sqrt{D_{11}D_{22}}}N_y \tag{3.31}$$

$$\mathcal{N}_{12} = \frac{R^2}{\sqrt[4]{D_{11}D_{22}^3}}N_{xy} \tag{3.32}$$

Combining the in-plane equations shown Eqs. (3.27) and (3.28) with the definitions of the nondimensional strains shown in Eqs. (3.24) and (3.25), and nondimensional stresses shown in Eqs. (3.30) and (3.31) and, operating, the following nondimensional in-plane relations are obtained:

$$E_{11}^0 = \frac{L^2}{R^2}\sqrt{\frac{a_{11}}{a_{22}}}\mathcal{N}_{11} + \frac{a_{12}}{\sqrt{a_{11}a_{22}}}\mathcal{N}_{22} \tag{3.33}$$

$$E_{22}^0 = \frac{a_{12}}{\sqrt{a_{11}a_{22}}}\mathcal{N}_{11} + \frac{R^2}{L^2}\sqrt{\frac{a_{22}}{a_{11}}}\mathcal{N}_{22} \tag{3.34}$$

Three new terms are highlighted in Eqs. (3.33) and (3.34). Upon inspection, these three terms can be expressed with the help of only two nondimensional parameters α_m and ν_m, as defined by Nemeth [125]:

$$\alpha_m = \frac{R}{L}\sqrt[4]{\frac{a_{22}}{a_{11}}} \tag{3.35}$$

$$\nu_m = -\frac{a_{12}}{\sqrt{a_{11}a_{22}}} \tag{3.36}$$

Combining the in-plane shear equation in Eq. (3.29) with the definition of the nondimensional strain from Eq. (3.26) and nondimensional in-plane shear stress in Eq. (3.32) and operating, the following relation is obtained:

$$\Gamma^0_{12} = \frac{L}{R}\frac{a_{66}}{\sqrt{a_{11}a_{22}}}\sqrt{\frac{D_{22}}{D_{11}}}\mathcal{N}_{12} \tag{3.37}$$

Operating it can become:

$$\Gamma^0_{12} = \frac{L}{R}\sqrt{\frac{D_{22}}{D_{11}}}2\left(\frac{2a_{12}+a_{66}}{2\sqrt{a_{11}a_{22}}} - \frac{a_{12}}{\sqrt{a_{11}a_{22}}}\right)\mathcal{N}_{12} \tag{3.38}$$

The above equation can be expressed with the help of three nondimensional parameters as defined by Nemeth [125]: ν_m which has already been defined in Eq. (3.36), and two new ones: α_b, and μ:

$$\alpha_b = \frac{R}{L}\sqrt[4]{\frac{D_{11}}{D_{22}}} \tag{3.39}$$

$$\mu = \frac{2a_{12}+a_{66}}{2\sqrt{a_{11}a_{22}}} \tag{3.40}$$

The parameters α_m defined in Eq. (3.35)) and α_b defined in Eq. (3.39) are called the stiffness weighted geometry parameters, because they relate the geometry of the shell: the radius and the length, with the stiffness of the composite laminate. The membrane orthotropy parameter, μ defined in Eq. (3.40)) and membrane Poisson ratio, ν_m defined in Eq. (3.36) relate to the membrane compliance and are mostly dependent on the material properties and facesheet layup.

If the nondimensional parameters defined in Eqs. (3.35), (3.36), (3.39) and (3.40) are included in the in-plane relations from Eqs. (3.33), (3.34) and (3.38) a more compact formulation can be expressed:

$$\begin{bmatrix} E^0_{11} \\ E^0_{22} \\ \Gamma^0_{12} \end{bmatrix} = \begin{bmatrix} \frac{1}{\alpha_m^2} & -\nu_m & 0 \\ -\nu_m & \alpha_m^2 & 0 \\ 0 & 0 & \frac{2(\mu+\nu_m)}{\alpha_b} \end{bmatrix} \begin{bmatrix} \mathcal{N}_{11} \\ \mathcal{N}_{22} \\ \mathcal{N}_{12} \end{bmatrix} \tag{3.41}$$

Under the current assumptions, the bend-twist anisotropy is treated as negligible. This means that even if the value is not zero, the influence of the bend-twist terms compared to other bending terms is considered small. This assumption might not be valid for all laminates especially for cases where the facesheets have a low ply number. Under this assumption, the moment per unit length resultants are defined as:

$$M_x = -\left(D_{11}\frac{\partial \beta_x}{\partial x} + D_{12}\frac{\partial \beta_y}{\partial y}\right) \tag{3.42}$$

$$M_y = -\left(D_{12}\frac{\partial \beta_x}{\partial x} + D_{22}\frac{\partial \beta_y}{\partial y}\right) \tag{3.43}$$

$$M_{xy} = -D_{66}\left(\frac{\partial \beta_y}{\partial x} + \frac{\partial \beta_x}{\partial y}\right) \tag{3.44}$$

In a similar way to the nondimensional force resultants described in Eqs. (3.30) to (3.32), the nondimensional moment resultants are introduced as follows:

$$\mathscr{M}_{11} = \frac{R^2}{\sqrt[4]{a_{11}a_{22}D_{11}^3D_{22}^3}}M_x \tag{3.45}$$

$$\mathscr{M}_{22} = \frac{L^2}{\sqrt[4]{a_{11}a_{22}D_{11}^3D_{22}^3}}M_y \tag{3.46}$$

$$\mathscr{M}_{12} = \frac{RL}{\sqrt[4]{a_{11}a_{22}D_{11}^3D_{22}^3}}M_{xy} \tag{3.47}$$

Combining the moment equations shown in Eqs. (3.42) and (3.43) with the definitions of the nondimensional change of slope to the normal of the undeformed midsurface described in Eqs. (3.12) and (3.13) and nondimensional moments from Eqs. (3.45) to (3.47) the following relations are obtained:

$$\mathscr{M}_{11} = -\frac{R^2}{L^2}\sqrt{\frac{D_{11}}{D_{22}}}\frac{\partial B_1}{\partial z_1} - \frac{D_{12}}{\sqrt{D_{11}D_{22}}}\frac{\partial B_2}{\partial z_2} \tag{3.48}$$

$$\mathscr{M}_{22} = -\frac{R^2}{L^2}\sqrt{\frac{D_{11}}{D_{22}}}\frac{\partial B_2}{\partial z_2} - \frac{D_{12}}{\sqrt{D_{11}D_{22}}}\frac{\partial B_1}{\partial z_1} \tag{3.49}$$

In these relations, two terms appear that can be expressed through the nondimensional parameters α_b and ν_b as introduced by Nemeth [125]. The parameter α_b, used in

the in-plane relations, is already defined in Eq. (3.39) and the parameter ν_b is expressed as:

$$\nu_b = \frac{D_{12}}{\sqrt{D_{11}D_{22}}} \tag{3.50}$$

The nondimensional parameter, ν_b, similarly to ν_m from Eq. (3.36), is called the flexural Poisson ratio and relates the bending stiffness terms of the sandwich composite.

If the moment equation Eq. (3.44) and the expression of nondimensional moment Eq. (3.47) are taken in combination with the definitions of the nondimensional change of slope to the normal of the undeformed mid-surface described in Eqs. (3.12) and (3.13), the following relation is obtained:

$$\mathscr{M}_{12} = -\frac{D_{66}}{\sqrt[4]{D_{11}D_{22}}}\left(\frac{\partial B_2}{\partial z_1} + \frac{\partial B_1}{\partial z_2}\right) \tag{3.51}$$

Manipulating this equation, it can be obtained that it is equivalent to:

$$\mathscr{M}_{12} = -\frac{1}{2}\left(\frac{D_{12}+2D_{66}}{\sqrt{D_{11}D_{22}}} + \frac{D_{12}}{\sqrt{D_{11}D_{22}}}\right)\left(\frac{\partial B_2}{\partial z_1} + \frac{\partial B_1}{\partial z_2}\right) \tag{3.52}$$

In this expression, two parameters can be extracted. On the one hand, the flexural Poisson ratio, ν_b described in Eq. (3.50). On the other hand, the flexural orthotropy parameter, β, defined as:

$$\beta = \frac{D_{12}+2D_{66}}{\sqrt{D_{11}D_{22}}} \tag{3.53}$$

The flexural orthotropy parameter β is analogous to the membrane orthotropy parameter μ defined in Eq. (3.40). It describes the interaction between the terms of the bending stiffness matrix and as such is highly dependent on the facesheet layup and material properties. The dependence on the core thickness is low because it affects similarly the terms on the numerator and denominator. This is particularly valuable to study separately the influence of the thickness and the influence of the material properties.

If the nondimensional parameters are included in the moment expressions defined in Eqs. (3.48), (3.49) and (3.52) the result is:

$$\begin{bmatrix} \mathscr{M}_{11} \\ \mathscr{M}_{22} \\ \mathscr{M}_{12} \end{bmatrix} = -\begin{bmatrix} \alpha_b^2 & \nu_b & 0 \\ \nu_b & \dfrac{1}{\alpha_b^2} & 0 \\ 0 & 0 & \dfrac{(\beta-\nu_b)}{2} \end{bmatrix} \begin{bmatrix} \dfrac{\partial B_1}{\partial z_1} \\ \dfrac{\partial B_2}{\partial z_2} \\ \dfrac{\partial B_2}{\partial z_1} + \dfrac{\partial B_1}{\partial z_2} \end{bmatrix} \tag{3.54}$$

Finally, the transverse shear stress resultants Q_x and Q_y can be expressed under the current model assumptions as:

$$Q_x = G_x h\left(\frac{\partial w}{\partial x} - \beta_x\right) \tag{3.55}$$

$$Q_y = G_y h\left(\frac{\partial w}{\partial y} - \beta_y\right) \tag{3.56}$$

In the nondimensional form, following a similar procedure as with the force and moment resultants, the transverse shear force resultants $\mathcal{Q}_{11}$ and $\mathcal{Q}_{22}$ are defined as:

$$\mathcal{Q}_{11} = \frac{LR^2}{\sqrt[4]{a_{11}a_{22}D_{11}^3D_{22}^3}}Q_x \tag{3.57}$$

$$\mathcal{Q}_{22} = \frac{L^2R}{\sqrt[4]{a_{11}a_{22}D_{11}^3D_{22}^3}}Q_y \tag{3.58}$$

Combining the transverse shear force resultant definition Eqs. (3.55) to (3.58) and the slope components Eqs. (3.12) and (3.13), the corresponding constitutive equations for the transverse shear force resultants in nondimensional form are obtained:

$$\mathcal{Q}_{11} = \frac{G_x hR^2}{\sqrt{D_{11}D_{22}}}\left(\frac{\partial W}{\partial z_1} - B_1\right) \tag{3.59}$$

$$\mathcal{Q}_{22} = \frac{G_y hL^2}{\sqrt{D_{11}D_{22}}}\left(\frac{\partial W}{\partial z_2} - B_2\right) \tag{3.60}$$

From this expressions, two clear terms emerge and thus two new nondimensional parameters can be defined as:

$$\chi_1 = \frac{G_x hR^2}{\sqrt{D_{11}D_{22}}} \tag{3.61}$$

$$\chi_2 = \frac{G_y hL^2}{\sqrt{D_{11}D_{22}}} \tag{3.62}$$

The nondimensional parameters χ_1 and χ_2 were not part of the nondimensionalization proposed by Nemeth [125]. The objective of the two new nondimensional parameters is to represent the influence of the core shear properties with respect to the sandwich bending stiffness and the geometry properties of the shell. The influence of

these parameters will give an indication of the importance of the transverse shear in the buckling loads of the shell.

Instead of considering χ_1 and χ_2 separately, a transverse ratio ϕ is defined:

$$\phi = \frac{\chi_2}{\chi_1} = \frac{G_y}{G_x}\left(\frac{L}{R}\right)^2 \tag{3.63}$$

This is a more convenient way of studying the problem since the properties of the core G_x and G_y are not independent from each other and must be considered together. The parameter ϕ also presents an advantage for cases with isotropic core materials, where the transverse ratio ϕ depends only on the geometry of the shell, as $G_x = G_y$.

With the inclusion of the χ_1 and χ_2 the transverse shear force resultants are:

$$\begin{bmatrix} \mathscr{Q}_{11} \\ \mathscr{Q}_{22} \end{bmatrix} = \begin{bmatrix} \chi_1 & 0 \\ 0 & \phi\chi_1 \end{bmatrix} \begin{bmatrix} \dfrac{\partial W}{\partial z_1} - B_1 \\ \dfrac{\partial W}{\partial z_2} - B_2 \end{bmatrix} \tag{3.64}$$

3.2.3. EQUILIBRIUM EQUATIONS

Assuming that the transverse normal stiffness of the sandwich shell is infinite, and considering the nondimensional formulation presented so far, the nondimensional equilibrium equations of forces and moments for a thin cylindrical shell are:

$$\frac{\partial \mathscr{N}_{11}}{\partial z_1} + \frac{1}{\alpha_b}\frac{\partial \mathscr{N}_{12}}{\partial z_2} = 0 \tag{3.65}$$

$$\frac{1}{\alpha_b}\frac{\partial \mathscr{N}_{12}}{\partial z_1} + \frac{\partial \mathscr{N}_{22}}{\partial z_2} = 0 \tag{3.66}$$

$$\frac{\partial \mathscr{Q}_1}{\partial z_1} + \frac{\partial \mathscr{Q}_2}{\partial z_2} + \mathscr{N}_{11}\frac{\partial^2 W}{\partial z_1^2} + \frac{2}{\alpha_b}\mathscr{N}_{12}\frac{\partial^2 W}{\partial z_1 \partial z_2} + \mathscr{N}_{22}\left(\frac{\partial^2 W}{\partial z_2^2} - \sqrt{12}Z\right) = 0 \tag{3.67}$$

$$\mathscr{Q}_{11} = \frac{\partial \mathscr{M}_{11}}{\partial z_1} + \frac{\partial \mathscr{M}_{12}}{\partial z_2} \tag{3.68}$$

$$\mathscr{Q}_{22} = \frac{\partial \mathscr{M}_{22}}{\partial z_2} + \frac{\partial \mathscr{M}_{12}}{\partial z_1} \tag{3.69}$$

The first two equations of equilibrium, Eqs. (3.65) and (3.66), are satisfied introducing the stress function $F(z_1, z_2)$ defined as:

$$\mathcal{N}_{11} = \frac{\partial^2 F}{\partial z_2^2} \tag{3.70}$$

$$\mathcal{N}_{22} = \frac{\partial^2 F}{\partial z_1^2} \tag{3.71}$$

$$\frac{\mathcal{N}_{12}}{\alpha_b} = -\frac{\partial^2 F}{\partial z_1 \partial z_2} \tag{3.72}$$

If equilibrium equations as expressed via the stress function F in Eqs. (3.70) to (3.72) are substituted in the third equilibrium equation Eq. (3.67), it yields:

$$\begin{aligned} &\frac{\partial^2 \mathcal{M}_{11}}{\partial z_1^2} + 2\frac{\partial^2 \mathcal{M}_{12}}{\partial z_1 \partial z_1} + \frac{\partial^2 \mathcal{M}_{22}}{\partial z_2^2} \\ &+ \frac{\partial^2 F}{\partial z_2^2}\frac{\partial^2 W}{\partial z_1^2} - 2\frac{\partial^2 F}{\partial z_1 \partial z_2}\frac{\partial^2 W}{\partial z_1 \partial z_2} + \frac{\partial^2 F}{\partial z_1^2}\left(\frac{\partial^2 W}{\partial z_2^2} - \sqrt{12}Z\right) = 0 \end{aligned} \tag{3.73}$$

If the moment expressions as defined in Eqs. (3.45) to (3.47) are introduced in Eq. (3.73), it yields:

$$\begin{aligned} &-\alpha_b^2\frac{\partial^3 B_1}{\partial z_1^3} - \beta\frac{\partial^3 B_1}{\partial z_1 \partial z_2^2} - \frac{1}{\alpha_b^2}\frac{\partial^3 B_2}{\partial z_2^3} - \beta\frac{\partial^3 B_1}{\partial z_1^2 \partial z_2} \\ &= -\frac{\partial^2 F}{\partial z_2^2}\frac{\partial^2 W}{\partial z_1^2} + 2\frac{\partial^2 F}{\partial z_1 \partial z_2}\frac{\partial^2 W}{\partial z_1 \partial z_2} - \frac{\partial^2 F}{\partial z_1^2}\left(\frac{\partial^2 W}{\partial z_2^2} - \sqrt{12}Z\right) \end{aligned} \tag{3.74}$$

Finally, if the moment expressions Eq. (3.54) and the transverse force expressions Eq. (3.64) are used in the moment equilibrium equations in Eqs. (3.68) and (3.69), the following relations are obtained:

$$\chi_1 B_1 - \alpha_b^2\frac{\partial^2 B_1}{\partial z_1^2} + \frac{1}{2}(\beta - \nu_b)\frac{\partial^2 B_1}{\partial z_2^2} - \frac{1}{2}(\beta + \nu_b)\frac{\partial^2 B_2}{\partial z_1 \partial z_2} = \chi_1\frac{\partial W}{\partial z_1} \tag{3.75}$$

$$\chi_2 B_2 - \frac{1}{\alpha_b^2}\frac{\partial^2 B_2}{\partial z_2^2} + \frac{1}{2}(\beta - \nu_b)\frac{\partial^2 B_2}{\partial z_1^2} - \frac{1}{2}(\beta + \nu_b)\frac{\partial^2 B_1}{\partial z_1 \partial z_2} = \chi_2\frac{\partial W}{\partial z_2} \tag{3.76}$$

The nondimensional equilibrium equations are represented in Eqs. (3.75) and (3.76) with the nondimensional transverse shear parameters highlighted.

3.2.4. COMPATIBILITY EQUATIONS

The compatibility equation restricts how the strains can vary over the shell so that a continuous displacement field could be found for the assumed strain field. The out of plane displacement variation, w, in terms of the mid-surface strains ϵ_x^0, ϵ_y^0 and γ_{xy}^0 is:

$$\frac{\partial^2 \epsilon_x^0}{\partial y^2} + \frac{\partial^2 \epsilon_y^0}{\partial x^2} - \frac{\partial^2 \gamma_{xy}^0}{\partial x y} = \frac{1}{R}\frac{\partial^2 w}{\partial x^2} + \left(\frac{\partial^2 w}{\partial y^2}\right)^2 - \frac{\partial^2 w}{\partial x^2}\frac{\partial^2 w}{\partial y^2} \tag{3.77}$$

Introducing the nondimensional mid-surface strains as described in Eqs. (3.21) to (3.23), the derivatives of the nondimensional out-of-plane displacement as defined in the Eq. (3.6), and the Batdorf-Stein parameter from Eq. (3.19), the Eq. (3.77) is converted into the following nondimensional compatibility equation.

$$\frac{\partial^2 E_{11}^0}{\partial z_2^2} + \frac{\partial^2 E_{22}^0}{\partial z_1^2} - \frac{\partial^2 \Gamma_{12}^0}{\partial z_1 z_2} = \sqrt{12} Z \frac{\partial^2 W}{\partial z_1^2} + \frac{L^2}{R^2}\left(\frac{\partial^2 W}{\partial z_2^2}\right)^2 - \frac{\partial^2 W}{\partial z_1^2}\frac{\partial^2 W}{\partial z_2^2} \tag{3.78}$$

Introducing the constitutive equations Eq. (3.41) and the described stress function F Eqs. (3.70) to (3.72) the nondimensional compatibility equation becomes:

$$\alpha_m^2 \frac{\partial^4 F}{\partial z_1^4} + \frac{1}{\alpha_m^2}\frac{\partial^4 F}{\partial z_2^4} + 2\mu \frac{\partial^4 F}{\partial z_1^2 \partial z_2^2} = \sqrt{12} Z \frac{\partial^2 W}{\partial z_1^2} + \frac{L^2}{R^2}\left(\frac{\partial^2 W}{\partial z_2^2}\right)^2 - \frac{\partial^2 W}{\partial z_1^2}\frac{\partial^2 W}{\partial z_2^2} \tag{3.79}$$

3.3. LINEARIZED BUCKLING EQUATIONS

THE linearized equations for the determination of the critical buckling load at the bifurcation point can be derived by the application of the adjacent equilibrium criterion [100]. To investigate the existence of adjacent equilibrium configurations, it is assumed that the following variables W, F, B_1 and B_2 are given by:

$$W = \bar{W} + \hat{W} \tag{3.80}$$

$$F = \bar{F} + \hat{F} \tag{3.81}$$

$$B_1 = \bar{B}_1 + \hat{B}_1 \tag{3.82}$$

$$B_2 = \bar{B}_2 + \hat{B}_2 \tag{3.83}$$

where $\bar{W}$, $\bar{F}$, $\bar{B}_1$ and $\bar{B}_2$ represent the prebuckling solutions along the fundamental path and $\hat{W}$, $\hat{F}$, $\hat{B}_1$ and $\hat{B}_2$ represent small perturbations at buckling. Assuming the shell is

sufficiently long, the prebuckling displacement $\bar{W}$ and the prebuckling slope $\bar{B}_1$ and $\bar{B}_2$ are considered constant. This means that previous to the buckling event, both the out-of-plane displacement and the slopes are independent of the spatial coordinates z_1 and z_2.

The scope of this study is limited to shells under only axial compression to investigate the influence of the transverse shear on the axial buckling load, P. However, the nondimensionalisation until here can be utilized for other load cases. The equations are to be solved for a value of the nondimensional buckling force. In the case of axial compression, the nondimensional buckling force, $\mathscr{F}$, expresses the buckling load P related to the bending stiffness of the shell and the cylindrical shell radius:

$$\mathscr{F} = -P\frac{R}{2\pi\sqrt{D_{11}D_{22}}} \tag{3.84}$$

The prebuckling force component in the axial direction, $\bar{\mathscr{N}}_{11}$, as defined in Eq. (3.70), represents the nondimensional axial buckling force, $\mathscr{F}$, as shown in Eq. (3.84). If only an axial load is considered, and deeming the expression of the stress function as defined in Eqs. (3.71) and (3.72), the prebuckling force components $\bar{\mathscr{N}}_{22}$ and $\bar{\mathscr{N}}_{12}$ are equal to zero.

$$\bar{\mathscr{N}}_{11} = \frac{\partial^2 \bar{F}}{\partial z_2^2} = \mathscr{F} \tag{3.85}$$

$$\bar{\mathscr{N}}_{22} = \frac{\partial^2 \bar{F}}{\partial z_1^2} = \frac{\bar{\mathscr{N}}_{12}}{\alpha_b} = -\frac{\partial^2 \bar{F}}{\partial z_1 \partial z_2} = 0 \tag{3.86}$$

Combining all the presented derivations shown in Eqs. (3.74) to (3.76), (3.79) to (3.83), (3.85) and (3.86) the following linearized buckling equations are obtained:

$$\alpha_b^2\frac{\partial^3 \hat{B}_1}{\partial z_1^3} + \beta\frac{\partial^3 \hat{B}_1}{\partial z_1 \partial z_2^2} + \frac{1}{\alpha_b^2}\frac{\partial^3 \hat{B}_2}{\partial z_2^3} + \beta\frac{\partial^3 \hat{B}_2}{\partial z_1^2 \partial z_2} = \mathscr{F}\frac{\partial^2 \hat{W}}{\partial z_1^2} - \sqrt{12}Z\frac{\partial^2 \hat{F}}{\partial z_1^2} \tag{3.87}$$

$$\alpha_m^2\frac{\partial^4 \hat{F}}{\partial z_1^4} + \frac{1}{\alpha_m^2}\frac{\partial^4 \hat{F}}{\partial z_2^4} + 2\mu\frac{\partial^4 \hat{F}}{\partial z_1^2 \partial z_2^2} = \sqrt{12}Z\frac{\partial^2 \hat{W}}{\partial z_1^2} \tag{3.88}$$

$$\chi_1\hat{B}_1 - \alpha_b^2\frac{\partial^2 \hat{B}_1}{\partial z_1^2} + \frac{1}{2}(\beta - \nu_b)\frac{\partial^2 \hat{B}_1}{\partial z_2^2} - \frac{1}{2}(\beta + \nu_b)\frac{\partial^2 \hat{B}_2}{\partial z_1 \partial z_2} = \chi_1\frac{\partial \hat{W}}{\partial z_1} \tag{3.89}$$

$$\chi_2\hat{B}_2 - \frac{1}{\alpha_b^2}\frac{\partial^2 \hat{B}_2}{\partial z_2^2} + \frac{1}{2}(\beta - \nu_b)\frac{\partial^2 \hat{B}_2}{\partial z_1^2} - \frac{1}{2}(\beta + \nu_b)\frac{\partial^2 \hat{B}_1}{\partial z_1 \partial z_2} = \chi_2\frac{\partial \hat{W}}{\partial z_2} \tag{3.90}$$

For simplicity, Eqs. (3.89) and (3.90) can be also expressed as follows:

$$\hat{B}_1 - \frac{\alpha_b^2}{\chi_1}\frac{\partial^2 \hat{B}_1}{\partial z_1^2} + \frac{1}{2\chi_1}(\beta - \nu_b)\frac{\partial^2 \hat{B}_1}{\partial z_2^2} - \frac{1}{2\chi_1}(\beta + \nu_b)\frac{\partial^2 \hat{B}_2}{\partial z_1 \partial z_2} = \frac{\partial \hat{W}}{\partial z_1} \tag{3.91}$$

$$\hat{B}_2 - \frac{1}{\chi_2 \alpha_b^2}\frac{\partial^2 \hat{B}_2}{\partial z_2^2} + \frac{1}{2\chi_2}(\beta - \nu_b)\frac{\partial^2 \hat{B}_2}{\partial z_1^2} - \frac{1}{2\chi_2}(\beta + \nu_b)\frac{\partial^2 \hat{B}_1}{\partial z_1 \partial z_2} = \frac{\partial \hat{W}}{\partial z_2} \tag{3.92}$$

Recalling that for simply supported boundary conditions: $\hat{W} = \partial^2 \hat{W}/\partial z_1^2 = 0$ at $z_1 = [0, 1]$; then these equations admit separable solutions of the form:

$$\hat{W} = A \sin(m\pi z_1)\sin(n z_2) \tag{3.93}$$

$$\hat{F} = B \sin(m\pi z_1)\sin(n z_2) \tag{3.94}$$

$$\hat{B}_1 = C \cos(m\pi z_1)\sin(n z_2) \tag{3.95}$$

$$\hat{B}_2 = D \sin(m\pi z_1)\cos(n z_2) \tag{3.96}$$

The non-dimensional buckling load $\mathscr{F}$, which is the desired solution of the derived equations, is obtained by solving the eigenvalue problem. The value is found for the combination of coefficients m and n that gives the lowest non-dimensional buckling load value. These values represent the buckling mode of the shell. The value of m is associated with the number of half-waves in the longitudinal direction, while the value of n is the value associated with the number of waves in the circumferential direction. In the case of an axisymmetric solution, the value of n is equal to 1.

To analyze the effect of the transverse shear, the equations without taking it into account are also considered. In this case, the transverse shear strains, ϵ_{xz}, ϵ_{yz} from Eqs. (3.10) and (3.11), or as defined in their nondimensional form Γ_{13}, Γ_{23} in Eqs. (3.17) and (3.18), are negligible compared to other strain components and, therefore:

$$B_1 = \frac{\partial W}{\partial z_1} \tag{3.97}$$

$$B_2 = \frac{\partial W}{\partial z_2} \tag{3.98}$$

This consideration simplifies some of the equations and reduces the number of variables to only the nondimensional out-of-plane displacement, W, and the nondimen-

sional stress function, F. The constitutive equation Eq. (3.54) becomes:

$$\begin{bmatrix} \mathscr{M}_{11} \\ \mathscr{M}_{22} \\ \mathscr{M}_{12} \end{bmatrix} = \begin{bmatrix} \alpha_b^2 & -\nu_b & 0 \\ -\nu_b & \dfrac{1}{\alpha_b^2} & 0 \\ 0 & 0 & \beta - \nu_b \end{bmatrix} \begin{bmatrix} \dfrac{\partial^2 W}{\partial z_1^2} \\ \dfrac{\partial^2 W}{\partial z_2^2} \\ \dfrac{\partial^2 W}{\partial z_1 \partial z_2} \end{bmatrix} \tag{3.99}$$

Therefore the equilibrium equation described in Eq. (3.73) becomes:

$$\begin{aligned} \alpha_b^2 \frac{\partial^4 W}{\partial z_1^4} + 2\beta \frac{\partial^4 W}{\partial z_1^2 \partial z_2^2} + \frac{1}{\alpha_b^2} \frac{\partial^4 W}{\partial z_2^4} \\ + \frac{\partial^2 F}{\partial z_2^2} \frac{\partial^2 W}{\partial z_1^2} - 2 \frac{\partial^2 F}{\partial z_1 \partial z_2} \frac{\partial^2 W}{\partial z_1 \partial z_2} + \frac{\partial^2 F}{\partial z_1^2} \left(\frac{\partial^2 W}{\partial z_2^2} - \sqrt{12} Z \right) = 0 \end{aligned} \tag{3.100}$$

The axial buckling load in this particular case is denotated as P_0 to differentiate it with the complete formulation with transverse shear. The nondimensional buckling force without transverse shear, $\mathscr{F}_0$, is thus defined in analogous way as the buckling load with transverse shear, $\mathscr{F}$, seen in Eqs. (3.84) and (3.85).

$$\bar{\mathscr{N}}_{11} = \frac{\partial^2 \bar{F}}{\partial z_2^2} = \mathscr{F}_0 = -P_0 \frac{R}{2\pi \sqrt{D_{11} D_{22}}} \tag{3.101}$$

The criterion is applied as described in Eqs. (3.80) and (3.81), where $\bar{W}$ and $\bar{F}$ represent the prebuckling solutions along the fundamental path and, $\hat{W}$ and $\hat{F}$, represent small perturbations at buckling. Considering that the initial prebuckling displacement, $\bar{W}$, is constant, the linearized buckling equations in this case become:

$$\alpha_b^2 \frac{\partial^4 \hat{W}}{\partial z_1^4} + 2\beta \frac{\partial^4 \hat{W}}{\partial z_1^2 \partial z_2^2} + \frac{1}{\alpha_b^2} \frac{\partial^4 \hat{W}}{\partial z_2^4} = \mathscr{F}_0 \frac{\partial^2 \hat{W}}{\partial z_1^2} - \sqrt{12} Z \frac{\partial^2 \hat{F}}{\partial z_1^2} \tag{3.102}$$

$$\alpha_m^2 \frac{\partial^4 \hat{F}}{\partial z_1^4} + \frac{1}{\alpha_m^2} \frac{\partial^4 \hat{F}}{\partial z_2^4} + 2\mu \frac{\partial^4 \hat{F}}{\partial z_1^2 \partial z_2^2} = \sqrt{12} Z \frac{\partial^2 \hat{W}}{\partial z_1^2} \tag{3.103}$$

These linearized equations were also described by Nemeth and Schultz [125] as the linearized governing equations for laminate configurations. Assuming again simply supported boundary conditions ($\hat{W} = \partial^2 \hat{W} / \partial z_1^2 = 0$ at $z_1 = [0, 1]$), and separable solutions defined in Eqs. (3.93) and (3.94), an eigenvalue problem can be solved to determine the nondimensional buckling load. The value is found for the combination of m and

n coefficients that gives the lowest nondimensional buckling load value, $\mathscr{F}_0$. The values of m and n describe the buckling mode of the shell, since they represent the number halfwaves in the longitudinal direction and the waves in the circumferential direction respectively.

Upon inspection of the linearized equations with and without transverse shear, the influence of χ_1 and χ_2 is revealed as the main difference between them. In the case where these nondimensional parameters have large values, Eqs. (3.89) and (3.90) become:

$$\hat{B}_1 = \frac{\partial \hat{W}}{\partial z_1} \tag{3.104}$$

$$\hat{B}_2 = \frac{\partial \hat{W}}{\partial z_2} \tag{3.105}$$

The remaining governing equations Eqs. (3.87) and (3.88) are as represented in Eqs. (3.102) and (3.103).

The values of χ_1 and χ_2, as defined in Eqs. (3.61) and (3.62), represent the influence of the transverse shear effects of the core. In the cases where the values of χ_1 and χ_2 are large, it indicates that the core material is very stiff and thus the influence of the transverse shear effects is negligible. In this case, the value of the nondimensional buckling load, with $\mathscr{F}$ and without $\mathscr{F}_0$ transverse shear effects will be the same.

This nondimensional formulation of the shell can be amended to include imperfections. When the imperfections are included the eigenvalue solution described here is no longer applicable.

3.4. DESIGN SPACE ANALYSIS VIA NONDIMENSIONAL PARAMETERS

BUILDING on the framework established in the previous section, and to demonstrate how nondimensional parameters can enhance the understanding of sandwich composite buckling behavior, various shell configurations are compared.

The goal is threefold. First, it highlights how cylindrical shells with different materials and dimensions can exhibit similar buckling behavior. Second, it shows how to effectively navigate the design space of sandwich composite shells, identifying the parameters that have the greatest influence on the buckling response. And third, it examines cases where the inclusion of transverse shear is necessary, thus requiring the use of the more complete formulation.

The dimensions of the shells, the facesheet laminate, core thickness and modulus are reported in Table 3.1. For all shell, the facesheets are made of the same carbon fiber material, with the properties: $E_x = 150GPa$, $E_y = 10GPa$, $G_{xy} = 6GPa$, $\nu_{xy} = 0.3$ and $t_f = 0.131mm$.

Table 3.1: Properties of the shells.

Properties	Shell 1	Shell 2	Shell 3	Shell 4	Shell 5	Shell 6
Radius, R [mm]	400	1400	400	400	400	400
Length, L [mm]	800	2800	800	800	800	1600
Facesheet laminate [°]	$(\pm 45)_s$	$(\pm 45)_{s2}$	$(\pm 45)_s$	$(\pm 45)_s$	$(\pm 45)_s$	$(\pm 45)_s$
Core thickness, t_{core} [mm]	2.5	10	2.5	1	1	2.5
Core shear modulus, G [MPa]	120	70	360	120	70	120

The nondimensional parameters α_m,α_b, μ, β, ν_b, Z, χ_1 and ϕ of the analyzed shells are reported in Table 3.2 together with the obtained nondimensional force with transverse shear $\mathscr{F}$, without transverse shear $\mathscr{F}_0$ and the ratio between them $\mathscr{F}/\mathscr{F}_0$.

Table 3.2: Nondimensional parameters of the shells.

Parameter	Shell 1	Shell 2	Shell 3	Shell 4	Shell 5	Shell 6
α_m	0.5	0.5	0.5	0.5	0.5	0.25
α_b	0.5	0.5	0.5	0.5	0.5	0.25
μ	-0.5	-0.5	-0.5	-0.5	-0.5	-0.5
β	2.4	2.4	2.4	2.4	2.4	2.4
ν_b	0.75	0.75	0.75	0.75	0.75	0.75
Z	50	50	50	100	100	50
χ_1	500	500	1500	970	570	500
ϕ	4	4	4	4	4	16
$\mathscr{F}$	294	294	341	567	478	293
$\mathscr{F}_0$	361	361	366	692	692	359
$\mathscr{F}/\mathscr{F}_0$	0.81	0.81	0.93	0.82	0.69	0.81

To demonstrate how nondimensional results are applicable to different shells of dif-

ferent scales, Shell 1 and Shell 2 are compared and their differences and similarities highlighted. Shell 2 is 3.5 times larger than Shell 1, and in both cases the length is double the radius. The laminate of the facesheet of Shell 1 is $(\pm 45°)_s$ with 4 plies, whereas the laminate of the facesheet in Shell 2 is $(\pm 45°)_{s2}$ with 8 plies. The core material, isotropic in both shells, is Rohacell 200 for Shell 1 and Rohacell 110 for Shell 2. The relevant difference between these materials is the shear moduli, G, as shown in Table 3.1. The thickness of the core of the two shells is also different.

In spite of these shells being of different scales, the set of nondimensional parameters that rule the nondimensional linearized equations is the same, as shown in Table 3.2. As a result, both the nondimensional force with transverse shear and without transverse shear are the same in both shells. Therefore, the ratio between both nondimensional buckling forces $\mathscr{F}/\mathscr{F}_0 = 0.81$ is the same as well.

In order to examine how the change in the different parameters affects the relation $\mathscr{F}/\mathscr{F}_0$ and explain how to navigate the design space of sandwich composite shells with the help of nondimensional parameters, another shell is considered, named Shell 3 as described in Table 3.1. This shell has the same geometry, both radius and length, as Shell 1. The Shell 3 facesheets are made of the same carbon fiber material as the Shell 1, the layup is also $(\pm 45°)_s$, and the core thickness is also 2.5 mm. The only difference between Shell 3 and Shell 1 is the type of core material, which in this case is Rohacell 300, which is an isotropic foam $G = 360$ MPa that is stiffer than the foam used in Shell 1.

The set of nondimensional parameters for Shell 1 and Shell 3 is the same except for the value of χ_1. In order to analyze the differences and study the trends, in Fig. 3.3 it is shown how the transverse shear buckling load ratio, $\mathscr{F}/\mathscr{F}_0$, is influenced by the nondimensional transverse shear χ_1 for the sandwich shell with the Batdorf-Stein parameter $Z = 50$.

Fig. 3.3 and Table 3.2 indicate that as the nondimensional transverse shear parameter χ_1 increases, the difference between the buckling loads with and without accounting for transverse shear becomes smaller. This suggests that higher values of χ_1 improve the accuracy of the buckling load prediction when transverse shear effects are not considered.

The curve in Fig. 3.3 is nonlinear and shows a steep increase for the values of χ_1 under 500. For the values over 500, the curve increase is more gradual. In the range depicted in Fig. 3.3, the curve also does not reach the value 1. This indicates that for this range of sandwich cylindrical shells, the transverse shear effects are not entirely negligible, inducing an error of at least 5% in the buckling load.

For the shells considered, as can be seen in Fig. 3.3, Shell 1 has a higher influence on the transverse shear in the solution $\mathscr{F}/\mathscr{F}_0 = 0.81$, than Shell 3 $\mathscr{F}/\mathscr{F}_0 = 0.93$. This is due to the fact that a stiffer core leads to a decrease in the influence of the transverse shear strains with respect to the rest of the strain components.

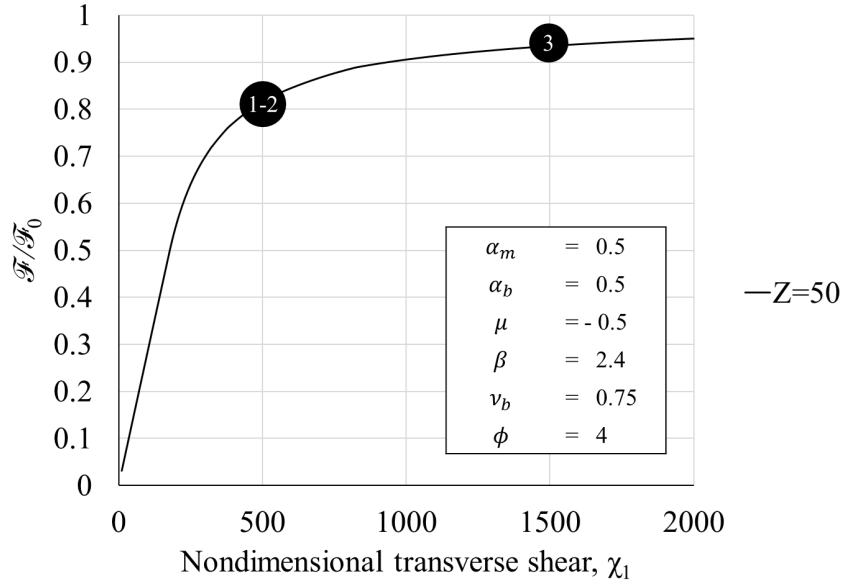

Figure 3.3: Effect of core shear parameter χ_1 on the transverse shear buckling load ratio $\mathscr{F}/\mathscr{F}_0$ for $Z = 50$, where the numbers in black are the shell numbers.

Shell 4 is now considered, where the geometry and facesheet laminate properties are the same as Shell 1 as seen Table 3.1. Regarding the core, Shell 4 has the same material as Shell 1 $G = 120MPa$, but the thickness of the core is reduced to only $1mm$. This case is a limit case because it goes close to infringing one of the assumptions of the methodology described in Section 3.1, that is, the core must be much thicker than the facesheet. In this case, the core is still double the thickness of the facesheet, so it is assumed that the method is still valid. Most nondimensional parameters remain the same as shown in Table 3.2, except the transverse shear parameter $\chi_1 = 970$ and the Batdorf-Stein parameter $Z = 100$.

Fig. 3.4 shows for a sandwich shell with Batdorf-Stein parameters $Z = 50$ and $Z = 100$ how the transverse shear buckling load ratio is influenced by the nondimensional transverse shear χ_1. This is important because a variation in the shell that produces a change in the value of Z (i.e. core thickness) also produces a change in the value of χ_1. A change in core thickness from 2.5 mm for Shell 1 to 1 mm in Shell 4 changes both parameters χ_1 and Z such that the influence is not easy to discern. In this particular scenario, the change in thickness does not produce a significant change in the influence of the transverse shear, going from $\mathscr{F}/\mathscr{F}_0 = 0.81$ for Shell 1 to $\mathscr{F}/\mathscr{F}_0 = 0.82$ for Shell 4.

Although the difference in the influence of the transverse shear remains similar, the buckling response of Shell 1 and Shell 4 is very different, as noted in the values of the nondimensional buckling load ranging from $\mathscr{F} = 294$ in Shell 1 to $\mathscr{F} = 567$ in Shell 4.

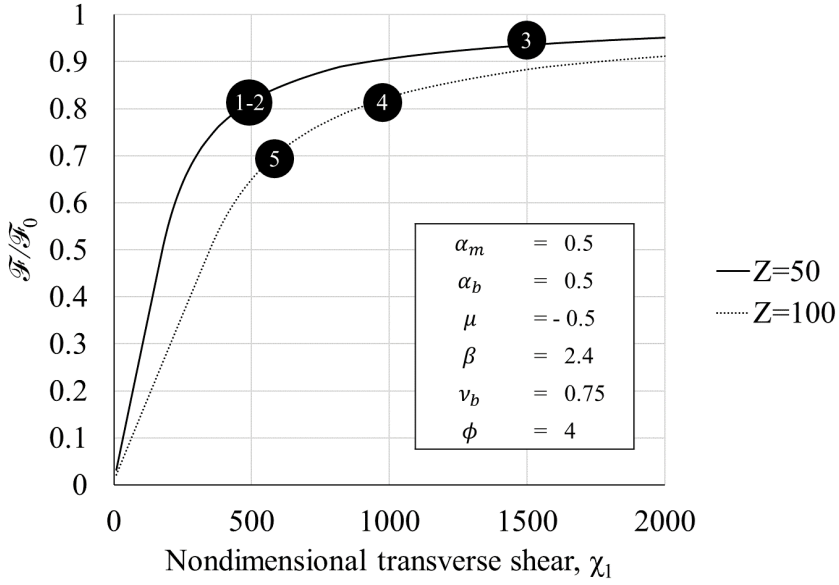

Figure 3.4: Effect of core shear parameter χ_1 on the transverse shear buckling load ratio $\mathscr{F}/\mathscr{F}_0$ for $Z = 50$ and $Z = 100$, where the numbers in black are the shell numbers.

Therefore the ratio $\mathscr{F}/\mathscr{F}_0$ is only an indication of the relevance of the transverse shear and not of the overall buckling response.

In Fig. 3.4, the influence of the transverse shear is higher for higher values of Z, which is a representative ratio of the radius versus the thickness. To observe this effect, Shell 5 is defined. The geometry and facesheet laminate properties of Shell 5 are the same as Shell 1 as seen in Table 3.1. Shell 5 has a core of a less stiff material $G = 70MPa$ than Shell 1, and the thickness is reduced to only $1mm$. Most nondimensional parameters remain the same, as shown in Table 3.2, except the Batdorf-Stein parameter $Z = 100$ and the transverse shear parameter $\chi_1 = 570$.

A higher value of Z with a similar value of χ_1, will have a more pronounced influence on the transverse shear. For instance, the Shell 5 ratio is $\mathscr{F}/\mathscr{F}_0 = 0.69$, considerably lower than the Shell 1 ratio $\mathscr{F}/\mathscr{F}_0 = 0.82$.

Another interesting observation can be made by analysing the difference between Shell 4 and Shell 5. Both shells have the same core thickness, and therefore the value of the nondimensional buckling load without transverse shear is the same: $\mathscr{F}_0 = 692$. However, when calculating the nondimensional buckling load including the transverse shear, for Shell 4 it is $\mathscr{F} = 567$ (18% lower than $\mathscr{F}_0$) and for Shell 5 it is $\mathscr{F} = 478$ (31% lower than $\mathscr{F}_0$). This is a significant disparity, especially given that the shell cores are composed of a similar material (isotropic foam), differing only in their shear modulus

properties. This speaks to the higher influence of the shear parameters for higher values of Batdorf-Stein parameters Z.

Finally, in order to study the influence of the length, Shell 6 is considered. Shell 6 has the same radius, facesheet laminate, core material and core thickness as Shell 1. However, the length of Shell 6 (L = 1600 mm) is double the length of Shell 1 (L = 800 mm). Therefore, Shell 1 and Shell 6 have different weighted geometry parameters α_m, α_b and different transverse ratio ϕ. In order to study the effect of these parameters, it is plotted the transverse shear buckling load ratio, $\mathscr{F}/\mathscr{F}_0$ versus the weighted geometry parameters (α_m, α_b) for the sandwich shells with shear ratios ϕ = 0.5, ϕ = 2, ϕ = 4 and ϕ = 16 in Fig. 3.5.

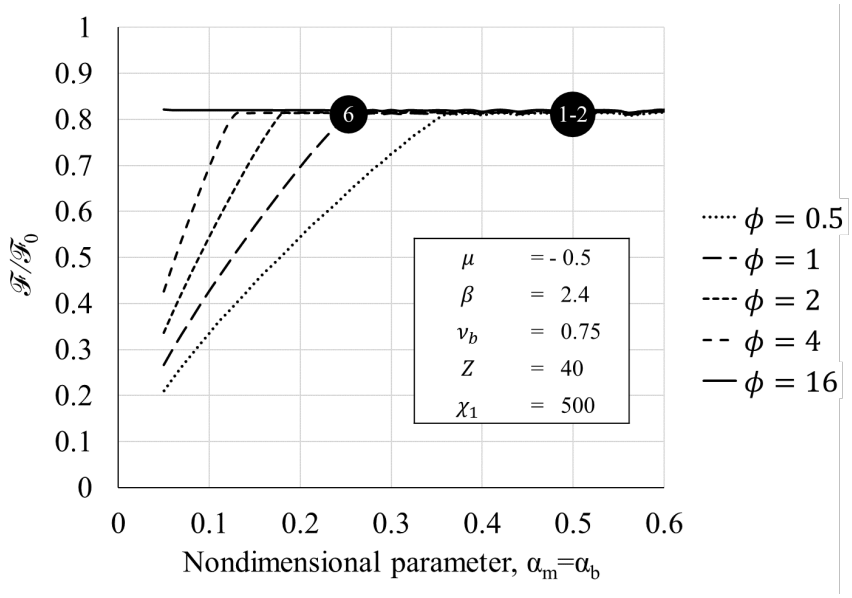

Figure 3.5: Effect of weighted geometry parameters (α_m, α_b) on the transverse shear buckling load ratio ($\mathscr{F}/\mathscr{F}_0$) for ϕ = 0.5, ϕ = 1, ϕ = 2, ϕ = 4 and ϕ = 16, where the numbers in black are the shell numbers.

If the same facesheet properties are kept, since the facesheet layup is $(\pm 45°)_s$, the variation of α_m and α_b is dependent only on the variation of geometry ratio (L/R). Fig. 3.5 shows that low values of α_m and α_b, in combination with low values of ϕ can produce a big change in the transverse shear buckling load ratio, $\mathscr{F}/\mathscr{F}_0$. However, the change between Shell 1 and Shell 6 is not significant enough to change either the buckling behavior or the influence of the transverse shear $\mathscr{F}/\mathscr{F}_0$ = 0.82. For shells with moderate length with respect to the radius, the influence of α_m, α_b and ϕ does not play a significant role.

3.5. FINITE ELEMENT VERIFICATION

IN order to verify the results and trends, for the shells described in Table 3.1 the buckling loads are compared with numerical results. The goal is to check the results obtained in Section 3.4, and analyze if the assumptions of the formulation hold even in the limit cases.

These numerical results are determined using the commercial general-purpose finite element code Abaqus, where a linear buckling analysis is performed. Since the considered sandwich cylindrical shells are assumed to be thin shells with thin cores, S4R reduced-integration four-noded shell elements are used in the finite element analysis. The models use elements of approximately 10mm x 10mm for Shell 1, 3, 4, 5 and 6 and 30mm x 30mm for Shell 2. Since the analytical equations are proposed considering simply supported conditions, simply supported conditions are used as well in the numerical analysis.

The results are reported in Table 3.3. The analytical load, P_0 is calculated using the formula in Eq. (3.101), and the analytical load, P is calculated using the formula in Eq. (3.84). The difference between the analytical load (P) and the numerical value (P_{num}) is also included in the table.

Table 3.3: Buckling load of the shells.

Results	Shell 1	Shell 2	Shell 3	Shell 4	Shell 5	Shell 6
Analytical load, P_0 [kN]	657	4707	675	328	328	653
Analytical load, P [kN]	534	3826	630	269	227	533
Numerical load, P_{num} [kN]	551	3881	631	290	265	551
Analytical-numerical difference [%]	-3.02	-1.40	-0.18	-7.17	-14.26	-3.16

The numerical results show reasonable agreement($< 5\%$) with the analytical formulation for Shell 1, Shell 2, Shell 3 and Shell 6. For Shell 4, which is considered a limit case, results show a higher difference (-7.17%) between the analytical and the numerical result. The case is a limit case because the thickness of the core is comparable to the thickness of the facesheets. The assumption that the transverse shear is only carried by the core is no longer true. In this case, the transverse shear properties of the facesheets should also be taken into account and therefore the Cheung and Tennyson shear model used here [123] is no longer applicable.

A large discrepancy can also be seen in Shell 5. For Shell 5, which has the same

thickness ($1mm$) but a less stiff core material as Shell 4, results show that the analytical formulation overestimates the influence of the transverse shear by -14.26%. This indicates that the reduction of the buckling load due to the transverse shear is significant ($P_{num}/P_0 = 0.81$) but not as high as predicted ($P/P_0 = 0.69$). This result reinforces the need to limit the application of the methodology to cases where the core thickness is significantly larger than the facesheets as established in the definition of the methodology.

Aside of the numerical buckling values, it is interesting to compare the buckling modes of the out-of-plane displacement w. The first comparison is between Shell 1 and Shell 2 which, as indicated, are shells of different scales, with different facesheet layup, core thickness and material. However, the nondimensional parameters that rule the buckling phenomena are the same and thus they have the same nondimensional buckling load ($\mathscr{F}$). The dimensional loads are different, as seen in Table 3.3, but they share the same eigenmode shape as seen in Fig. 3.6. The figure shows the first eigenmode shape for the out-of-plane displacement w.

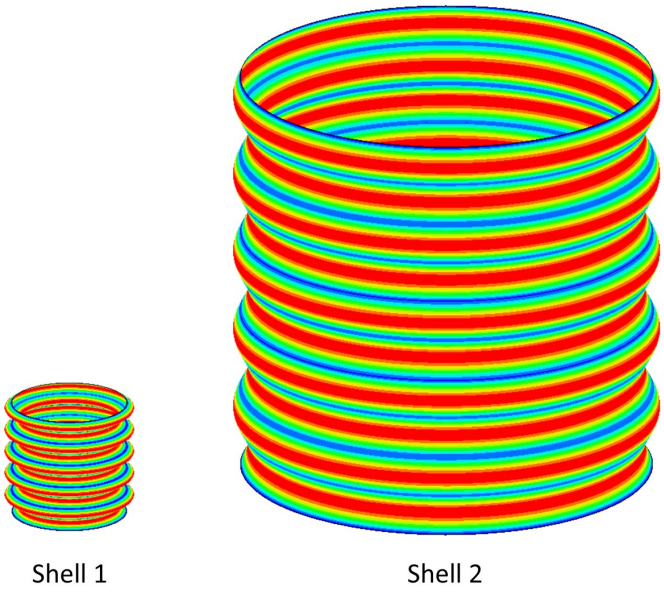

Figure 3.6: Comparison of the first buckling mode of Shell 1 and Shell 2.

Regarding the comparison between shells of the same geometry (radius and length) it can be observed that they all have axisymmetric shape in Fig. 3.7. This is consistent with the eigenvalue solution obtained analytically as indicated in Eq. (3.93). Fig. 3.7 also shows the out-of plane displacement (w) for the first eigenmode. Each solution has a different number of half-waves: 11 for Shell 1, 10 for Shell 3, 14 for Shell 4 and 16 for Shell 5.

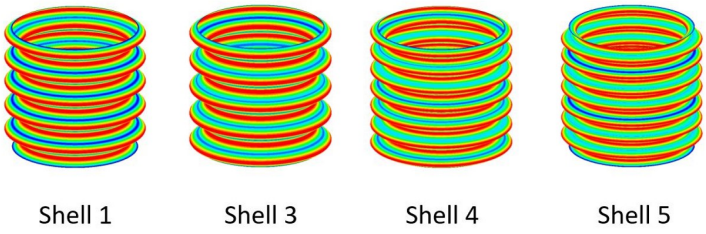

Figure 3.7: Comparison of the first buckling mode of Shell 1, Shell 3, Shell 4 and Shell 5.

Finally, the buckling shapes of Shell 1 and Shell 6, for which the buckling load (P) as well as the buckling nondimensional load ($\mathscr{F}$) are very similar, are compared in Fig. 3.8. The buckling shape is axisymmetric in both cases but the number of half-waves is 11 for Shell 1 and 21 for Shell 2.

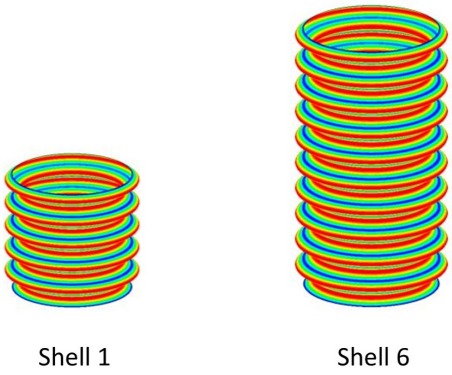

Figure 3.8: Comparison of the first buckling mode of Shell 1 and Shell 6.

3.6. CONCLUSIONS

THIS chapter presents the development of nondimensional equations for axial buckling of sandwich composite cylindrical shells with and without a shear deformable core. A systematic nondimensionalization is applied from the coordinates of the shell up to the linearized buckling equations. The equations offer the advantage to present a similar format as their dimensional counterparts making their use more intuitive.

A solution for the nondimensional buckling load is derived from the linearized nondimensional equations. The nondimensional buckling load is an effective parameter to compare the buckling phenomena for different types of shells of different scale. The nondimensional buckling load $\mathscr{F}$ obtained considering the core transverse shear is com-

pared to the nondimensional buckling load $\mathscr{F}_0$ obtained neglecting the core transverse shear.

Using the nondimensional parameters, it is possible to navigate the design space of different shells and to investigate the impact of changes in the properties of the shells towards the buckling response. More specifically, the focus is on the reduction of the buckling load due to the influence of the core transverse shear effects and the relation between the load and other factors of the shells. The transverse shear buckling load ratio $\mathscr{F}/\mathscr{F}_0$ represents this influence.

The study shows that the Batdorf-Stein parameter Z and the nondimensional transverse shear parameter χ_1 influence the transverse shear buckling load ratio $\mathscr{F}/\mathscr{F}_0$ the most. Shells with a stiffer core material, represented with a higher nondimensional transverse shear parameter χ_1, are less influenced by the core transverse shear. For the same value of χ_1, thinner shells, as represented by a higher Batdorf-Stein parameter Z, exhibit a higher transverse shear influence.

The study also investigates the influence of the shear modulus ratio ϕ and the weighted geometry nondimensional parameters α_m, α_b on the transverse shear buckling load ratio $\mathscr{F}/\mathscr{F}_0$. For the applications considered (shells of moderate length with respect to the radius), the influence of these parameters is small.

Overall, the analysis and results can be used to design sandwich composite cylindrical shells. However, these results are only valid for the perfect shell case. Accounting for the imperfection will be introduced in the next chapter.

4

IMPERFECTIONS IN THE NONDIMENSIONAL BUCKLING FORMULATION

No tengas miedo de la perfección,
nunca la alcanzarás.

Salvador Dalí

The goal of this chapter is to extend the nondimensionalization formulation developed in Chapter 3 to include shells with imperfections. As outlined in Chapter 2, imperfections can be modeled in a variety of ways. In this nondimensionalization, a trigonometric function is used, similar to the approach taken by Schultz et al. [126]. The trigonometric function approach is particularly useful when the position and magnitude of imperfections are unknown. Additionally, the trigonometric function approach allows for imperfections to be accounted for efficiently, as the function provides a global description of the imperfection pattern.

In this case, to solve the nondimensional equations including a trigonometric imperfection signature, the use of the eigenvalue problem as described in Chapter 3 is not possible. A homogeneous partial differential equation with constant coefficients is produced, where the solution is dependent on the imperfection amplitude. By using the

amplitude of the imperfection as a parameter, a set of solutions can be found that describe how the shells behave at different levels of imperfection. These solutions, along with the nondimensional parameters, can then be used to find the buckling load of the shell at different scales.

4.1. MODELING OF IMPERFECTIONS

THE nondimensional formulation of the cylindrical shell described in Chapter 3 can be amended to include imperfections. In order to do so, first it must be considered that the normalized coordinates, as shown in Figs. 3.1 and 3.2, are defined for $0 < z_1 < 1$, $0 < z_2 < 2\pi$ and $-1/2 < z_3 < 1/2$.

The shell reference surface is defined by $z_3 = 0$, and therefore the nondimensional components of the displacement of the reference shell surface are $U(z_1, z_2)$, $V(z_1, z_2)$ and $W(z_1, z_2)$, where z_1 and z_2 are the coordinates for the reference surface. These surface displacements are measured with respect to a geometrically perfect, idealized reference surface. This displacement function is normalized with the following expression, analogous to the normalization of the W component of the displacement in Eq. (3.6):

$$W_I = \frac{1}{\sqrt[4]{a_{11}a_{22}D_{11}D_{22}}}\omega_I \tag{4.1}$$

where ω_I denotes the dimensional expression of surface displacements.

The imperfections in the cylindrical shell geometry are often introduced by deviations in the shell's reference surface, denoted as $W_I(z_1, z_2)$, which represent the out-of-plane displacements. These imperfections can originate from various manufacturing defects, material inconsistencies, or loading-induced deformations, and are generally superimposed on the idealized reference geometry. To account for these imperfections in the nondimensional formulation, a perturbation method is often employed, where the displacement field of the imperfect shell is expressed as a sum of the displacement field of the perfect shell and a perturbation term that represents the imperfections.

Mathematically, this can be represented as:

$$W_{\text{total}}(z_1, z_2) = W(z_1, z_2) + W_I(z_1, z_2) \tag{4.2}$$

where W_{total} is the total displacement field, W is the displacement field for the perfect shell, and $W_I(z_1, z_2)$ is the perturbation due to imperfections. It assumed that $W_I(z_1, z_2) << W(z_1, z_2)$, because these imperfections are typically small. The magnitude and pattern of the imperfection field W_I can be derived from experimental data or assumed based on common manufacturing tolerances.

4.2. EQUILIBRIUM AND COMPATIBILITY EQUATIONS

To analyze the response of a shell with relatively small initial imperfections, measured with respect to this idealized shell reference, an imperfection function W_I is introduced. When the shell is unloaded and free of stress and strain, this imperfection function is a distribution of small deviations in the z_3 direction that are always perpendicular to the tangent of the reference surface.

Once the axial load is applied, the nondimensional normal displacement is given by the equation presented in Eq. (4.2). The nondimensional shell normal displacement is the sum of two components: W, which describes the response to an axially loaded shell, and W_I, which is a measure of the magnitude of initial imperfections on the shell. If this normal displacement is applied to the strain displacement-relations from Eqs. (3.21) to (3.23), the strain-displacement relations can be updated to:

$$E_{11}^0 = \frac{\partial U}{\partial z_1} + \frac{1}{2}\left(\frac{\partial W}{\partial z_1}\right)^2 + \left(\frac{\partial W}{\partial z_1}\right)\left(\frac{\partial W_I}{\partial z_1}\right) \tag{4.3}$$

$$E_{22}^0 = \frac{\partial V}{\partial z_2} + \sqrt{12}\,Z\,W + \frac{1}{2}\left(\frac{\partial W}{\partial z_2}\right)^2 + \left(\frac{\partial W}{\partial z_2}\right)\left(\frac{\partial W_I}{\partial z_2}\right) \tag{4.4}$$

$$\Gamma_{12}^0 = \frac{\partial V}{\partial z_1} + \frac{\partial U}{\partial z_2} + \frac{\partial W}{\partial z_1}\frac{\partial W}{\partial z_2} + \frac{\partial W_I}{\partial z_1}\frac{\partial W}{\partial z_2} + \frac{\partial W}{\partial z_1}\frac{\partial W_I}{\partial z_2} \tag{4.5}$$

Once the new strain displacement relations are defined, then the equilibrium equations, defined in Eqs. (3.74) to (3.76), are updated as follows:

$$\begin{aligned} &\alpha_b^2\frac{\partial^3 B_1}{\partial z_1^3} + \beta\frac{\partial^3 B_1}{\partial z_1 \partial z_2^2} + \frac{1}{\alpha_b^2}\frac{\partial^3 B_2}{\partial z_2^3} + \beta\frac{\partial^3 B_2}{\partial z_1^2 \partial z_2} + \sqrt{12}Z\frac{\partial^2 F}{\partial z_1^2} = \\ &= \frac{\partial^2 F}{\partial z_2^2}\frac{\partial^2 (W+W_I)}{\partial z_1^2} + \frac{\partial^2 F}{\partial z_1^2}\frac{\partial^2 (W+W_I)}{\partial z_2^2} - 2\frac{\partial^2 F}{\partial z_1 \partial z_2}\frac{\partial^2 (W+W_I)}{\partial z_1 \partial z_2} \end{aligned} \tag{4.6}$$

$$\chi_1 B_1 - \alpha_b^2\frac{\partial^2 B_1}{\partial z_1^2} + \frac{1}{2}(\beta - \nu_b)\frac{\partial^2 B_1}{\partial z_2^2} - \frac{1}{2}(\beta + \nu_b)\frac{\partial^2 B_2}{\partial z_1 \partial z_2} = \chi_1\frac{\partial W}{\partial z_1} \tag{4.7}$$

$$\chi_2 B_2 - \frac{1}{\alpha_b^2}\frac{\partial^2 B_2}{\partial z_2^2} + \frac{1}{2}(\beta - \nu_b)\frac{\partial^2 B_2}{\partial z_1^2} - \frac{1}{2}(\beta + \nu_b)\frac{\partial^2 B_1}{\partial z_1 \partial z_2} = \chi_2\frac{\partial W}{\partial z_2} \tag{4.8}$$

Similarly the nondimensional compatibility equations from Eq. (3.79) becomes:

$$\begin{aligned}\alpha_m^2\frac{\partial^4 F}{\partial z_1^4}+\frac{1}{\alpha_m^2}\frac{\partial^4 F}{\partial z_2^4}+2\mu\frac{\partial^4 F}{\partial z_1^2\partial z_2^2}-\sqrt{12}Z\frac{\partial^2 W}{\partial z_1^2}=\\ =\frac{1}{2}\left(\frac{\partial^2 W}{\partial z_2^2}\frac{\partial^2(W+W_I)}{\partial z_1^2}+\frac{\partial^2 W}{\partial z_1^2}\frac{\partial^2(W+W_I)}{\partial z_2^2}-2\frac{\partial^2 W}{\partial z_1\partial z_2}\frac{\partial^2(W+W_I)}{\partial z_1\partial z_2}\right)\end{aligned} \tag{4.9}$$

4.3. NONLINEAR DEFORMATIONS OF IMPERFECT CYLINDRICAL SHELLS

4

IN order to solve this new set of nonlinear equations Eqs. (4.6) to (4.9), a radial displacement approximation is taken. The slopes of the median surfaces B_1 and B_2 are also defined as a functional representation that meets the simply supported boundary conditions.

$$W = w_0 + w_1 sin(2\pi m_I z_1) sin(n_I z_2) \tag{4.10}$$

$$B_1 = b1_0 + b1_1 cos(2\pi m_I z_1) sin(n_I z_2) \tag{4.11}$$

$$B_2 = b2_0 + b2_1 sin(2\pi m_I z_1) cos(n_i z_2) \tag{4.12}$$

where w_0 and w_1 are the unknown radial displacement amplitudes, and $b1_0$, $b1_1$, $b2_0$, and $b2_1$ are the unknown median surface slope amplitudes. These unknown amplitudes will have to be calculated in order to describe the shell displacements.

The compatibility equation Eq. (4.9) is a nonhomogeneous partial differential equation with constant coefficients in terms of the stress function F and can be expressed as follows:

$$\alpha_m^2\frac{\partial^4 F(z_1,z_2)}{\partial z_1^4}+\frac{1}{\alpha_m^2}\frac{\partial^4 F(z_1,z_2)}{\partial z_2^4}+2\mu\frac{\partial^4 F(z_1,z_2)}{\partial z_1^2\partial z_2^2}=H(z_1,z_2) \tag{4.13}$$

where $H(z_1,z_2)$ is a function that is dependent on the solution of W and the imposed imperfection.

A simple trigonometric function that is dependent on the buckling shape of the perfect shell and an amplitude parameter is chosen as the imperfection function. This function is presented in Eq. (4.10).

$$W_I = w_I sin(2\pi m_I z_1) sin(n_I z_2) \tag{4.14}$$

where w_I represents the nondimensional amplitude of the imperfection, m_I is associated with the number of halfwaves in the longitudinal direction, and n_I is the value associated with the number of waves in the circumferential direction.

Regarding the stress function F, it was already described in Eqs. (3.70) to (3.72) and the solution takes the form of:

$$F = F_h + F_p \tag{4.15}$$

The particular solution (F_p) is found using the method of undetermined coefficients in terms of the unknown radial displacement amplitudes: w_0 and w_1 from Eq. (4.10).

The homogeneous solution (F_h) to equation Eq. (4.13) is constructed with the following form:

$$F_h = k_1 z_2^2 + k_2 z_1^2 \tag{4.16}$$

where the coefficients k_1 and k_2 are such that they satisfy the boundary conditions and are related to the stresses in the axial and circumferential directions.

The first boundary condition that must be met is that the nondimensional force $\mathcal{N}_{11}$ is equal to the applied nondimensional force at $z_1 = 0$ and $z_1 = 1$. This condition is assumed to be true in an integrated matter of the coordinate z_2 from 0 to 2π. Therefore, taking Eq. (3.70) and integrating for z_2 from 0 to 2π, the k_1 coefficient can be defined as follows:

$$k_1 = \frac{\mathscr{F}_{applied}}{4\pi} \tag{4.17}$$

were $\mathscr{F}_{applied}$ is the nondimensional axial load applied to the cylinder.

The second boundary condition relates to the circumferential displacement. This boundary condition establishes that for $z_1 = 0$ and $z_1 = 1$, the value of the circumferential displacement must be zero, as both edges have simply supported conditions. In order to calculate it, first, the Eq. (4.4) is used to express the derivative of the circumferential displacement ($\partial V/\partial z_2$) in terms of the W and F.

$$\frac{\partial V}{\partial z_2} = -\nu_m \frac{\partial^2 F}{\partial z_2^2} - \sqrt{12} Z W + \alpha_m^2 \frac{\partial^2 F}{\partial z_2^2} - \frac{1}{2}\left(\frac{\partial W}{\partial z_1}\right)^2 - \frac{\partial W}{\partial z_2}\frac{\partial W_I}{\partial z_2} \tag{4.18}$$

The circumferential displacement V is found by integrating Eq. (4.18) with respect to the z_2 coordinate. From this equation, the coefficient k_2 is determined in terms of $w0$ and $w1$.

Once the function F has been defined, applying the Galerkin method to the equilibrium equations Eqs. (4.6) to (4.8), 6 arithmetic equations can be obtained with 6 unknowns: $w0$, $w1$, $b1_0$, $b1_1$, $b2_0$ and $b2_1$.

Finally, the nondimensional axial displacement can be calculated by rearranging Eq. (4.3) as:

$$\frac{\partial U}{\partial z_1} = \frac{1}{\alpha_m^2}\frac{\partial^2 F}{\partial z_2^2} - \nu_m \frac{\partial^2 F}{\partial z_1^2} - \frac{1}{2}\left(\frac{\partial W}{\partial z_1}\right)^2 - \left(\frac{\partial W}{\partial z_1}\right)\left(\frac{\partial W_I}{\partial z_1}\right) \tag{4.19}$$

This equation (Eq. (4.19)) can be integrated to obtain the displacement U as a function of z_2. For comparison purposes, this study uses the shortening Δ which is the average nondimensional displacement obtained integrating U from 0 to 2π. The dimensional form of the shortening δ is calculated in the same way in Eq. (4.20):

$$\Delta = \frac{L}{\sqrt{a_{11}a_{22}D_{11}D_{22}}}\delta \tag{4.20}$$

A complete solution path is obtained by solving Δ for monotonically increasing values of the load $\mathscr{F}_{applied}$ over the desired loading range. Eventually, a further increase of the load in the solution path can't be sustained and the cylinder must buckle to acquire a stable equilibrium configuration. This is the load where buckling of the cylindrical shell with imperfection occurs, denoted from now on as $\mathscr{F}_i$. This value is lower than the value of linear buckling load ($\mathscr{F}$) calculated in Eq. (3.84). This linear buckling load includes the transverse shear effects described in Chapter 3.

To describe this relation, the imperfection sensitivity (IS) is defined as the load of the shell with imperfections($\mathscr{F}_i$) divided by the load of the shell without imperfections ($\mathscr{F}$). Since the nondimensionalisation of these two variable is analogous, the IS can also express the ratio between the buckling load of the imperfect shell P_i(kN) and the buckling load of the perfect shell P (kN), as seen in Eq. (4.21).

$$IS = \frac{\mathscr{F}_i}{\mathscr{F}} = \frac{P_i}{P} \tag{4.21}$$

The load path of the solution is dependent on the value of the imperfection amplitude w_I (Eq. (4.10)), which can be introduced to study different imperfection amplitudes.

4.4. INFLUENCE OF NONDIMENSIONAL PARAMETERS IN THE IMPERFECTION SENSITIVITY OF CYLINDRICAL SHELLS

To illustrate the results derived from the presented nondimensional imperfection formulation, the shells from Section 3.4 are compared. The comparison is used to show how different shells are influenced by different imperfection amplitude values as well as to evaluate the influence of the nondimensional parameters presented in Chapter 3.

Due to the nondimensional nature of the parameter, the imperfection amplitude w_I produces different values of dimensionsional imperfection amplitude, ω_I for each shell. This is shown in Table 4.1. Although the expression for w_I, shown in Eq. (4.1)), includes other parameters, it is mainly dominated by the shell thickness. Shell 1, Shell 3 and Shell 6 have similar shell thicknesses, and thus the imperfection amplitude is similar. Similar phenomena happens for Shell 4 and Shell 5. Shell 2 is much larger than the rest and therefore it has a larger imperfection amplitude.

Table 4.1: Imperfection amplitude $\omega_I[mm]$ for the different shells.

	Shell 1	Shell 2	Shell 3	Shell 4	Shell 5	Shell 6
$w_I = 0.1$	0.23mm	0.79mm	0.22mm	0.12mm	0.12mm	0.23mm
$w_I = 0.2$	0.45mm	1.59mm	0.44mm	0.23mm	0.23mm	0.45mm
$w_I = 0.3$	0.68mm	2.38mm	0.66mm	0.35mm	0.35mm	0.68mm
$w_I = 0.4$	0.91mm	3.17mm	0.88mm	0.47mm	0.47mm	0.91mm

For the six different shells the load imperfection sensitivity (IS) can be seen in the following figure (Fig. 4.1) for different values of imperfection amplitude w_I.

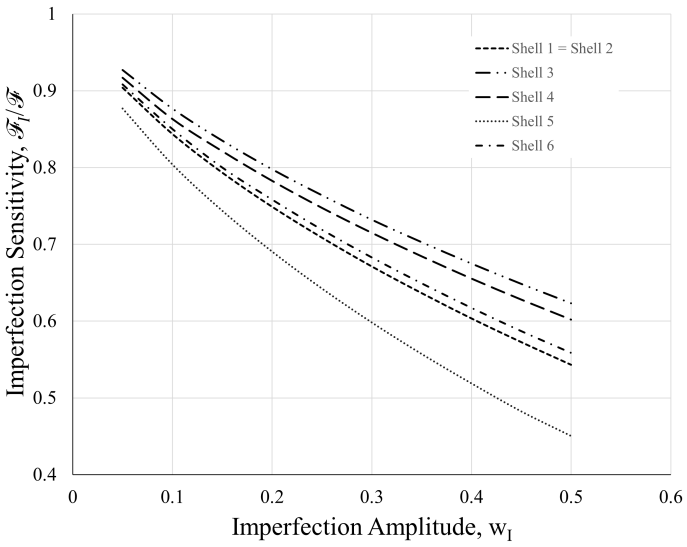

Figure 4.1: Imperfection Sensitivity with respect to imperfection amplitude w_I.

Shell 1 and Shell 2 share all the nondimensional parameters, and this translates to the imperfection sensitivity. This means that for the same level of nondimensional imperfection amplitude (w_I), the imperfection sensitivity (IS) is the same. Both shells also have the same nondimensional load ($\mathscr{F}_i$) vs. shortening curve (Δ) that can be seen in Fig. 4.2.

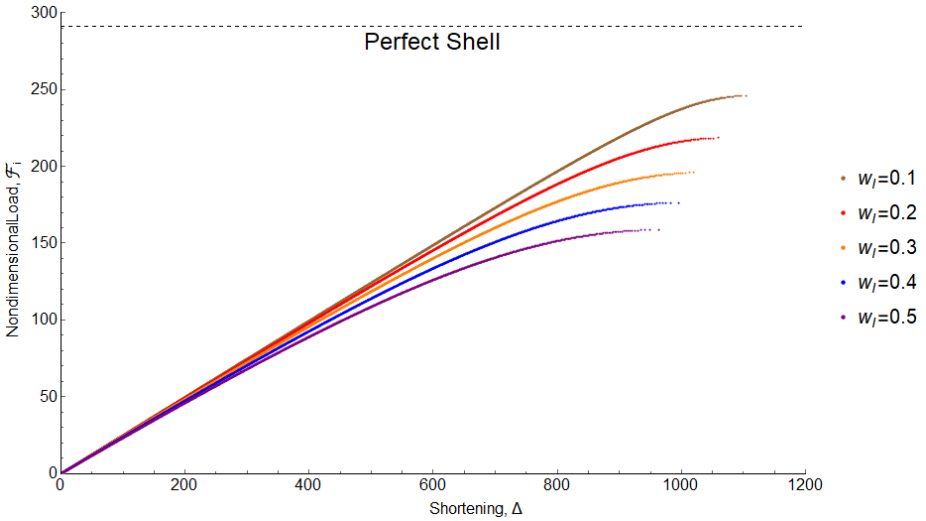

Figure 4.2: Nondimensional load ($\mathcal{F}_i$) against the nondimensional shortening (Δ) for Shell 1 and Shell 2.

This demonstrates that nondimensional results are applicable to different shells of different scales. Since Shell 2 is much larger than Shell 1, the critical load and maximum shortening are also much larger in the dimensional form. This can be seen in Table 4.2.

Table 4.2: Load and shortening for Shell 1 and Shell 2.

	Shell 1		Shell 2	
Imperfection Amplitude	Load, P_i [kN]	Shortening, δ [mm]	Load, P_i [kN]	Shortening, δ [mm]
$w_I = 0.1$	447.8	2.9	3166.4	24.6
$w_I = 0.2$	396.5	2.5	2810.6	23.7
$w_I = 0.3$	356.7	2.3	2514.8	23.0
$w_I = 0.4$	321.0	2.1	2264.7	22.2
$w_I = 0.5$	287.4	1.8	2037.9	21.5

Aside of Shell 1 and Shell 2, it can be seen in Fig. 4.1 that the different shells respond differently to the same imperfection amplitude (w_I). This can also been seen clearly in their respective load-shortening curves shown in Fig. 4.3. However, it is hard to elucidate from these figures which parameters drive the change in the imperfection sensitivity (IS), so a step by step approach must be taken.

First, a comparison between Shell 1 and Shell 3 is made. The main difference between those two shells is the χ_1 parameter, due to change in the core material. The rest

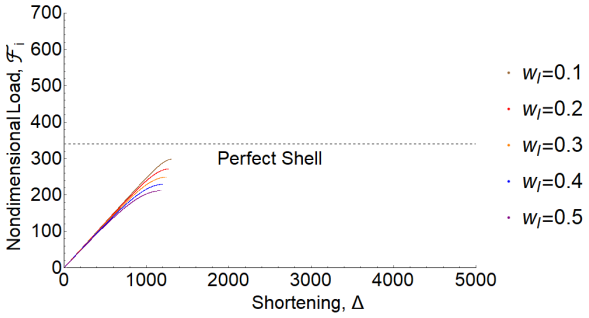

(a) Shell 3

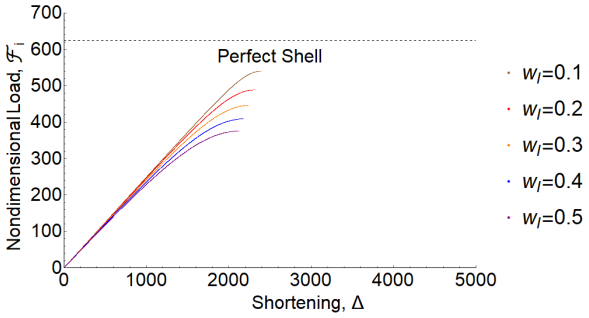

(b) Shell 4

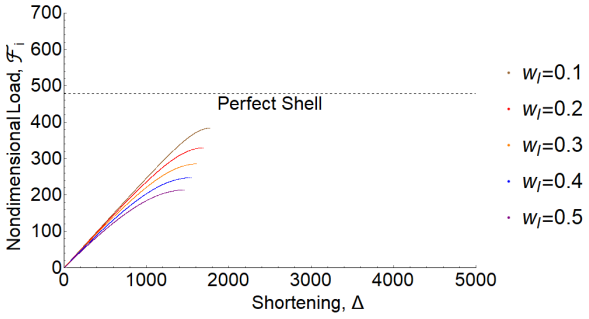

(c) Shell 5

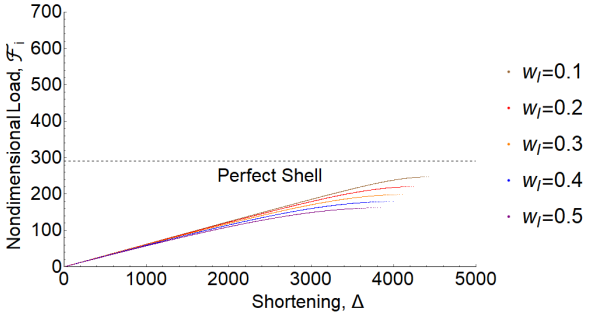

(d) Shell 6

Figure 4.3: Nondimensional load ($\mathcal{F}$) against the nondimensional shortening (Δ) for Shell 3, Shell 4, Shell 5, and Shell 6.

of the set of nondimensional parameters for Shell 1 and Shell 3 is the same. In Fig. 4.4, the influence of the nondimensional transverse shear χ_1 on the imperfection sensitivity IS is illustrated for a sandwich shell with the Batdorf-Stein parameter $Z = 50$ to analyze the differences and study the trends. The figure includes the values for five different imperfection amplitudes $w_I = 0.1$, $w_I = 0.2$, $w_I = 0.3$, $w_I = 0.4$ and $w_I = 0.5$

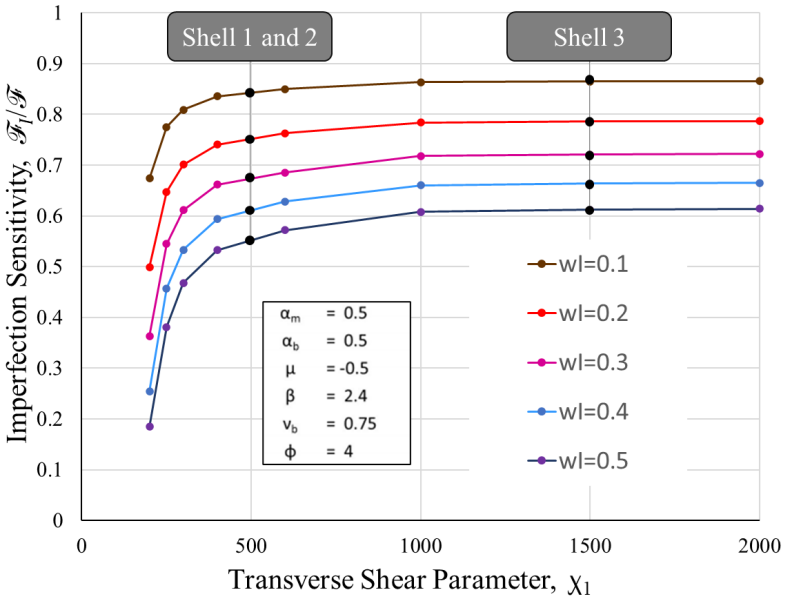

Figure 4.4: Effect of core shear parameter (χ_1) on the Imperfection Sensitivity ($\mathscr{F}_i/\mathscr{F}$) for $Z = 50$.

The curve in Fig. 4.4 is not linear. There is a sharp increase in the value of IS under $\chi_1 < 500$, then the curve stabilizes and converges to a value depending on the level of imperfection amplitude. This indicates that for a shell with high values of χ_1 the importance of this parameter is reduced. This is aligned with the conclusion in Chapter 2, where it was demonstrated that the influence of the transverse shear parameters is relevant for low χ_1 values. A lower transverse shear parameter is linked to a less stiff core, which lowers the critical buckling load both in the case of the shell with and without imperfections.

For the shells considered, as can be seen in Fig. 4.4, the difference due to the change is small and, as already established, dependent on the imperfection amplitude. For instance, for an imperfection amplitude of $w_I = 0.1$, the difference in the imperfection sensitivity between Shell 1 and 3 is of 3% and for an imperfection amplitude of $w_I = 0.5$ the difference is of 12%. For subsequent analysis, just the imperfection amplitude $w_I = 0.5$ is shown to better spot trends.

Then, to study the influence of both the transverse shear parameter χ_1 and the Batdorf-Stein parameter Z, Shell 4 and Shell 5 are considered. These two parameters respond to

changes in the core material and the core thickness. For Shell 4, the thickness of the core is much smaller than in Shell 1. This directly influences a change in the transverse shear parameter χ_1 and the Batdorf-Stein parameter Z. Shell 5 has the same thickness as Shell 4 as well as a much less stiff core material, which reduces the value of χ_1.

In order to analyze the differences and study the trends, Fig. 4.5 shows, for a sandwich shell with Batdorf-Stein parameters $Z = 50$ and $Z = 100$,the imperfection sensitivity $IS = \mathscr{F}_i/\mathscr{F}$ with respect to the nondimensional transverse shear χ_1.

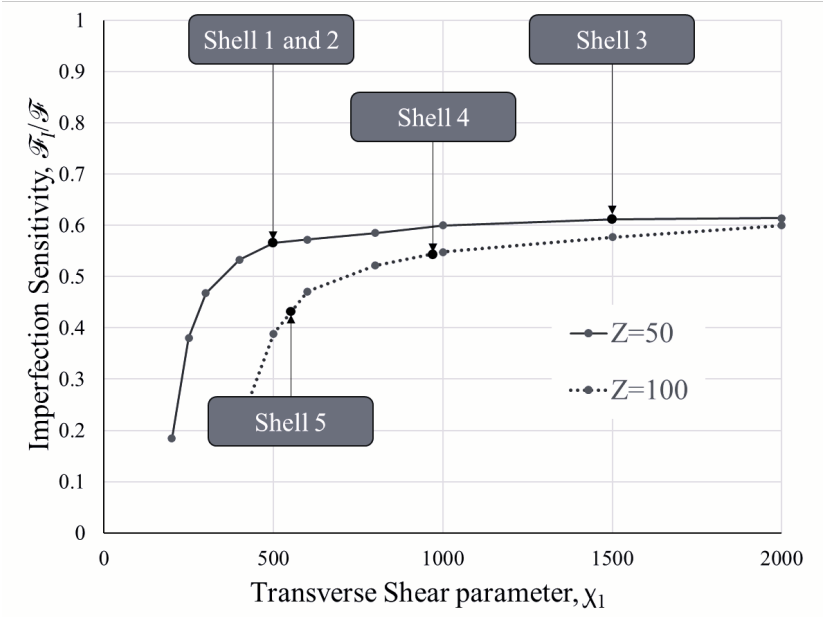

Figure 4.5: Effect of core shear parameter (χ_1) on the Imperfection Sensitivity ($\mathscr{F}_i/\mathscr{F}$) for $Z = 50$ and $Z = 100$ with imperfection amplitude $w_I = 0.5$.

It can be seen that an increase in the Batdorf-Stein parameter for the same value of the transverse shear parameter χ_1, reduces the imperfection sensitivity value (IS). This means that the shell is more sensitive to imperfections for higher Batdorf-Stein parameters. A clearer way to expose this result is depicted in Fig. 4.6. The Imperfection Sensitivity (IS) is displayed versus the Batdorf-Stein parameter Z for the following transverse shear parameter values: $\chi_1 = 500$, $\chi_1 = 1000$, and $\chi_1 = 1500$.

In Fig. 4.6, the importance of Z parameter is highlighted. Although the relationship in non-linear and dependent on the transverse shear value as well as the imperfection sensitivity, there is a significant reduction of the IS value for higher values of Z, indicating that slender shells are more influenced by the imperfections. This conclusion is aligned with the available literature [124, 127].

For the shells considered, as can be seen in Figs. 4.5 and 4.6, there is some significant

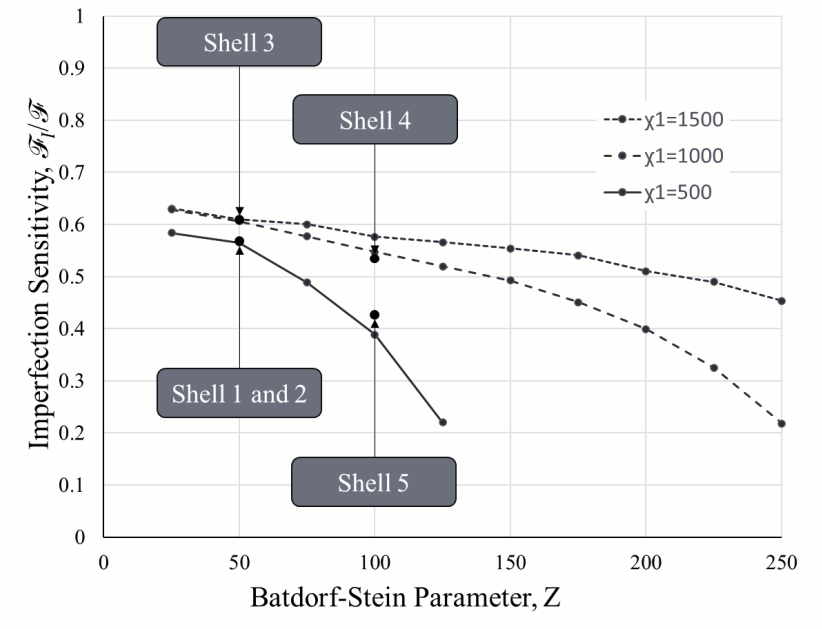

Figure 4.6: Effect of the Batdorf Stein parameter (Z) on the Imperfection Sensitivity ($\mathscr{F}_i/\mathscr{F}$) for $\chi_1 = 500$,$\chi_1 = 1000$, and $\chi_1 = 1500$ with imperfection amplitude $w_I = 0.5$.

differences in their imperfection amplitude. For instance, for an imperfection amplitude of $w_I = 0.5$, between Shell 1 and Shell 5 the difference is of 24%, whereas between Shell 1 and Shell 5 the difference is of only 3%. This is due to two factors, that compound on each other. First, Shell 4 and Shell 5 are more slender compared to Shell 1, which increases their sensitivity to imperfection. And second, Shell 5 has a core material with very low stiffness which in turn also increases the imperfection sensitivity. The results also prove that for sandwich shells, the transverse shear effects must be taken into account in order to have accurate results. The Batdorf-Stein parameter Z is insufficient to explain the variation between shells.

Then, the other parameters, namely the α_m and α_b are considered. These parameters, if only a facesheet with an orthotropic facesheet layup ($(\pm 45)_s$) is considered, act as a geometry ratio parameters, which is turn highlights the importance of the stiffness.

In order to study the influence of the geometry ratio, Shell 6 is considered. Shell 1 and Shell 6 have different weighted geometry parameters (α_m, α_b) and different transverse ratio (ϕ) because the length of Shell 6 (L = 1600 mm) is double the length of Shell 1 (L = 800 mm). To examine the impact of these factors, the IS is displayed against the weighted geometric parameters for the sandwich shells with shear ratios $\phi = 1$, $\phi = 2$, $\phi = 4$, and $\phi = 16$ in Fig. 4.7.

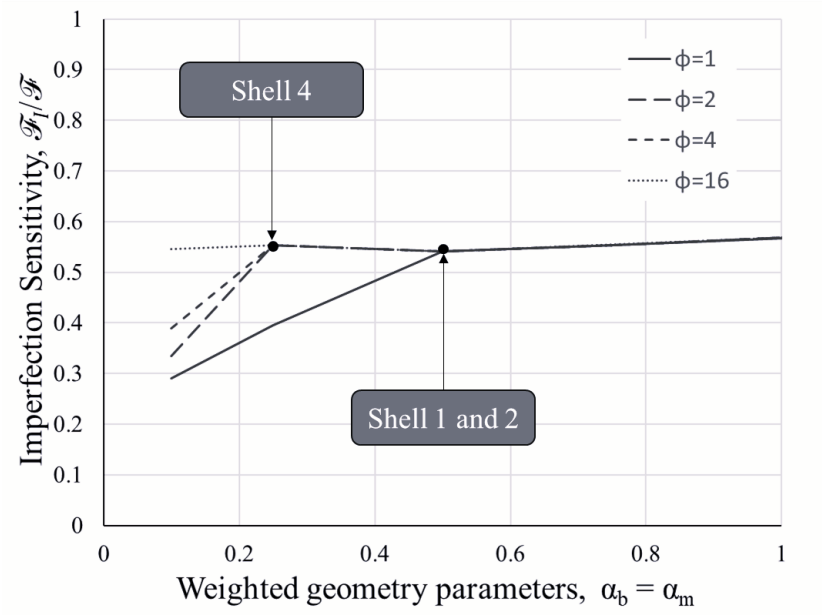

Figure 4.7: Effect of weighted geometry parameters (α_m, α_b) on the IS $(\mathscr{F}_I/\mathscr{F})$ for $\phi = 0.5$, $\phi = 1$, $\phi = 2$, $\phi = 4$ and $\phi = 16$.

Fig. 4.7 shows that low values of α_m and α_b (<0.2), in combination with low values of $\phi < 4$ can produce a large variation, between 15-25%, in the imperfection sensitivity. This is an unrealistic scenario for most shells considered since the length needs to be much larger than the radius, which makes Euler buckling more likely than shell buckling. In this particular example, the change between Shell 1 and Shell 6 is very small. For shells with orthotropic facesheet layup $(\pm 45°)_s$ with moderate length with respect to the radius, the influence of α_m, α_b and ϕ does not play a significant role.

Finally, the influence of the facesheet lay-up needs to be considered. In theory, this is best done using the nondimensional parameters μ and β, who represent the in-plane and out-of-plane stiffness of the shell. However, a change on the facesheet lay-up directly affects all the rest of the nondimensional parameters, so these two parameters cannot be studied in isolation. For this reason, a specific lay-up is considered: $(\pm\theta)_s$, and the rest of the parameters are the same as in Shell 1. The angle θ is varied from 0º to 90º and the variation on the nondimensional parameters μ and β as well as the imperfection sensitivity for each Shell is reported in Fig. 4.8.

Fig. 4.8 illustrates that the fluctuation of the angle θ has a little impact on the imperfection sensitivity of the shell, contingent upon the imperfection amplitude. In general, the highest value of IS is found for shells closer to 0°. The difference between the shells with 45° is from 4% for the lowest imperfection amplitude up to 16% for the highest imperfection amplitude. The values close to 90° are not as high as the values at 0°. The

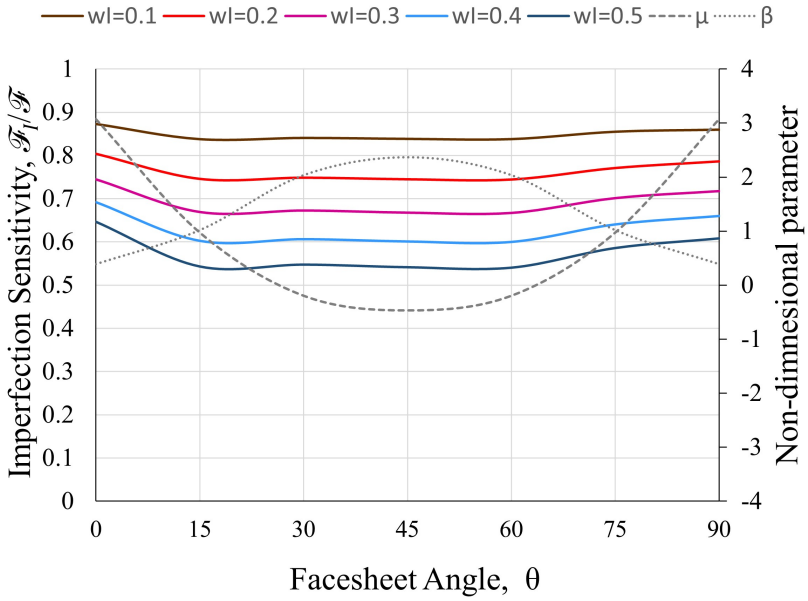

Figure 4.8: Effect of the facesheet Angle (θ) on the orthotropy parameters (μ,β) and the IS ($\mathscr{F}_I/\mathscr{F}$) for $w_I = 0.1$, $w_I = 0.2$, $w_I = 0.3$, $w_I = 0.4$ and $w_I = 0.5$.

difference ranges between 2% up to 6%.

Finally, it must be pointed out that the similar imperfection sensitivity does not signify similar buckling response. In fact, as can be seen in Fig. 4.9, the buckling loads for the shells with the same imperfection amplitudes are also impacted up to 40% by changes in the θ angle, and therefore by the change in the μ and β parameters.

It can be seen in both the nondimensional buckling load graph of Fig. 4.9a and the buckling load graph of Fig. 4.9b, that the highest buckling load happens when the values of μ and β are the closest in value. The larger difference between those two parameters produces a lower buckling load. This is also consistent with the available literature [125].

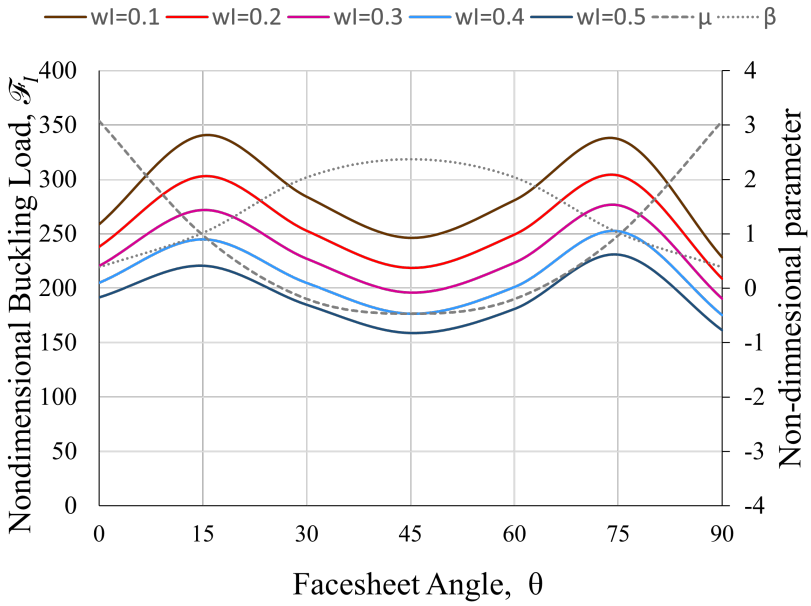

(a) Nondimensional Buckling Load , $\mathscr{F}_I$ [kN].

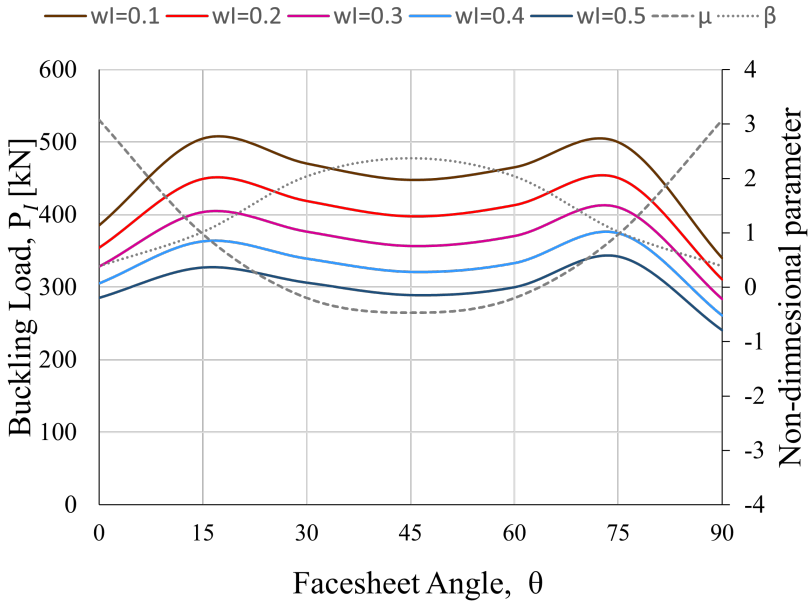

(b) Buckling Load, P_I [kN].

Figure 4.9: Effect of the facesheet Angle (θ) on the buckling load for $w_I = 0.1$, $w_I = 0.2$, $w_I = 0.3$, $w_I = 0.4$ and $w_I = 0.5$.

4.5. CONCLUSIONS

THE derivation of nondimensional equations for axial buckling of sandwich composite cylindrical shells including a trigonometric imperfection is discussed in this chapter. A systematic nondimensionalization is applied because nondimensional imperfection parameters are useful for comparing buckling phenomena for various shell types and scales.

A solution for the nondimensional buckling load is derived from the equilibrium and compatibility equations including an initial geometric imperfection. This model uses the bifurcation buckling modes of the shell without imperfections as initial geometric imperfections. The limit buckling load $\mathscr{F}_i$ for each imperfection amplitude w_I occurs when the shell cannot support more load. The Imperfection Sensitivity (IS) is defined as the ratio between $\mathscr{F}_i$ and $\mathscr{F}$.

Using the nondimensional parameters, it is possible to navigate the design space of different shells and to investigate the impact of changes in the properties of the shells towards imperfection sensitivity. The study shows that the nondimensional imperfection amplitude w_I plays the largest role in the solution.

The study also shows that the Batdorf-Stein parameter Z and the nondimensional transverse shear parameter χ_1 play a large role as well in the imperfection sensitivity $\mathscr{F}_i/\mathscr{F}$. Shells with a stiffer core material, represented with a higher nondimensional transverse shear parameter χ_1, are less sensitive to imperfections. For the same value of χ_1, shells with a higher Batdorf-Stein parameter Z, present a higher sensitivity to imperfections.

The study also investigates the influence of the geometry of the shell via the weighted geometry parameters on the imperfection sensitivity. In the examples examined, the impact of these parameters in the imperfection sensitivity is minimal in moderately long shells with relation to the radius.

Finally, the influence of the in-plane and out-of-plane stiffness of the facesheets is considered. These factors are best represented by the nondimensional parameters μ and β. However, altering these parameters only had a minor impact on imperfection sensitivity.

Overall, the analysis and results can be used to design sandwich composite cylindrical shells as well as to account for an initial imperfection factor in the scaling methodology developed in the following chapter.

5

SCALING METHODOLOGY

Entonces fue cuando empecé a darme cuenta
de que se aguantan mucho mejor
las contrariedades grandes
que las pequeñas nimiedades de cada día

Carmen Laforet

An analytical scaling methodology for compression-loaded sandwich composite cylindrical shells is presented is this chapter. This scaling methodology is based on the nondimensionalization of the buckling equations presented in Chapters 3 and 4. The goal of this methodology is to provide a tool to facilitate the study of the buckling behavior of large shell structures via reduced-scale shell structures.

The appeal of developing a systematic analysis-based scaling methodology stems from the drawbacks of performing multiple full-scale tests. Testing is expensive, not only due to the high number of tests required but also due to the large scale of the structures considered. An analysis-based methodology would allow for the rapid formulation of scaled-down structures suitable for smaller laboratories. The analytical, numerical, and experimental results of these scaled-down structures can then be used in the design of large-scale structures, thereby reducing the number of large-scale tests.

The difficulty in developing such an analysis-based methodology lies in the high de-

Parts of this chapter have been published in AIAA Journal **1–10**, 107393 (2020) [128].

pendency of test results on geometry variations and the shell's imperfection signature. A successful methodology requires accurate modeling of the phenomena, the selection of appropriate scaling laws, and the investigation of feasibility areas. The approach taken in this chapter makes use of a nondimensional formulation of the equations, where the components of the equations become the scaling laws.

The use of nondimensional governing equations requires comprehensive nondimensional formulations to describe the problem, such as the one developed by Nemeth [125]. These equations offer the advantage of having a similar format to their dimensional counterparts, making their use more intuitive. A systematic nondimensionalization is applied from the coordinates of the shell up to the buckling equations of the sandwich composite cylindrical shell [120]. Two particular challenges in the modeling are the inclusion of transverse shear effects in the sandwich core which were discussed in Chapter 3 and the inclusion of imperfections in the shell which were discussed in Chapter 4.

Once the nondimensional governing equations are developed, this methodology takes advantage of the fact that shells of different sizes can share the same set of nondimensional parameters. Therefore, as shown in detail in Chapters 3 and 4, the buckling load, the influence of transverse shear on the buckling load, and the influence of imperfections can be observed and studied through this set of parameters.

For this reason, the nondimensional parameters are used as metrics to describe similarity. If different cylindrical shells have identical nondimensional parameters, their nondimensional buckling responses must also be identical. Therefore, the goal is to develop a methodology to design scaled configurations with nondimensional parameters that match as closely as possible the nondimensional parameters of the baseline configurations.

The innovative aspect of this methodology is that the parameters are decoupled, allowing each parameter to be calculated in a specific order. The potential of this approach is very high, but finding an exact match of all nondimensional parameters can be challenging. Manufacturing and material constraints can limit the applicability of the results. Feasibility areas must be defined depending on the structures that need to be scaled. These structures will be discussed in detail in the following section.

5.1. BASELINE STRUCTURES

FOR the purposes of demonstrating the scaling methodology, several baseline structures, shown in Table 5.1), will be analyzed. These baseline structures were considered during the Shell Buckling Knock-Down Factor program [129]. In particular, they were considered in the part of the program dealing with large sandwich composite structures [92].

The main properties of these baseline designs are described in Table 5.1. All baseline

structures have the same radius of 1.2 m [47 in] and length of 2.3 m [91 in]. All baseline structures are made of carbon fiber facesheets, and the core is made of aluminum honeycomb. More details regarding the materials can be found in the technical reports of each baseline structure [9, 10, 16, 130].

Table 5.1: Baseline Structures Properties.

Parameter	Baseline 1	Baseline 2	Baseline 3	Baseline 4
Facesheet lay-up	$[\pm 45/0/\bar{90}]_s$	$[\pm 60/0]_s$	$[\pm 30/\bar{90}]_s$	$[\pm 30/90/0]_s$
Ply Thickness [mm]	0.145 [0.0057 in]	0.180 [0.0071 in]	0.137 [0.0054 in]	0.137 [0.0054 in]
Core thickness [mm]	6.35 [0.25 in]	5.08 [0.20 in]	5.08 [0.20 in]	7.62 [0.30 in]
Total Thickness [mm]	8.38 [0.33 in]	7.24 [0.28 in]	6.45 [0.25 in]	9.82 [0.39 in]

Table 5.2: Baseline Structures Nondimensional Parameters, Z is highlighted due to its importance.

Parameter	Baseline 1	Baseline 2	Baseline 3	Baseline 4
α_m	0.56	0.52	0.58	0.59
α_b	0.56	0.52	0.58	0.59
μ	0.75	1.00	0.64	1.59
β	1.17	1.00	1.25	0.78
Z	87.9	106.7	111.0	77.6
χ_1	2039.6	2167.3	3959.3	1467.9
χ_2	3403.7	3616.8	6607.3	2449.8

These designs were chosen because they have nondimensional parameters within the range of real-scale launch vehicle structures. For instance, for the real-scale launch vehicle structures, the values of Z are estimated to be between 65 and 120. A selection of suitable structures from this range was chosen. The nondimensional parameters that correspond to these baseline structures are shown in Table 5.2. It can be seen that the values of Z fall within the estimated values of the structures of the real-scale launch vehicle.

The test article cited as CTA8.1 in the Schultz et al. report [16] corresponds with the first design, Baseline 1. The tested design included some manufacturing and load introduction details. The shell had a six-ply padup, and aluminum end rings were mounted

to the shell to allow integration with the test setup. Moreover, the specimen underwent several repairs to address some flaws discovered during the non-destructive evaluation. The other structures are Baseline 2, which corresponds to the test article CTA8.2 [10], Baseline 3, which corresponds to the test article CTA8.3 [9] and Baseline 4, which corresponds to test article CTA8.4 [130]; all with similar design of load introduction details.

5.2. SCALING STRATEGIES

DURING this PhD research, two different scaling strategies were developed. Both use a similar method, but each is suitable for a different case and has its own advantages and disadvantages. The two scaling methods are presented in Fig. 5.1.

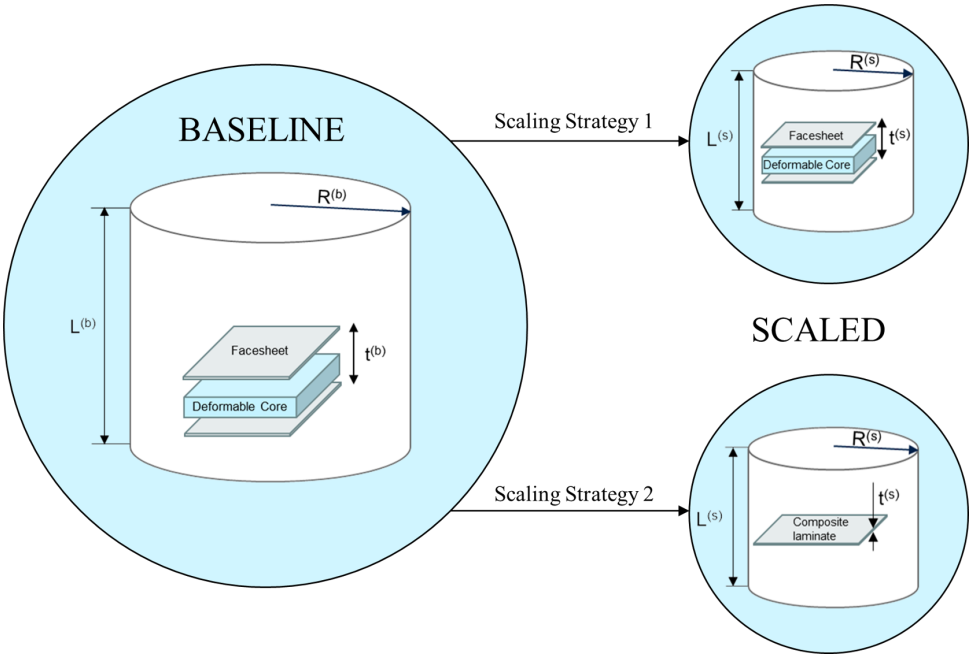

Figure 5.1: Sketch of the two different scaling strategies.

The first strategy scales from a baseline sandwich structure to a scaled sandwich structure. This method is constrained by the manufacturing limits in the thickness of the core of the scaled structure. Depending on the size of the baseline structure, the scaled structure can produce thickness values that are not feasible. Furthermore, as shown in Chapter 3, the transverse shear parameter (χ_1) decreases substantially for lower thickness values. In some scale cases, it is not feasible to replicate this parameter with existing materials. These reasons amount to a manufacturing challenge where, even if a scaled structure is possible in theory, it cannot be produced.

The second strategy scales from a baseline sandwich structure to a monolithic laminate structure. This strategy avoids the manufacturing problems described for the previous strategy, but has the issue of obtaining the desired thickness with a specific layout. The main challenge in this case is to compare the two different types of structures. It is particularly challenging to compare imperfection levels.

5.2.1. SCALING STRATEGY 1

IN Scaling strategy 1 (as shown in Fig. 5.1), the cylindrical structure that needs to be scaled, called the baseline configuration, is a cylindrical sandwich composite shell with carbon fiber facesheets and an aluminum honeycomb core. The result of the structural scaling, referred to as the scaled configuration, is also a cylindrical sandwich composite shell. The scaled cylindrical shell may have different material properties for both the facesheets and the core. The full Scaling strategy outline is depicted in Fig. 5.2 and will be described step by step in this section.

In this study, for the composite laminate facesheets in a scaled configuration, two families of stacking sequences are considered. The methodology is amenable to other families of stacking sequences.

- Family I: A symmetric balanced laminate $[\theta/-\theta]_s$
- Family II: An unsymmetric balanced three-ply laminate $[\theta/0/-\theta]$

In both families, the ply stacking sequence is a function of only the variable θ. This is done to reduce the number of parameters involved in the methodology. Note that although the second stacking sequence family is an unsymmetric laminate, when used for the facesheets in the sandwich cylinder, the resulting full sandwich shell is symmetric about the midsurface. The equations considered treat the entire sandwich structure as a balanced and symmetric laminate, neglecting bend-twist anisotropy effects.

For the purposes of these analyses, the Rohacell WF foams [131] were considered as core materials. Other materials such as balsa wood could also be considered for the core if higher shear stiffness is required. Rohacell WF foams were developed for the aerospace industry and are based on polymethacrylimide (PMI) chemistry. Rohacell WF foams have an isotropic nature, meaning they exhibit uniform mechanical properties in all directions. This means that the parameter ϕ described in Eq. (3.63) depends only on the geometry of the shell, as $G_x = G_y$.

These foams enable highly efficient manufacturing processes, as they allow the production of sandwich components in a single co-curing step, and they are compatible with autoclave and vacuum infusion processes. In addition to the processing advantages, the closed-cell structure of the foam ensures that resin remains only at the core-face sheet interface, preventing excess resin from adding unnecessary weight. For these

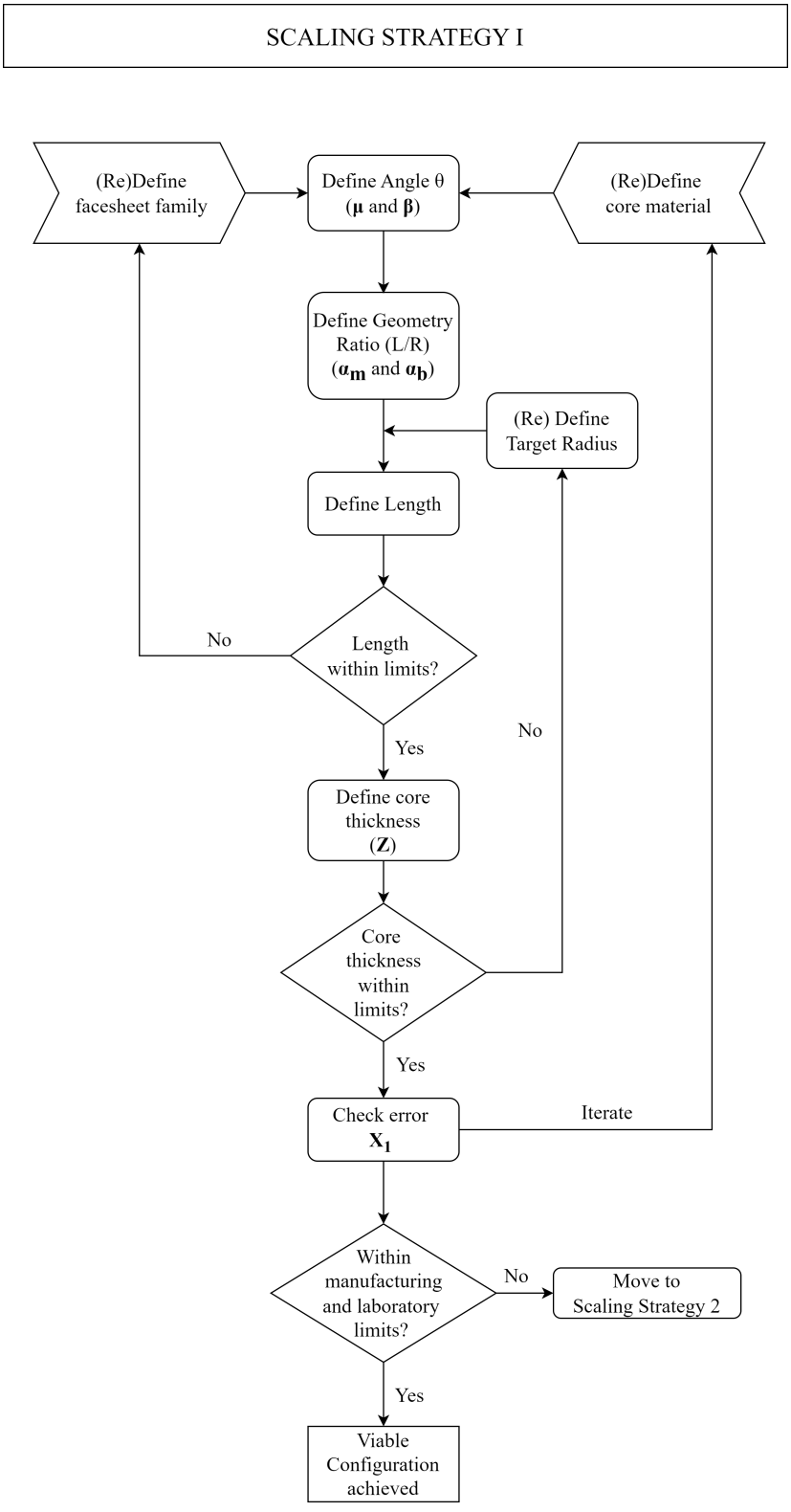

Figure 5.2: Diagram of Scaling Strategy 1.

reasons, the Rohacell WF foams are a good choice for applying the scaling methodology to the baseline structures discussed in Table 5.1.

The scaling methodology is based on the nondimensional form of the buckling equations defined in Chapter 3. The buckling response is formulated by the six nondimensional parameters: μ, β, α_m, α_b, Z, and χ_1 and the scaling laws are the nondimensional parameters in these equations.

The first pair of parameters considered in the scaling methodology are the membrane orthotropy parameter, μ, from Eq. (3.40), and the flexural orthotropy parameter, β, from Eq. (3.53). These two parameters relate the in-plane compliance matrix and the bending stiffness matrix parameters, and are independent of geometry. They are a function of the material properties, the ply stacking sequence, and the core thickness.

For the two families of stacking sequences defined, the parameters μ and β only depend strongly on the ply angle θ. This is because μ and β are not highly sensitive to changes in the core and facesheet thickness. This insensitivity is due to the fact that thickness contributes to the numerator and denominator in similar ways in both Eq. (3.40) and Eq. (3.53), and the high in-plane stiffness of the facesheets compared to typical core materials makes the influence of the core stiffness negligible.

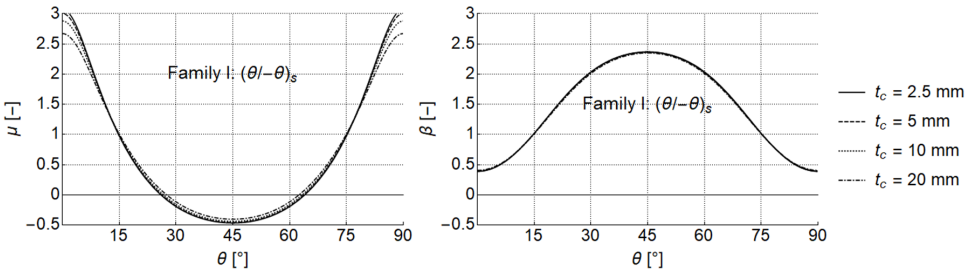

Figure 5.3: Variation of μ and β with respect to θ for Family I.

This phenomenon can be seen in Fig. 5.3, where the values of the parameters μ and β are obtained as a function of the angle θ for the Family I stacking sequence $[\theta/-\theta]_s$ for different core thicknesses. Here, it can be seen that the variation of the values of μ with the thickness of the core is less than 10% for all ply angles. The maximum difference occurs near the 0 and 90-degree ply angles. For β, there are no differences in the values for the different core thicknesses.

A similar distribution of the parameters μ and β as a function of the angle θ for the Family II stacking sequence for different core thicknesses is shown in Fig. 5.4. In this case, up to 15% can be found close to 0°. Again, for the parameter β, there is no difference in the values for the different core thicknesses.

From the curves in Figs. 5.3 and 5.4, it can be seen that for most values of μ and β, there are two possible angles that produce equivalent membrane and flexural orthotropy

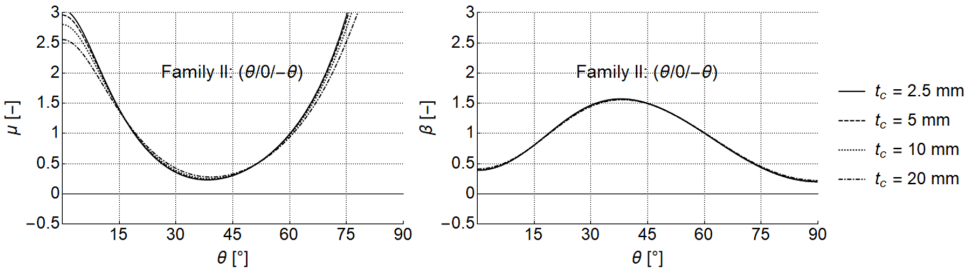

Figure 5.4: Variation of μ and β with respect to θ for Family II.

parameters, and therefore two possible configurations for the scaled cylindrical shells.

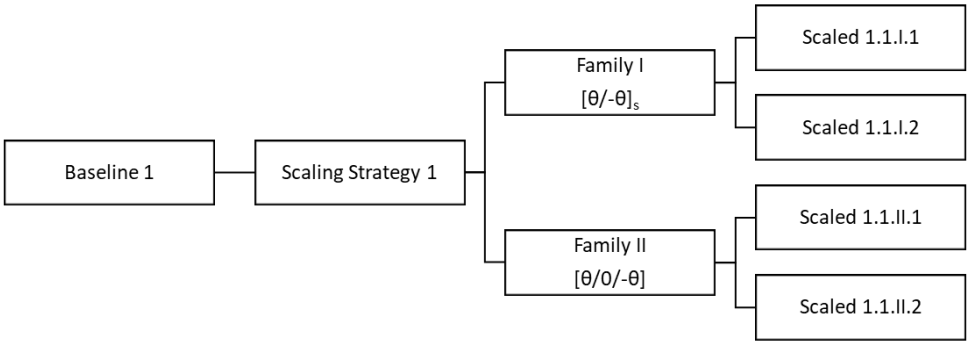

Figure 5.5: Labeling scheme for the scaled configurations in Scaling strategy 1.

Therefore, in most cases, there will be two possible solutions for scaled configurations. Thus, the naming convention that will be used is that the two configurations obtained from Baseline 1 via Scaling strategy 1 will be referred to as Scaled 1.1.I.1 and Scaled 1.1.I.2 for the first family $[\theta/-\theta]_s$ and Scaled 1.1.II.1 and Scaled 1.1.II.2 for the second family $[\theta/0/-\theta]$. This labeling scheme, shown in more detail in Fig. 5.5, can be extended to as many baseline configurations as desired. It can also be extended to other facesheet stacking sequence families.

After the ply angle for each stacking sequence has been defined, the next parameters to be evaluated are α_m (Eq. (3.35)) and α_b (Eq. (3.39)). Both parameters are a function of the ratio R/L, the ply angle (θ), and the thickness of the core (t_c).

The ply angle θ has already been determined, and it can be demonstrated that the influence of the thickness of the core is also negligible for these two parameters. This is attributed to the fact that thickness contributes to the numerator and denominator

in similar ways in both Eq. (3.35) and Eq. (3.39). Moreover, the values of α_m and α_b are equal for low thickness values. The values of α_m have more variation with respect to the thickness and will require reiteration at the end of the process to obtain an exact match. This phenomenon can be seen in Fig. 5.6, where the values of the parameters α_m and α_b are obtained as a function of the geometry ratio R/L for different thicknesses of the core.

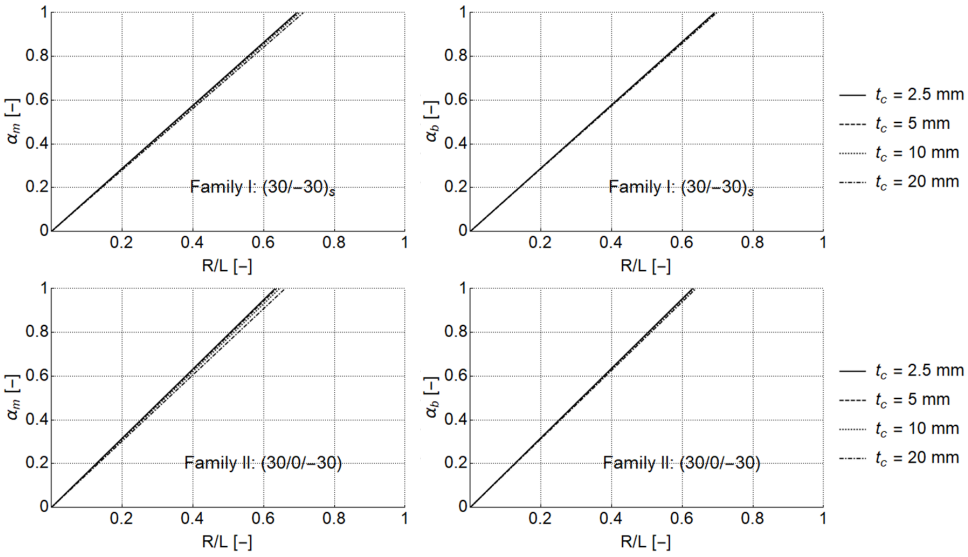

Figure 5.6: Variation of α_m and α_b with respect to to R/L for Family I and Family II.

Based on these trends and pending a final iteration, the thickness of the core is set aside in this step. As a result, it is considered that for a given facesheet stacking sequence, the relationships between the parameters α_m and α_b and R/L are linear. This means that for each value of the α_m and α_b parameters, a single solution can be found for R/L.

Extremes in the value of the ratio R/L can raise concerns about the validity of the equations used. If the cylinder is relatively long, with a low R/L ratio, the dominant structural phenomenon could be global bending instead of axial buckling. If the cylinder is relatively short, with a high R/L ratio, the influence of the boundary conditions can change the buckling response and the imperfection sensitivity. To stay within the assumptions described in Chapter 3 and Chapter 4, the values of R/L are fixed to be between 0.2 and 0.6.

As described in Fig. 5.5, each family produces two solutions for the angle θ. One solution is closer to 0°, making it more axially stiff, and the second one is closer to 90 degrees, making it more circumferentially stiff. Given that the parameters α_m and α_b are also a ratio between the axial and circumferential stiffness (see Eqs. (3.35) and (3.39)), the first scaled solution will produce a lower R/L than the second scaled solution. This phenomenon can be seen in Fig. 5.7. It can also be inferred from the equations that a more axially stiff configuration will produce higher values of critical buckling load, even

if the nondimensional buckling load is the same in both configurations.

Since the scaled solutions from Family II have a middle ply with 0 degrees orientation, by definition, they will be more axially stiff than the scaled solution from Family I. Therefore, as seen in Fig. 5.7, they will tend to have a lower R/L. This trend is particularly noticeable in the scaled configurations with high values of θ.

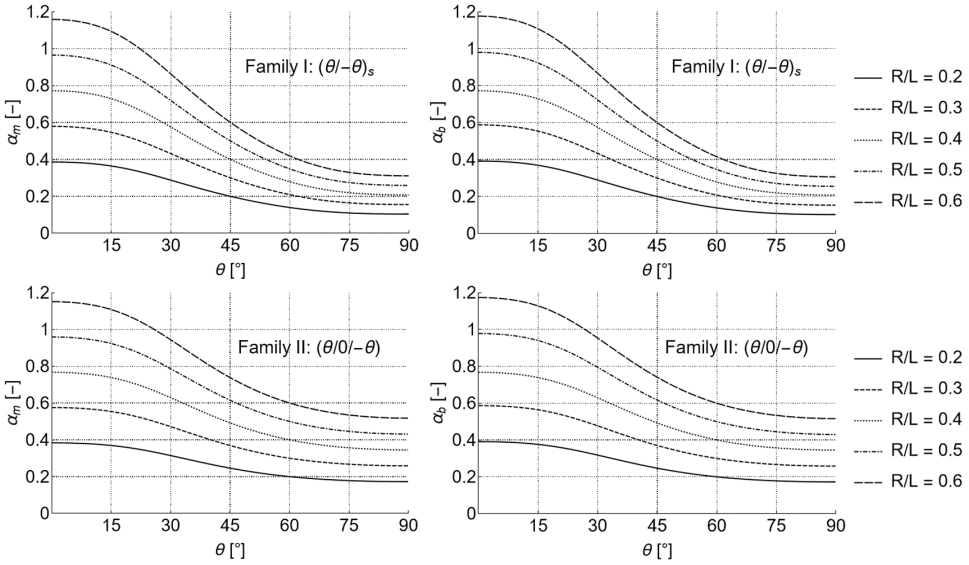

Figure 5.7: Variation of α_m and α_b with respect to θ for different values of R/L for fixed core thickness $t_c = 2.5$.

The next parameter to evaluate is the Batdorf-Stein Z (Eq. (3.19)), which is a function of radius, axial and circumferential membrane compliances, and bending stiffness. This parameter represents the ratio between radius and equivalent thickness. Given that the facesheet stacking sequence and R/L for the scaled configurations have been selected, the baseline value of Z can be maintained in the scaled configurations with the right combination of radius, R, and core thickness, t_c.

From the formulation of the Batdorf-Stein parameter Z in Eq. (3.19), a linear correlation between Z and the radius is observed. As shown in Fig. 5.8, Z also exhibits a particularly pronounced sensitivity to core thickness. These findings highlight the significant influence of core thickness on the behavior of the Z parameter.

It is important to note that Rohacell 200WF foam, an isotropic material with a shear modulus of $G = 120$ MPa, was selected as the material for the core in this particular illustration (Fig. 5.8). However, as seen in the Fig. 5.9, the effect of the core material on the Batdorf-Stein parameters is virtually negligible. These observed patterns are consistent with the findings discussed in Chapter 3, highlighting the predominance of core thickness over core material with regard to the Z parameter.

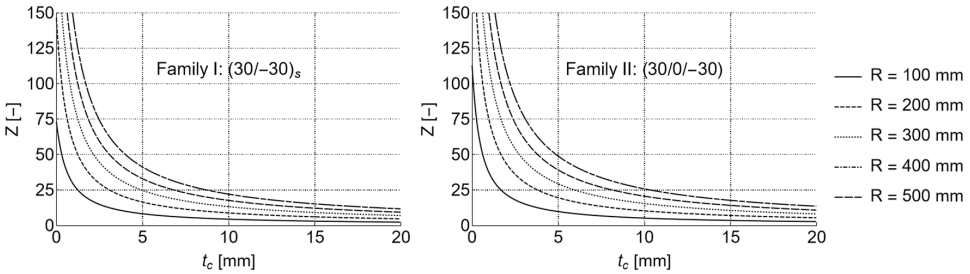

Figure 5.8: Variation of Z with respect to the core thickness for different values of shell radius with Rohacell 200WF as core material.

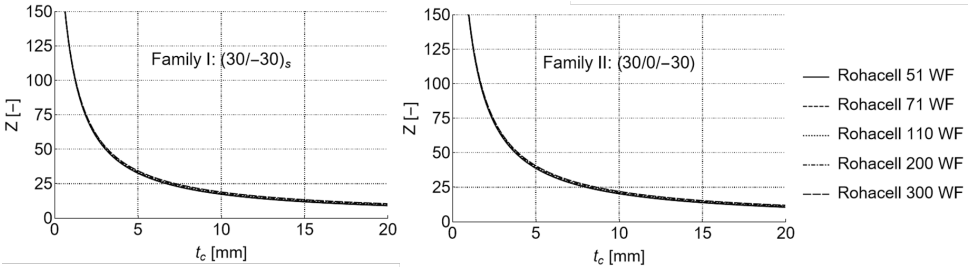

Figure 5.9: Variation of Z with respect to the radius for different foam core materials ($R = 400$ mm).

As previously discussed, the nondimensional buckling load is extremely sensitive to changes in Z, and therefore, achieving good agreement for this parameter is paramount to establish a reliable scaling strategy. The linear relationship between Z and the radius, along with its strong dependency on core thickness, emphasizes the need for accurate characterization and control of these factors in this methodology. This precision is essential to ensure that the scaling strategy effectively captures the critical buckling behavior, enabling us to extrapolate meaningful results for various structures and conditions.

However, it is important to note that the two main parameters that can be modified, namely the radius and the core thickness, are often subject to limitations imposed by manufacturing and laboratory constraints. These constraints may include practical limitations on the range of sizes that can be produced or tested, as well as restrictions related to available materials and equipment. A sensitivity analysis of these parameters is discussed in Section 5.3, as they are integral to determining the feasibility and applicability of the scaling approach in real-world engineering contexts.

The final parameter to evaluate is the transverse shear parameter: χ_1, which is a function of radius, axial and circumferential membrane compliances, and bending stiffness.

Given that the facesheet stacking sequence and R/L for the scaled configurations have been selected, as well as the radius and core thickness, the baseline value of χ_1 could be maintained with the appropriate core material. Of course, this is less straight-

forward than the other choices because, the core material has multiple variable coupled together.

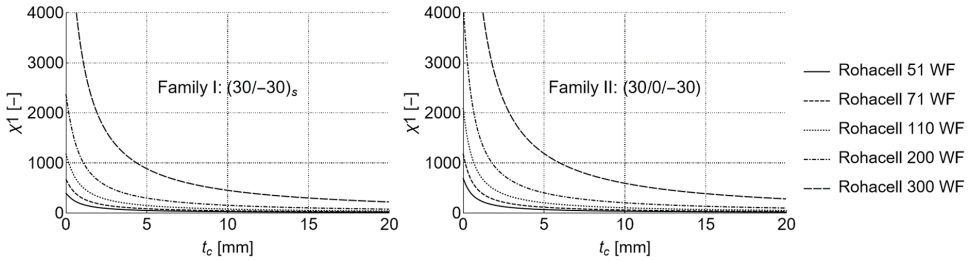

Figure 5.10: Variation of χ_1 with respect to the core thickness for different foam core materials (R=400mm).

It is important to note that the χ_1 parameter, like the Z parameter, has a strong influence of the radius and core thickness. However, the trends are quite distinct. It is observed in Fig. 5.11 that the value of χ_1 varies with the changes in the radius.

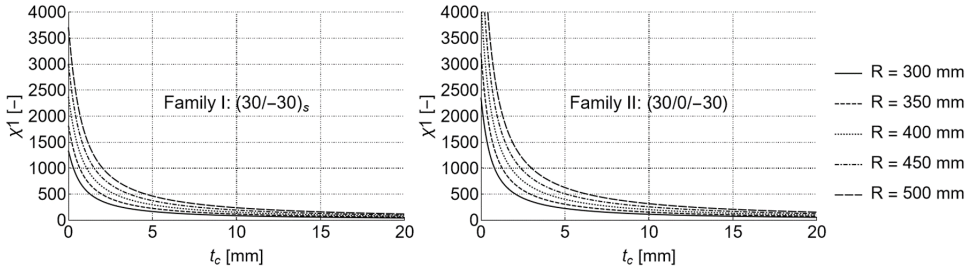

Figure 5.11: Variation of χ_1 with respect to the thickness for a core material Rohacell 200WF for different values of core thickness.

It can also be observed, that, unlike the Z parameter, χ_1 parameter does have a strong dependence in the core material, specially of the shear modulus. This phenomena can be seen in Fig. 5.10, where material with a higher shear modulus (Rohacell 300WF, G=360 MPa) will have much higher values of χ_1, than a material with a lower shear modulus (Rohacell 71WF, G=34 MPa). This phenomena can be utilized to achieve reasonable agreement with the value of the baseline structure, without modifying the obtained core thickness and radius from parameter Z. Reevaluating the core material at this late stage allows for a better agreement in all non-dimensional parameters without compromising the value of Z.

The process outlined can be summarized in Fig. 5.2, where the values of the facesheet angle, length, core thickness and core material are set up. All the configurations that correspond to the baseline structures described in Table 5.1 are presented in Appendix A.

To discuss the quality of the scaling, the scaled structures of Baseline 1 are also presented in Table 5.3. These scaled structures correspond to the closest match of parameters in each of the scaling steps. However, matching exactly all the parameters is not

possible. It is particularly hard to match exactly the value of χ_1, because the suitable materials are not available at a required precise transverse shear value.

Table 5.3: Scaled Structures Properties for the Scaling Strategy 1 of Baseline 1.

Shell	Lay-up	Length [mm]	Core thickness [mm]	Core Material	Buckling Load [kN]
Scaled 1.1.I.1	(17/-17)s	1261	1.8	Rohacell 300 WF	730
Scaled 1.1.I.2	(73/-73)s	388	1.8	Rohacell 300 WF	713
Scaled 1.1.II.1	(23/0/-23)	1220	2.0	Rohacell 300 WF	586
Scaled 1.1.II.2	(56/0/-56)	731	1.9	Rohacell 300 WF	786

Table 5.4: Buckling Response.

Shell	Nondimensional Buckling Load [-]	Buckling Load [kN]	m [-]	n [-]
Baseline 1	565	4706	10	1
Scaled 1.1.I.1	556	730	11	1
Scaled 1.1.I.2	543	713	11	1
Scaled 1.1.II.1	567	586	10	1
Scaled 1.1.II.2	551	786	11	1

A way to visualize the error is shown in Fig. 5.12, where the nondimensional parameters involved in the scaling methodology are plotted, along with the final nondimensional load. The graph represents the relative error of each nondimensional parameter of the scaled structures with respect to Baseline 1, as detailed in Table 5.2. From the graph, it is evident that structure 1.1.II.1 offers the best overall match, including a low 6% discrepancy in χ_1, resulting in the smallest error in the final nondimensional buckling load, $\mathscr{F}$ (less than 1%). This suggests that 1.1.II.1 is a strong candidate for scaled testing.

However, this choice must be weighed against manufacturing constraints. For instance, structure 1.1.II.1 requires a core thickness of 2 mm using Rohacell 300WF foam. The typical thickness tolerance for this material is ±0.2 mm, representing a 10% variation. Due to the linear dependency of Z on the thickness, this variation could have a substantial influence on the actual buckling load in the manufactured specimen. Nev-

ertheless, this limitation is shared by all the configurations under consideration, as they all use the same material and have similar core thicknesses (1.8–1.9 mm).

The observed error values for μ and β stem from their strong sensitivity to the precise angle used, as shown in Fig. 5.3. In particular, these parameters change rapidly in the ranges between 0–30° and 60–90°, making them especially susceptible to small angular deviations. On the contrary, for ranges between 30–60°, the error is very small as testified by 1.1.II.2. Also in this case manufacturing considerations play a role, as producing structures with angles defined to decimal precision is impractical.

Another interesting observation is that although a better match of χ_1 typically improves scaling accuracy, the nondimensional buckling load $\mathscr{F}$ can still be closely approximated if other parameters, especially Z, are accurately scaled.

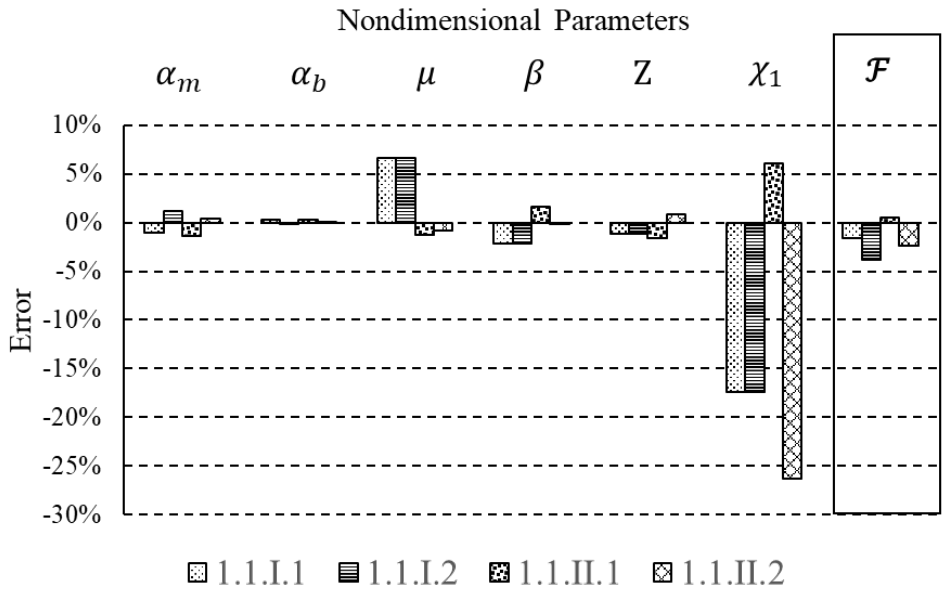

Figure 5.12: Error in the Nondimensional Parameters between Baseline 1 and the Scaled Structures with Scaling Strategy 1.

When comparing the Baseline 1 and the Scaled 1.1.II.1 more closely, we can see that not only the nondimensional buckling load is matched but also the buckling pattern (m,n). The dimensional and nondimensional buckling values for the structures depicted in Fig. 5.12 are reported in the Table 5.4.

5.2.2. SCALING STRATEGY 2

IN the Scaling strategy 2, as shown in Fig. 5.1, the cylindrical structure that needs to be scaled (the baseline configuration) is still a cylindrical sandwich composite shell with carbon fiber facesheets and an aluminum honeycomb core. However, unlike Scaling strategy 1, the result of structural scaling (scaled configuration) is not a cylindrical sandwich composite shell. In this case, the scaled configuration is a composite laminate. The material of this composite laminate may be different from the material of the composite laminate that conforms to the facesheets of the baseline configuration. The full strategy outline is depicted in Fig. 5.13 and will be described step by step in this section.

For the scaled cylindrical composite shell, a large number of different stacking sequences are possible. For the purpose of this study, six families of stacking sequences are considered for the facesheets. Again like in the Scaling strategy 1, the methodology is amenable to other families of stacking sequences. All stacking sequences are a function of only two variables: the ply angle θ and the number of repetitions r. These facesheet stacking sequence families are:

- Family I: A unsymmetric laminate with 2r layers $([\theta/-\theta])_r$
- Family II: A unsymmetric laminate with 3r layers $([\theta/0/-\theta])_r$
- Family III: A symmetric laminate with 4r layers $([\theta/-\theta]_s)_r$
- Family IV: A symmetric laminate with 5r layers $([\theta/-\theta/9\bar{0}]_s)_r$
- Family V: A symmetric laminate with 6r layers $([\theta/0/-\theta]_s)_r$
- Family VI: A symmetric laminate with 7r layers $([\theta/0/-\theta/9\bar{0}]_s)_r$

Note that in this case, unlike in the Scaling strategy 1, in order to be able to compare the sandwich shell from the baseline shell and composite laminate from the scaled shell, the buckling equations: Eq. (3.102) and Eq. (3.103)) are formulated under the assumptions that transverse-shear deformations can be neglected. The considered equations also neglect the bend-twist anisotropy effects. In particular, as shown in detail in Chapter 3, neglecting transverse-shear deformations may not be universally valid. This assumption will limit the effectiveness of the scaling and thus must be closely monitored.

The buckling response in this strategy is formulated with the five nondimensional parameters: μ, β, α_m, α_b, and Z. The transverse deformation parameter χ_1 is not included here because the scaled structure does not include a core material. The nondimensional parameters are used as the metrics to describe similarity, and, as in the previous strategy, the nondimensional buckling responses of different cylinders with identical nondimensional parameters should be identical.

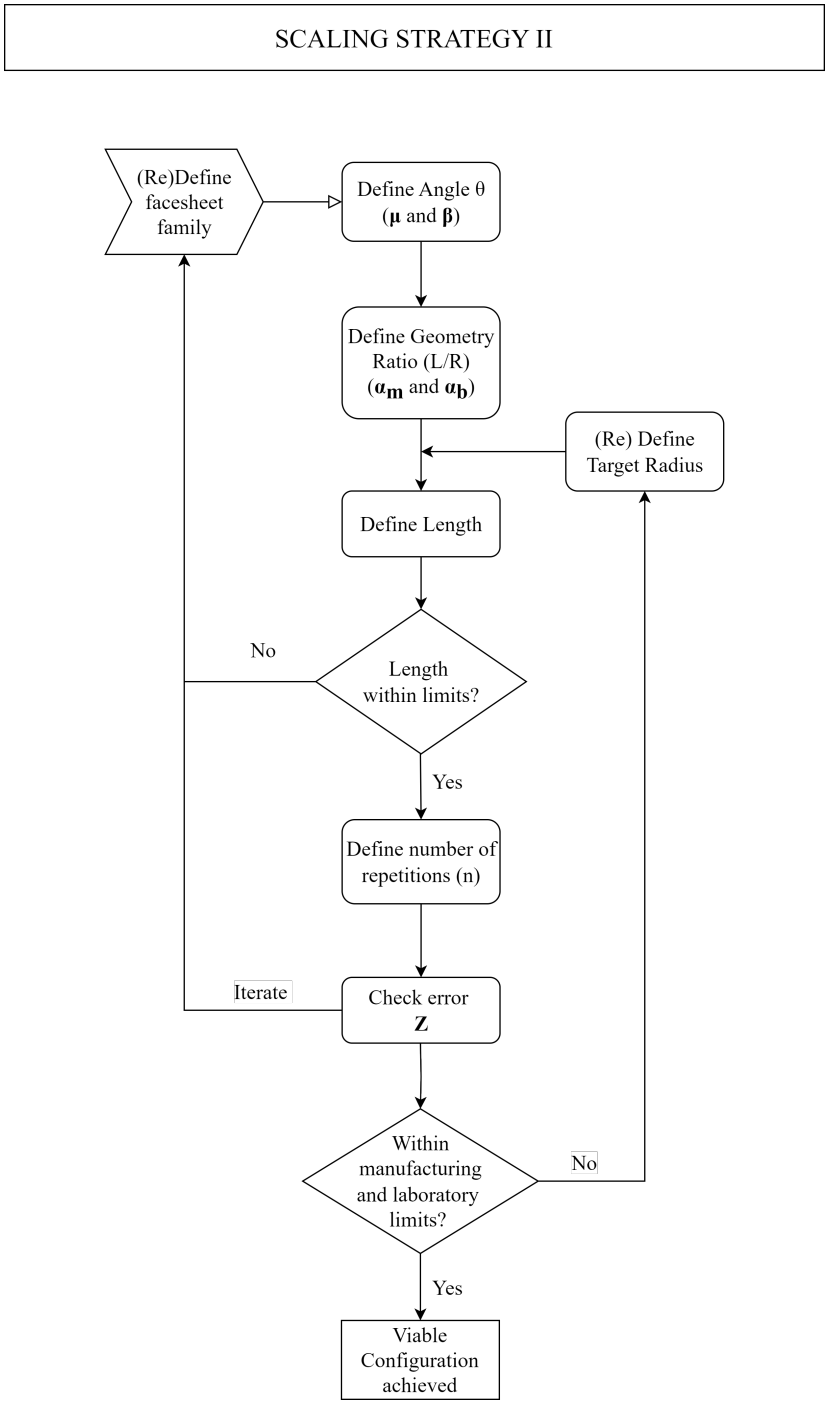

Figure 5.13: Diagram of Scaling Strategy 2.

Similarly to Section 5.2.1, the first pair of parameters considered in the scaling methodology are the membrane orthotropy parameter, μ, from Eq. (3.40), and the flexural orthotropy parameter, β, from Eq. (3.53). The two parameters relate the in-plane compliance matrix and the bending stiffness matrix parameters, and in this case, they are a function of the material properties and the ply stacking sequence. Therefore, given a specific facesheet material, the membrane and the flexural orthrotopy parameter can be established by the angle value θ and the number of repetitions r.

From the curves in Figs. 5.14 to 5.19, it can be seen that there's no variation of the orthotropy parameter μ on the number of repetitions.

On the other hand there is a substantial variation of the orthotropy parameter β depending on the number of repetitions for some families. In particular, Family II (Fig. 5.15), Family IV (Fig. 5.17), Family V (Fig. 5.18) and Family VI (Fig. 5.19) show some variability, while Family I (Fig. 5.14) and Family III (Fig. 5.16) don't.

The influence of the number of repetitions is quite high for a low number of repetitions (low laminate thickness). Therefore it is recommended to start the scaling process assuming a number of repetitions equal to 3 and iterate later if necessary. By assuming that the number of repetitions is equal to 3 or higher, the influence of the facesheet repetitions can be considered negligible for all the considered patterns, and thus establishing that the driving parameter is the angle θ.

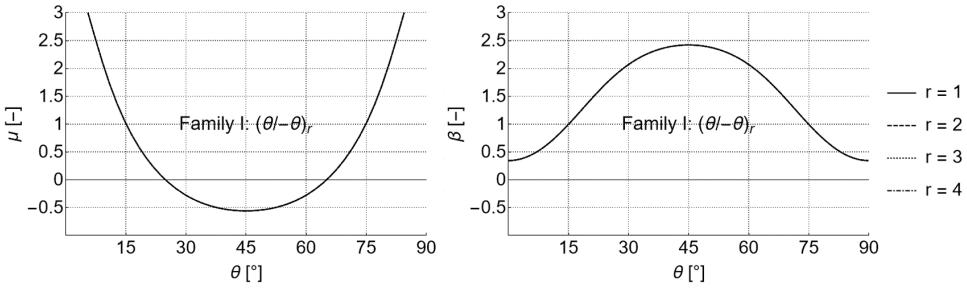

Figure 5.14: Variation of μ and β with respect to θ for Family I.

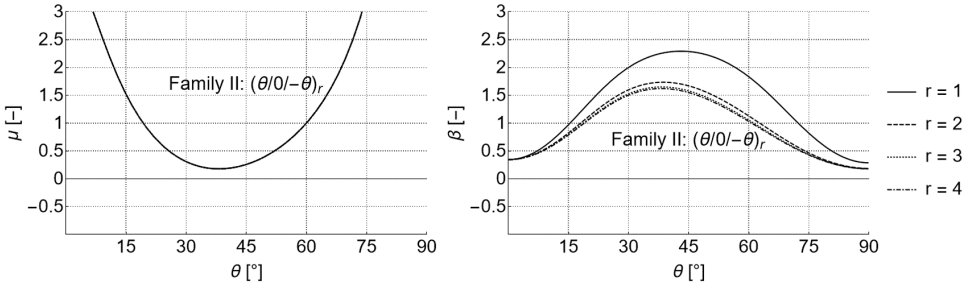

Figure 5.15: Variation of μ and β with respect to θ for Family II.

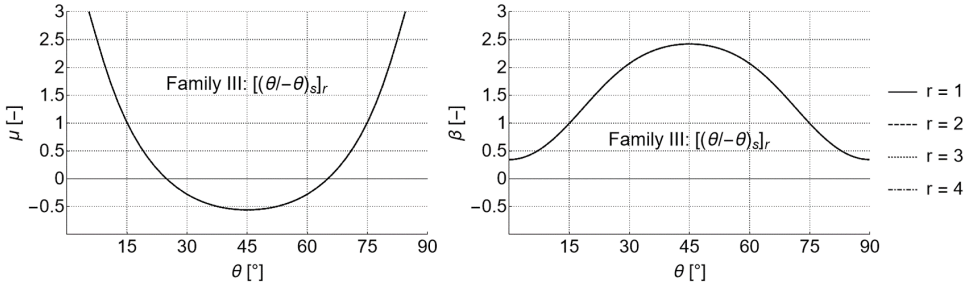

Figure 5.16: Variation of μ and β with respect to θ for Family III.

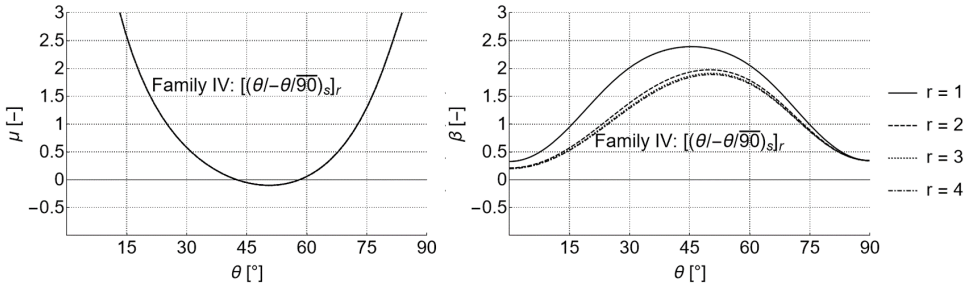

Figure 5.17: Variation of μ and β with respect to θ for Family IV.

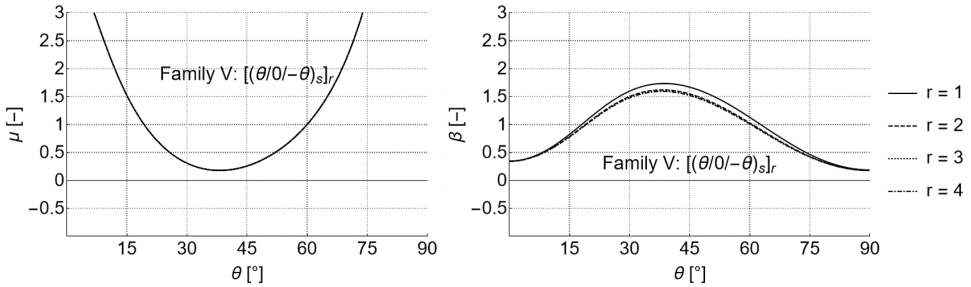

Figure 5.18: Variation of μ and β with respect to θ for Family V.

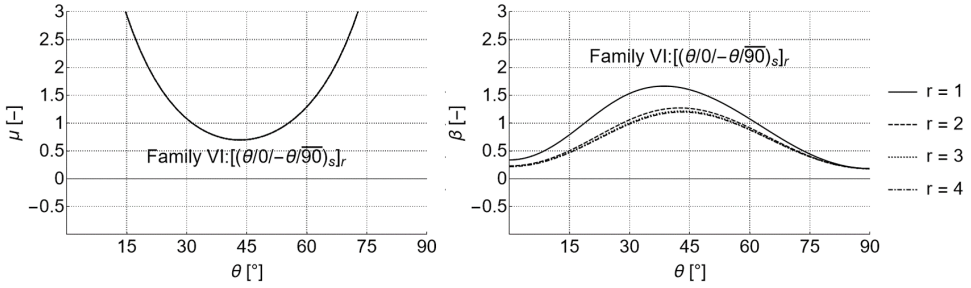

Figure 5.19: Variation of μ and β with respect to θ for Family VI.

Examining the distinctions among families facilitates an understanding of their differences and clarifies the contexts in which certain families are more appropriate for specific purposes. For example, Family I and Family III exhibit a perfectly symmetrical curve, while the other families display a slight inclination towards either the 0 or 90 direction, contingent upon the values incorporated in the stacking sequence.

From the curves in Figs. 5.14 to 5.19, the angles required for each family to maintain the baseline values of μ and β are obtained. For the laminate families considered, there are two possible angles that produce equivalent membrane and flexural orthotropy parameters, and therefore two possible configurations for the scaled cylindrical shells.

Therefore, in most cases, there will be two possible solutions for scaled configurations. In this case, a similar labeling scheme to that defined in Scaling strategy 1 shown in Fig. 5.5 will be used. For instance, the scaled models from Baseline 1 will range from Scaled 1.2.I.1 to Scaled 1.2.VI.2. The labeling scheme can be seen in the Fig. 5.20.

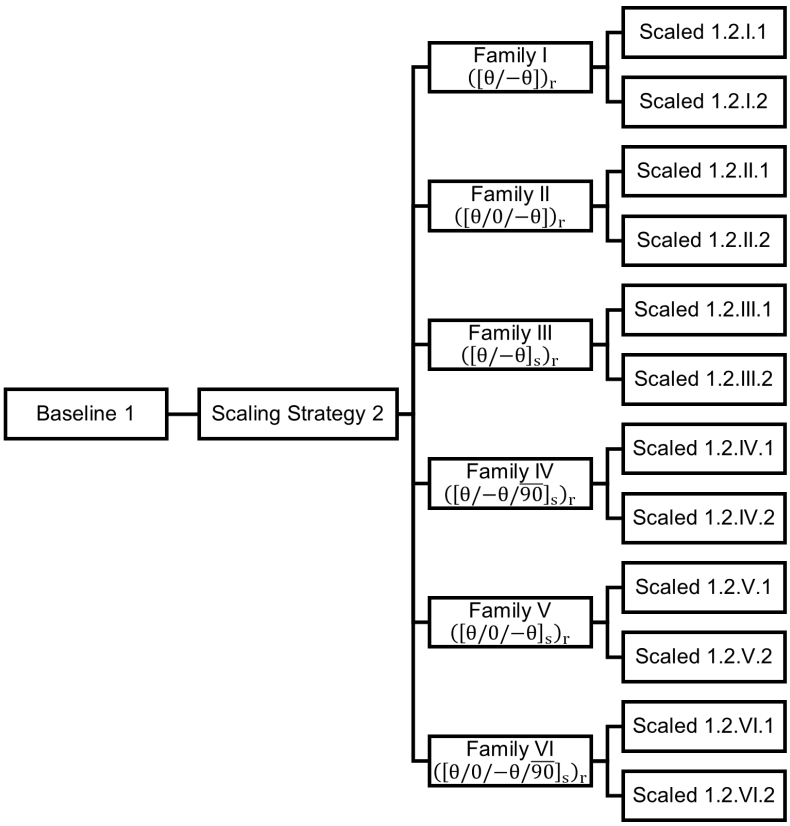

Figure 5.20: Labelling scheme for the scaled configurations in the Strategy 2.

After the ply angle for each stacking sequence has been defined, the next parameters

to be evaluated are α_m (Eq. (3.35)) and α_b (Eq. (3.39)). Both parameters are a function of the ratio (R/L), the ply angle (θ) and the number of repetitions (r) .

Given that the ply angle θ has been established, it can be proven that the impact of the pattern repetition is also negligible for these two parameters. This is attributed to the fact that the pattern repetition (r) contributes to numerator and denominator in similar ways in both Eq. (3.35) and Eq. (3.39), a similar phenomenon already observed for in Scaling strategy 1 with the thickness. Thus, pending a final iteration, the pattern repetition is set aside in this step.

As a result, it is considered that for a given facesheet stacking sequence, the relationships between the parameters α_m and α_b and R/L are linear. This means that for each value of the α_m and α_b parameters, a single solution can be found for R/L.

This can be observed in Figs. 5.21 to 5.26 where the values of the parameters α_m and α_b are obtained as a function of the geometry ratio R/L for Family I, for different ply angles θ.

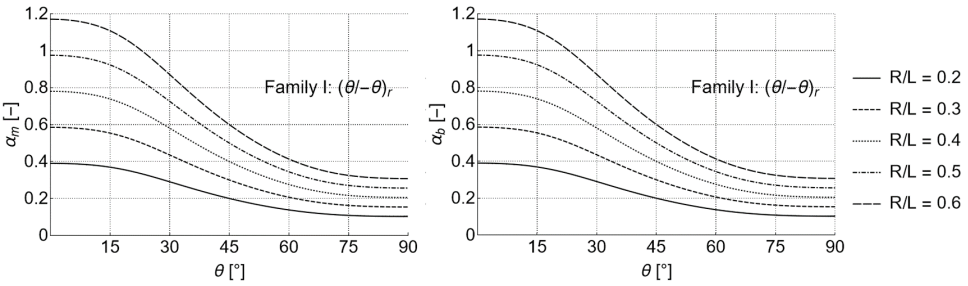

Figure 5.21: Variation of α_m and α_b with respect to θ for Family I.

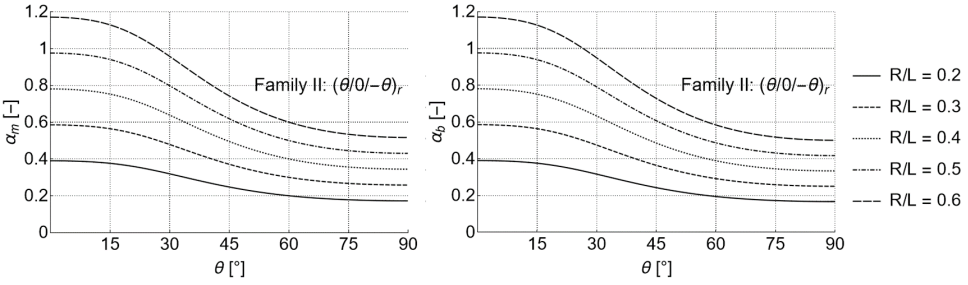

Figure 5.22: Variation of α_m and α_b with respect to θ for Family II.

The final parameter to evaluate is the Batdorf-Stein Z (Eq. (3.19)) which is a function of radius, axial and circumferential membrane compliances, and bending stiffness. This parameters represents the ratio between Radius and equivalent thickness. Given that the facesheet stacking sequence and R/L for the scaled configurations have been down selected, the baseline value of Z can be maintained in the scaled configurations with the

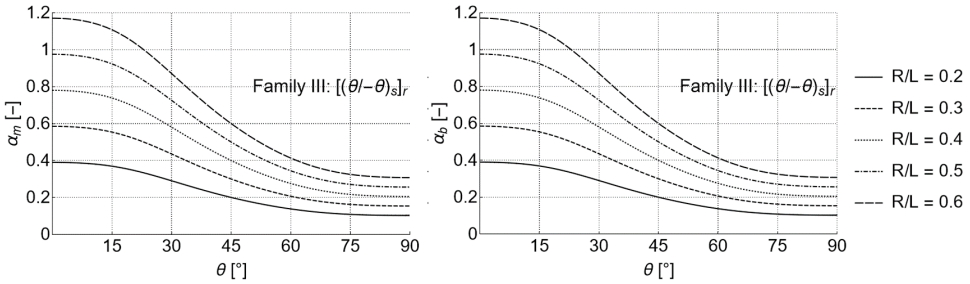

Figure 5.23: Variation of α_m and α_b with respect to θ for Family III.

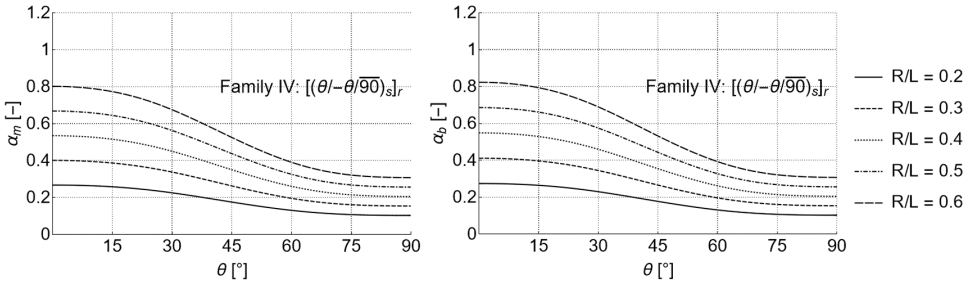

Figure 5.24: Variation of α_m and α_b with respect to θ for Family IV.

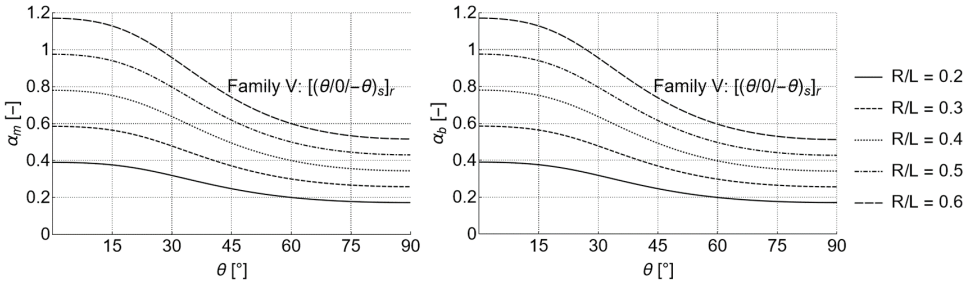

Figure 5.25: Variation of α_m and α_b with respect to θ for Family V.

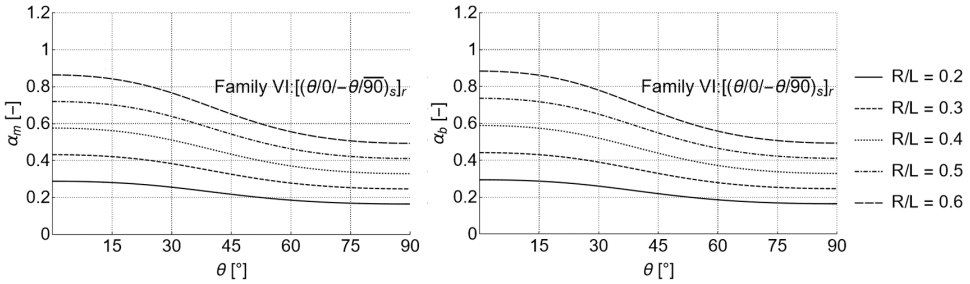

Figure 5.26: Variation of α_m and α_b with respect to θ for Family VI.

right combination of radius, R, and facesheet repetition, r.

The observations shown in Figs. 5.27 to 5.29 reveal a linear correlation between the Z parameter and the radius, with a particularly pronounced sensitivity to the repetition parameters, especially evident at lower values. These findings demonstrate the significant impact of repetition parameter on the Z parameter.

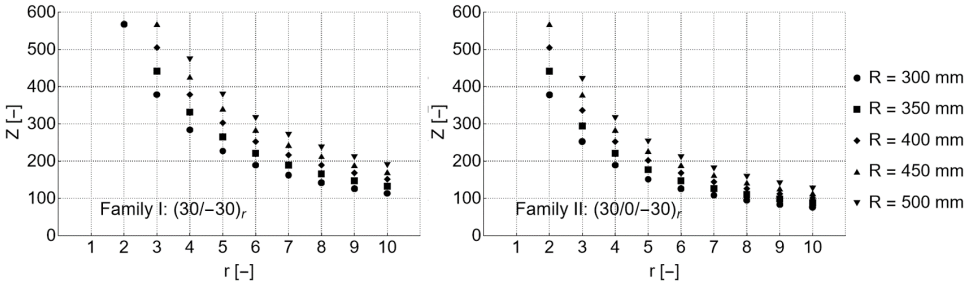

Figure 5.27: Variation of Z with respect to the radius for Families I-II for $\theta = 30°$.

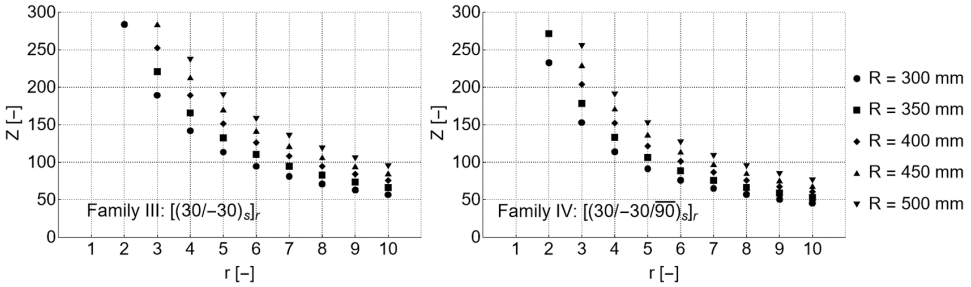

Figure 5.28: Variation of Z with respect to the radius for Families III-IV for $\theta = 30°$.

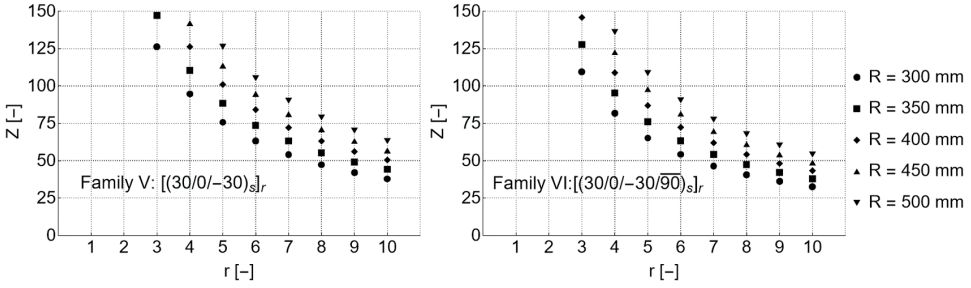

Figure 5.29: Variation of Z with respect to the radius for Families V-VI for $\theta = 30°$.

The process outlined can be summarized in Fig. 5.13, where the values of the facesheet angle, number of lay-up repetitions and length are set up. The configurations for Scaling strategy 2 that correspond to the baseline structures described in Table 5.1 are also presented in Appendix A.

However, to discuss the quality of the scaling, the scaled structures of Baseline 1 are isolated in this case and shown in Table 5.5. These scaled structures correspond to the closest match of parameters in each of the scaling steps.

The first observation that can be made is that some of the scaled structures are identical. The scaled structures from Family II and Family V are the same due to the even number of repetitions in Family II. The same happens with the scaled configurations of Family I and Family III. This even repetition results in no distinction between the two families, leading to the same properties for both and, logically, the same buckling response.

Table 5.5: Scaled structures properties for the Scaling Strategy 2 of **Baseline 1**.

Shell	Facesheet lay-up	Total thickness [mm]	Length [mm]	Buckling Load [kN]
Scaled 1.2.I.1	$(17/-17)_{12}$	4.21	1267	2214
Scaled 1.2.I.2	$(73/-73)_{12}$	4.21	387	2210
Scaled 1.2.II.1	$(23/0/-23)_8$	4.21	1229	2278
Scaled 1.2.II.2	$(56/0/-56)_8$	4.21	733	3431
Scaled 1.2.III.1	$([17/-17]_s)_6$	4.21	1267	2214
Scaled 1.2.III.2	$([73/-73]_s)_6$	4.21	387	2210
Scaled 1.2.IV.1	$([28/-28/9\bar{0}]_s)_5$	4.38	811	3666
Scaled 1.2.IV.2	$([70/-70/9\bar{0}]_s)_5$	4.38	392	2441
Scaled 1.2.V.1	$([23/0/-23]_s)_4$	4.21	1229	2278
Scaled 1.2.V.2	$([56/0/-56]_s)_4$	4.21	733	3431
Scaled 1.2.VI.1	$([40/0/-40/9\bar{0}]_s)_4$	4.91	808	4566
Scaled 1.2.VI.2	$([47/0/-47/9\bar{0}]_s)_4$	4.91	744	4681

One of the drawbacks of this methodology is that the number of repetitions (r), unlike the core thickness of the Scaling strategy 1, is an integer, and therefore an exact match of the Batdorf-Stein parameter is not possible for all families. For instance, for Family VI which is the family with the highest number of plies, the error for Z, as seen in Fig. 5.30, is 13%, which is larger than for other families. Choosing the right family for each baseline structure will be an essential part of the process.

The error of all the nondimensional parameters included in this scaling strategy is shown in Fig. 5.30. The graph represents the difference between the value of the baseline nondimensional parameter of each scaled structure with respect to the values of Baseline 1 as reported in Table 5.2.

Another interesting detail is that even in cases where the error in all parameters is under 4%, such as Scaled Structures 1.2.III.1 and 1.2.III.2, the nondimensional buckling load error is larger, approximately 9%. This difference is built in the assumptions of the second scaling strategy that tries to replicate the buckling response of sandwich composite laminate.

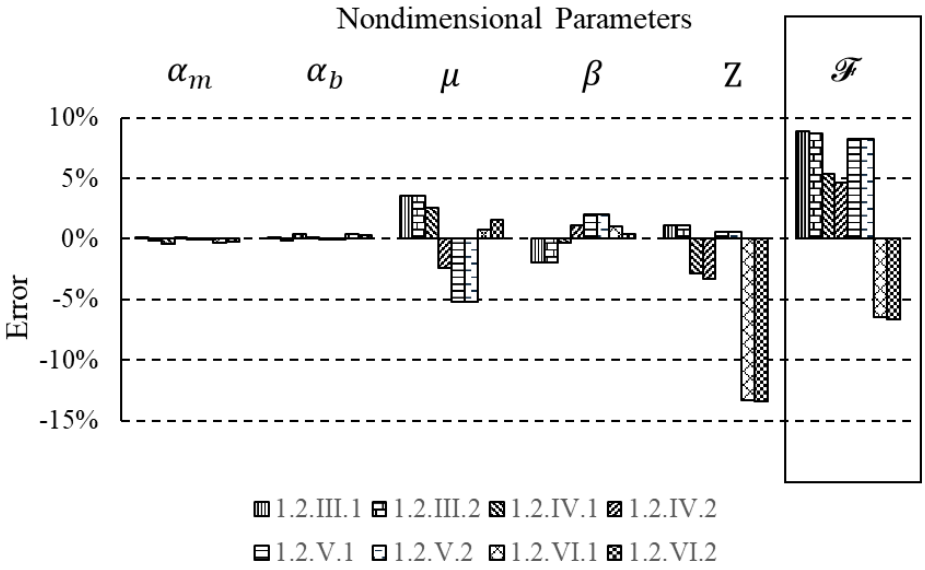

Figure 5.30: Error in the Nondimensional Parameters between Baseline 3 and the Scaled Structures with Scaling Strategy 2.

For Baseline 1 where $\chi_1 \approx 2000$ and $Z \approx 90$, as show in Chapter 3, the difference between the buckling load including or not including the transverse shear effects is already 8%. This built-in discrepancy must be accounted for when selecting the right scaling strategy.

When comparing Baseline 1 and the Scaled Structures more closely, another important thing to consider in the buckling pattern (m,n). The nondimensional and dimensional buckling load values as well as the buckling pattern are reported in Table 5.6. Overall it seems that this second scaling strategy, even accounting for the implicit error of neglecting the transverse shear effects, also produces reasonable results that would be able to replicate the buckling response of the Baseline structure.

Table 5.6: Buckling Response

Shell	Nondimensional Buckling Load [-]	Buckling Load [kN]	m [-]	n [-]
Baseline 1	565	4706	10	1
Scaled 1.2.III.1	616	2214	10	1
Scaled 1.2.III.2	615	2210	10	1
Scaled 1.2.IV.1	596	3666	10	1
Scaled 1.2.IV.2	592	2441	10	1
Scaled 1.2.V.1	612	2278	10	1
Scaled 1.2.V.2	612	3431	10	1
Scaled 1.2.VI.1	529	4566	9	1
Scaled 1.2.VI.2	528	4681	9	1

5.3. SENSITIVITY STUDY OF THE GEOMETRICAL PARAMETERS

EACH scaling approach has advantages and disadvantages. For the most part, it would be ideal to use the first methodology, since the scaled and baseline structures have a similar construction. However, this is not always possible. For instance, available laboratory testing equipment constrains radius (R) values, and the minimum manufacturable core thickness constrains the lower bound for this variable (t_{core}).

For this reason, it is important to assess how robust are the structures produced with the different methodologies to parameter variations. Thus, the sensitivity of the different input parameters into the nondimensional parameters is discussed in the section. As described, each of the scaling strategies can generate multiple design options. These scaled designs also provide a range of options to choose from. Each of these design options offers a variety of advantages and drawbacks, depending on the specific application. The user must select the design option that best suits their needs, taking into account the manufacturing constraints, the size of the available laboratory facilities and the required scaling accuracy.

There are four parameters that were considered in the sensitivity analysis of Scaling strategy 1: ply thickness, core thickness, radius and length. For the scaled configurations reported in Table 5.3, the nominal ply thickness used is 0.175 mm, as reported by the manufacturer. For the ply angle, in the scaled configurations reported, the closest integer was chosen for determining the ply angle. The shell radius, fixed to a nominal value of $R = 400$ mm for the reported configurations in Table 5.3. Finally, for the shell length, in the scaled configurations reported, the closest integer was chosen.

For these four factors, the sensitivity analysis is shown in Fig. 5.31. As anticipated, the core thickness and the radius have an large importance in the quality of the scaling.

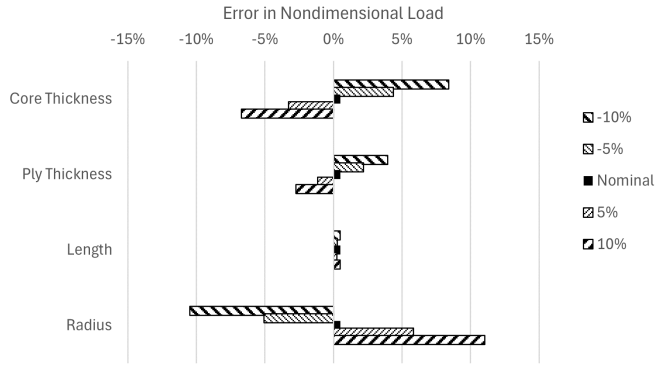

Figure 5.31: Sensitivity to geometrical parameters for Scaled 1.1.II.1 in the Buckling Nondimensional Load.

On the other hand, there are only three parameters that were considered in the sensitivity analysis of Scaling strategy 1: ply thickness, core thickness, radius and length. For the scaled configurations reported, the nominal ply thickness used is 0.175 mm, as reported by the manufacturer. For the ply angle, in the scaled configurations reported, the closest integer was chosen for determining the ply angle. The shell radius, fixed to a nominal value of R=400mm for the reported configurations. Finally, for the shell length, in the scaled configurations reported, the closest integer was chosen.

For these three factors, the sensitivity analysis is shown in Fig. 5.32. Since the nominal case here has an already much larger error in the Nondimensional Load, this is compounded with the importance of the ply thickness, the length and the radius.

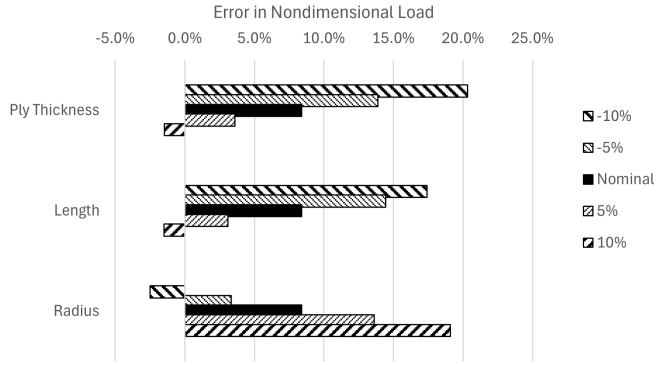

Figure 5.32: Sensitivity to geometrical parameters for Scaled 1.2.V.1 in the Buckling Nondimensional Load.

5.4. CONCLUSIONS

THIS chapter presents an analytical scaling methodology designed to study the buckling behavior of large, compression-loaded sandwich composite cylindrical shells. This approach is based on the nondimensionalization of buckling equations presented in Chapters 3 and 4.

The baseline structures analyzed are from the Shell Buckling Knock-Down Factor (SBKF) program [129], focusing on large sandwich composite cylindrical shells made from carbon fiber facesheets and aluminum honeycomb cores. All the baseline configurations share similar dimensions, with a radius of 1.2 meters and a length of 2.3 meters, though they differ in the thickness and stacking sequence of the materials. These baseline designs serve as references for applying the scaling methodology.

Two scaling strategies are introduced in the study. The first strategy scales from a baseline sandwich structure to a smaller sandwich shell, maintaining the same structural characteristics but encountering manufacturing challenges, particularly with producing scaled thicknesses. This method works by adjusting the geometry and material properties to match the nondimensional buckling response of the original structure. The second strategy scales the sandwich composite shell to a monolithic laminate structure. While this approach avoids the manufacturing limitations of the first strategy, it introduces new challenges, especially in comparing the buckling behavior of two different structural types. In this strategy, transverse shear deformations are neglected, leading to inaccuracies in predicting the buckling response.

A sensitivity study of the geometrical parameters, such as core thickness, ply thickness, radius, and length, was conducted for both strategies. The results show that the thickness and radius are the most influential factors in determining the accuracy of the scaled models. Scaling strategy 1 is more sensitive to these variations, though it provides a closer match to the buckling behavior of the baseline structures. Strategy 2, although easier to implement due to fewer manufacturing constraints, introduces inherent errors, particularly when transverse shear effects are significant.

In conclusion, the scaling strategies outlined in this dissertation effectively facilitate the examination of buckling behavior in large composite shell structures through testing at reduced dimensions. While Scaling strategy 1 provides a more accurate reproduction of the original structure's behavior, it faces practical manufacturing constraints. Scaling strategy 2, on the other hand, is more practical but less accurate due to the assumptions made in the modeling process. Both strategies provide valuable insights and contribute to the broader understanding of scaling techniques in structural analysis.

6

Numerical Analysis and Comparison with Available Data

Observar sin pensar
es tan peligroso como
pensar sin observar.

Santiago Ramon y Cajal

The objective of this chapter is to contrast the theoretical results obtained from the nondimensional formulation outlined in Chapters 3 and 4 as well as the scaling methodology of Chapter 5 with the numerical analysis and available experimental results. Two particular cases are examined, one at the full scale (CTA8.1) and the other at the laboratory scale (NDL-1), as the results of both experiments have been published [16, 132].

The outcomes of these tests will yield insights into the structural behavior and the validity of the scaling methodology, as the test specimen NDL-1 was developed using the second strategy of the scaling methodology. The specimen NDL-1 was designed using configuration Scaled 1.2.V.1 as the starting point.

Scaled 1.2.V.1 may appear to be an odd choice among all of the configurations proposed in Chapter 5 for Baseline 1. For example, Scaled 1.1.II.1 had a significantly lower

error in the nondimensional buckling load than Scaled 1.2.V.1, with an error of 0.5% versus 8.4%. The reason for choosing a structure of the second scaling strategy instead of the first one lies in the difficulty of manufacturing precisely the core thickness of 2 mm, required for this configuration. As shown in Fig. 5.31, there is a high sensitivity to the core thickness on the scaling quality. Manufacturing tolerances for this foam are reported to be 1 mm, which would be a large variation and therefore the lower nondimensional error would not be achieved.

Even then, other configurations of the second scaling strategy have lower nondimensional error than Scaled 1.2.V.1. For instance Scaled 1.2.IV.1 and Scaled 1.2.IV.2, as well as Scaled 1.2.IV.1 and Scaled 1.2.IV.1 both have values around 5% error. The reason for avoiding these configurations was the difficulty in using the 90° ply in the hand-laid manufacturing that was used here. Other reasons for rejecting configurations were a high buckling load, higher than the maximum 2500 kN the machine provided, and a very short length, which would have made the load introduction path challenging.

Scaled 1.2.V.1 was also modified with respect to the ideal configuration due to laboratory limitations. The length required was 1229 mm was reduced to 1220 due to the maximum mandrel size available. However, this reduction in the length is only 1% and the influence of the length has already proved in Fig. 5.32 to be small in the quality of the scaling.

The process of designing NDL-1 from CTA8.1 is depicted in Fig. 6.1. The scaling strategies proposed in Chapter 6 only apply to the idealized shells; they do not apply to test articles with additional features required for experiments. Therefore, Baseline 1 and Scaled 1.2.V.1, two simplified shell designs, were used as a bridge between the CTA8.1 and NDL-1 designs.

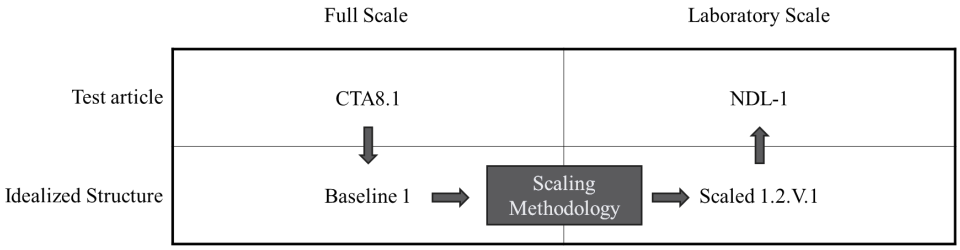

Figure 6.1: Chart showing the test articles and idealized structures considered.

A major difference between CTA8.1 and Baseline 1, and between NDL-1 and Scaled 1.2.V.I are the pad-ups and potting surfaces. Pad-ups assist in transferring load from the edge regions to the central portion of the shell. Furthermore, they induce buckling to occur in this central acreage during testing, thus ensuring that the stability phenomenon can be studied in a controlled manner. The introduction of the pad-ups reduced the effective length of the shell further, as well as added some increased stiffness due to the extra plies.

On top of the pad-ups, the test specimens also include potting and end rings. They act as stabilizing media that provide a partial clamping effect on the shell's edges; this is not a fully clamped condition because the potting itself is able to deform. The potting's surface area also helps facilitate load transfer from the test apparatus into the shell by minimizing the risk of damage to the the shell's edges.

The structures were studied first via numerical analysis. The simulations were performed using the finite element analysis (FEA) software Abaqus. First, the goal is to show that the analytical model produced accurate results that closely matched those obtained from numerical simulations. Then, the results of numerical simulations are compared to determine the efficacy of the scaling method. Finally the test results are contrasted and the quality of the scaling this case assessed.

6.1. NUMERICAL ANALYSIS

IN this section, numerical analysis will be applied to the idealized structures described in Fig. 6.1. Broadly speaking, Abaqus offers two types of elements that are suitable for the three-dimensional analysis of thin-walled shells: conventional shell elements and continuum shell elements seen in Fig. 6.2.

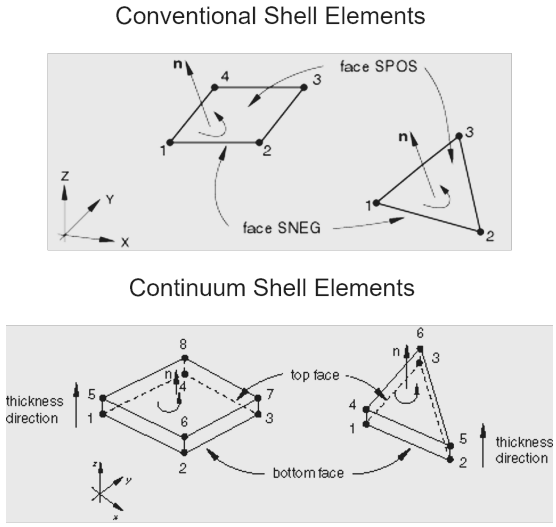

Figure 6.2: Element types used in the simplified analysis. [1]

Both static and dynamic methods can utilize the conventional shell elements included in Abaqus. Some elements, such as S4S, incorporate the influence of transverse shear deformation and thickness variation. Continuum shells fully discretize a three-

[1] From the Abaqus Analysis User's Manual

dimensional body, as opposed to conventional shells that just discretize a reference surface. The continuum shell elements are versatile because they enable finite membrane deformation and significant rotations, making them well-suited for nonlinear geometric analysis. These factors encompass the influence of transverse shear deformation and variations in thickness, which are relevant to the proposed analysis.

Continuum shell elements utilize the principles of first-order layer-wise composite theory. Unlike traditional shells, continuum shell elements allow for stacking to achieve a more precise response throughout the thickness. By stacking continuum shell pieces, it becomes possible to make more accurate predictions of transverse shear stress and force, as well as anticipate the force that causes pinching across the thickness. It is important to use caution while stacking a limited number of continuum shell parts, as the convergence may not follow a consistent pattern.

To assess the different elements and their suitability to capture the transverse shear impact in the buckling behaviour for the different scale changes, the set of linear analyses was executed by using the two types of elements: S4R, and SC8R. The S4R is a conventional stress/displacement shell element with 4 nodes and reduced integration, and the SC8R eight-node continuum shell element with reduced integration.

The comparison of both elements resulted from initial uncertainty about which was best for this particular problem. In Chapter 3, the conventional element was used for the initial analytical model verification. However, thinner core shells demonstrated a greater effect of transverse shear, suggesting the need for a more complex element to accurately depict the transverse shear for the sandwich structure.

6.1.1. LINEAR ANALYSIS

The linear eigenvalue analyses of the baseline and scaled cylindrical shell will be the primary focus of this section. These analyses were carried out to provide a set of buckling loads before making the transition to non-linear analyses. A linear perturbation step, which calculates the stiffness matrix eigenvalues, is commonly used to calculate cylindrical sandwich shell critical buckling loads. The lowest eigenvalue indicates the basic buckling load, while each eigenvalue is a scaling factor used to the specified load to attain a critical buckling situation. The related eigenmodes reveal shell buckling patterns under loads.

The analytical equations are formulated under simply supported conditions; therefore, these conditions are also applied in the numerical analysis. Axial compressive forces are applied uniformly along the shell's top using a surface load. Mesh size also has an impact on the accuracy of eigenvalue buckling analysis. A highly meshed model better represents local deformations and stress gradients, especially near high curvature or abrupt geometry changes. Mesh convergence investigations should ensure that refinement does not affect eigenvalues. For the Baseline 1, as defined in table Table 5.1,

the mesh convergence analysis can be seen in Fig. 6.3. It can be seen that both types of elements (S4R and SC8R) converge to a solution below 1% of error in under 2000 elements.

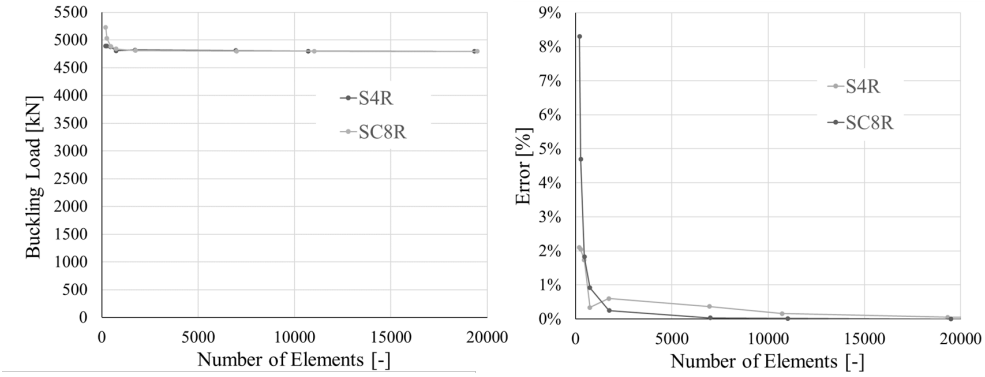

Figure 6.3: Mesh Convergence analysis of Baseline 1.

Looking directly at the buckling load values, in Table 6.1, as expected based on the literature, the numerical buckling load and the analytically calculated results with the formulation including transverse shear, are in good agreement for both types of elements S4R and SC8R.

Table 6.1: Buckling Load comparison for Baseline Structures

Shell	Analytical Calculation	Conventional Shell (S4R)	Continuum Shell (SC8R)
Baseline 1	4706 kN	4806 kN	4805 kN
Scaled 1.2.V.1	2278 kN	2217 kN	2207 kN

Moreover, the modeshapes resulting from the eigenvalue analyses were used as imperfections in subsequent sections. For Baseline 1, the first modeshapes calculated using S4R elements are shown in Fig. 6.4. These modeshapes have an overall axisymmetric shape, with minor differences in the deformation patterns. The axisymmetric character of the modeshapes corresponds to the expected analytically determined buckling behavior. The visual representation of these eigenmodes provides useful insights into the structure's global deformation trends, which are necessary for understanding the load redistribution mechanisms that contribute to buckling.

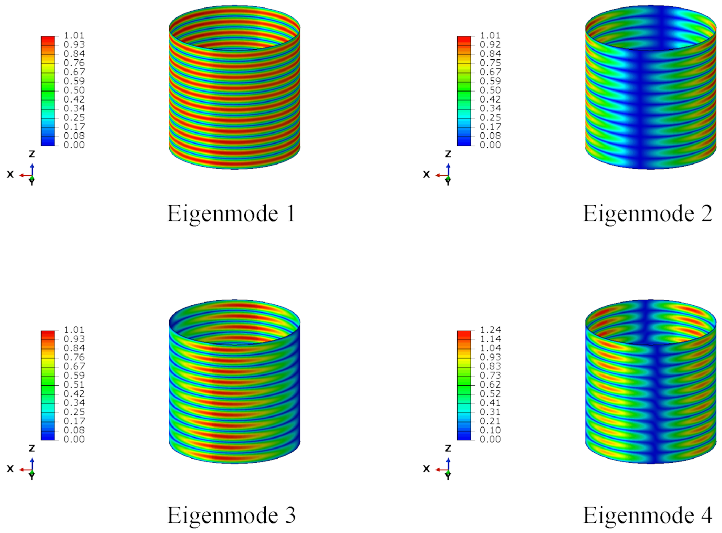

Figure 6.4: Magnitude of the radial displacement of Baseline 1 for the first 4 Eigenmodes.

6.1.2. NON-LINEAR ANALYSIS

For the non-linear analysis of shell buckling, implicit and explicit numerical time integration schemes were considered since each of them offers advantages over the other, which results in certain trade-offs. Implicit analysis solves a system of equations using information from the current and next-time steps simultaneously. This requires a large matrix inversion for every increment, which can be computationally expensive. Explicit analysis does not have this constraint, only solving one increment at a time, and then moving on to the next. However, this requires much smaller time increments than implicit analysis because the time step must be less than the time it takes a sound wave to pass across an element, as well as to avoid error accumulating over large periods of simulation.

The advantage of explicit analysis is that it can capture the inertial effects present in models. Whether or not axial compression buckling simulations require these inertial effects to be included, however, is not entirely straightforward for investigation of pre- and initial buckling behavior (in contrast to post-buckling). This is because end-shortening rates used in experiments are on the order of millimeters per minute or less, whereas the overall scale of the cylindrical shells is often on the order of meters.

However, even with this consideration and based on the literature results, the type of analysis that was used is dynamic implicit. The main advantage of the choice for implicit analysis is due to the computational efficiency compared to explicit analysis. That said, the choice for a dynamic type of analysis also presents the advantage of capturing better

the drop in stiffness and load-carrying ability of the cylindrical structure when it buckles. In general space structures are designed to not buckle for their design load, but the post-buckling field is interesting to capture to see when failure would happen.

For these analyses, the boundary conditions are simply supported conditions in both ends of the shells, which allow rotation while preventing translational movement except in the top surface axial direction. In this case, instead of introducing a surface load, a displacement-driven boundary condition will be added. For displacement-driven loading, one end of the cylinder is constrained to move axially while maintaining uniform displacement across the edge. The rate of the displacement plays an important role in obtaining accurate results.

For a more detailed analysis, an imperfection signature must be included in the simulation. Previous to the manufacturing of the specimen, there is a lack of detail regarding the real imperfection. Numerous approaches can be taken regarding this issue, as discussed previously in Chapter 2 which is at the core of the problem of the imperfection sensitivity of cylindrical shells.

The most conservative approach is to include an axisymmetric imperfection for different amplitudes concerning the thickness. This allows for a verification of the analytical formulation of Chapter 4, and an easy comparison between the nondimensional results and the buckling loads. The process begins with performing an eigenvalue analysis to identify the dominant buckling mode shapes and their corresponding eigenvalues. A scaled version of the dominant eigenmode is then introduced into the finite element model as an imperfection. This imperfection is defined with the amplitude expressed as a fraction of the shell thickness.

Table 6.2: Buckling Load comparison for Baseline 1 with Imperfection Amplitude.

Imperfection Amplitude	Analytical Calculation [kN]	Analytical Knock-Down Factor	Numerical Value [kN]	Numerical Knock-Down Factor
$w_I = 0.1$ ($\omega_I = 0.4$ mm)	4075	0.87	4228	0.88
$w_I = 0.2$ ($\omega_I = 0.8$ mm)	3717	0.79	3844	0.80
$w_I = 0.5$ ($\omega_I = 2.0$ mm)	2901	0.62	3027	0.63

In this study, since the objective is to study the influence of the nondimensional imperfection values reported in Chapter 4 case the imperfection included are the values calculated from Eq. (4.1). In Table 6.2 the numerical and analytical results for Baseline 1 can be seen. These results were calculated with a 5 mm/s displacement rate. For each calculated nondimensional imperfection, the corresponding buckling load and Knock-Down Factor (KDF) are reported. The numerical KDF is calculated with respect to the buckling load obtained from the eigenvalue analysis. It can be observed that for the idealized shell Baseline 1 the numerical and analytical results are in good agreement.

Then, the values of CTA8.1 numerical analysis reported by Schultz et al. [16] are compared with the equivalent Baseline 1 structure. This numerical prediction introduced the measurements of the structure into the formulation. Moreover, the test specimen was modeled in detail, including load introduction pad-ups and potting end rings.

For this post-test prediction, adjusting for material nonlinearities was 3758 kN [845 kips]. This value falls closely to the nondimensional imperfection amplitude $w_I = 0.2$. The stiffness obtained in this case is also similar as can be seen in Fig. 6.5a in their dimensional format and in Fig. 6.5b in their nondimensional format. It is important to mention that the conversion to the nondimensional values which depend on the shell length (L), Radius (R), components of the compliance matrix (a_{ij}), and components of the bending stiffness matrix (D_{ij}) are all taken from the idealized structure: Baseline 1.

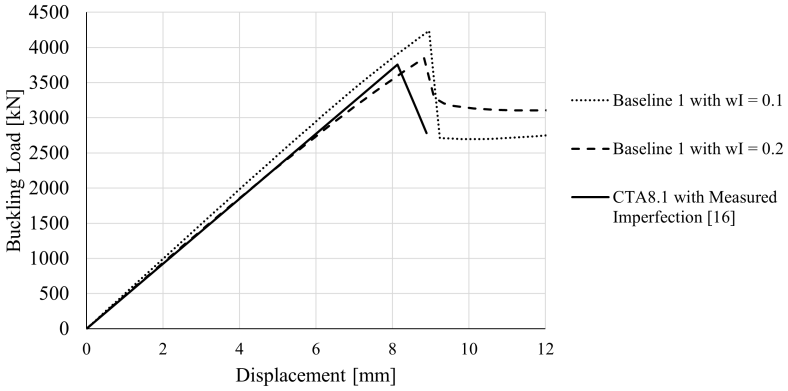

(a) Comparison of the dimensional numerical results with nondimensional imperfection amplitude $w_I = 0.1$ and $w_I = 0.2$, compared with the numerical results of CTA8.1.

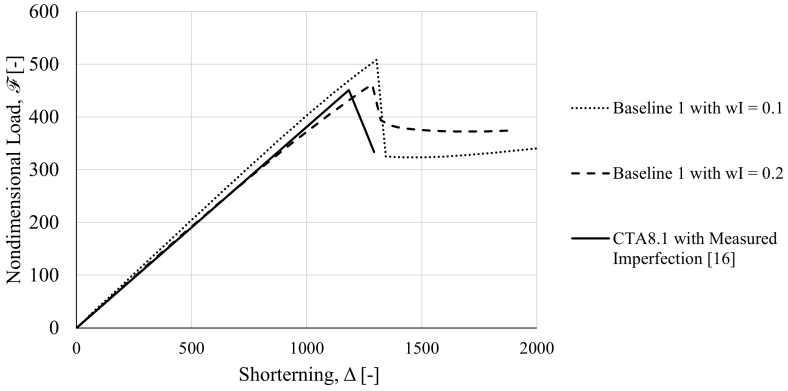

(b) Comparison of the nondimensional numerical results with nondimensional imperfection amplitude $w_I = 0.1$ and $w_I = 0.2$, compared with the numerical results of CTA8.1.

Figure 6.5: Comparison numerical results of Baseline 1 with nondimensional imperfection amplitude $w_I = 0.1$ and $w_I = 0.2$, compared with the numerical results of CTA8.1. [16]

The postbuckling shapes of these three imperfection levels can be seen in Fig. 6.6. The magnitude of the displacement at postbuckling is reported in mm. The images are taken at a displacement in the Z component equal to 9mm.

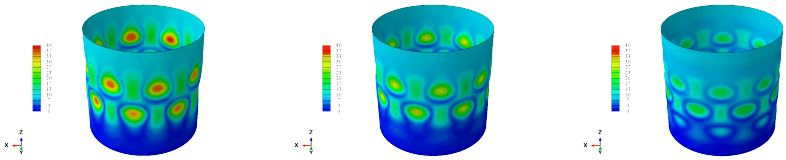

(a) Baseline 1 with $w_I = 0.1$ ($\omega_I = 0.8$ mm) (b) Baseline 1 with $w_I = 0.2$ ($\omega_I = 0.8$ mm) (c) Baseline 1 with $w_I = 0.5$ ($\omega_I = 2.0$ mm)

Figure 6.6: Magnitude of the displacement (expressed in mm) at postbuckling for Baseline 1.

A similar analysis can be performed for the scale structure, which compares the idealized structure Scaled 1.2.V.1 with the test model NDL-1. First, the comparison of the dynamic implicit analysis results for Scaled 1.2.V.1 with their analytical counterparts can be seen in Table 6.3. The analysis had simply supported boundary conditions and a displacement-driven boundary condition on the top edge. The results were calculated with a 1 mm/s displacement rate.

Table 6.3: Buckling Load comparison for Scaled 1.2.V.1 with Imperfection Amplitude

Imperfection Amplitude	Analytical Calculation [kN]	Analytical Knock-Down Factor	Numerical Value [kN]	Numerical Knock-Down Factor
$w_I = 0.1$ ($\omega_I = 0.13$ mm)	1887	0.83	1884	0.85
$w_I = 0.2$ ($\omega_I = 0.26$ mm)	1732	0.76	1707	0.77
$w_I = 0.5$ ($\omega_I = 0.66$ mm)	1357	0.60	1352	0.61

The comparison between analytical and numerical values shows good agreement in this case, between 1% and 3% difference. However, most notably, the numerical KDF for the same level of nondimensional imperfection amplitude remains similar in both scales: Baseline 1 and Scaled 1.2.V.1. For example, for Baseline 1 the numerical KDF for $w_I = 0.1$ is 0.88 (see Table 6.2, whereas for Scaled 1.2.V.1 the numerical KDF for $w_I = 0.1$ 0.85, a difference of only 3.5%. For $w_I = 0.2$, the difference between the numerical KDF in the scales is 3.8% and for $w_I = 0.5$ is 3.2%.

Then a comparison of the idealized shell with the numerical analysis of the test model NDL-1, as described by Rudd et al. [132] is done. The shell of NDL-1 was manufactured via hand layup of 12.5-mm wide tows of the preimpregnated carbon-fiber-epoxy composite IM7-8552. Four layups comprise the shell: a primary layup (the same as the simplified shell, Scaled 1.2.V.1) and three pad-up sections found on either end of the shell. On top of the Pad-ups, the test specimen NDL-1 also includes potting and end rings, but

these, unlike in the analysis of CTA8.1 were not included in the fully detailed numerical analysis.

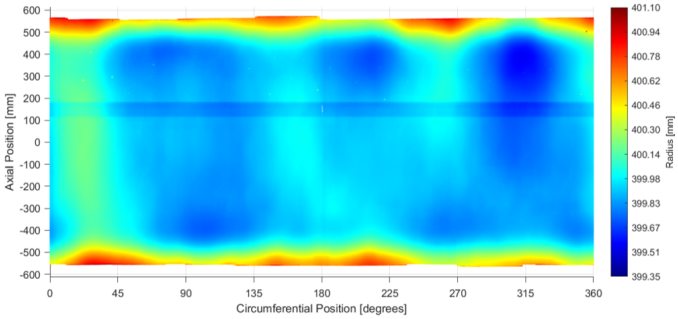

(a) Inner Surface data.

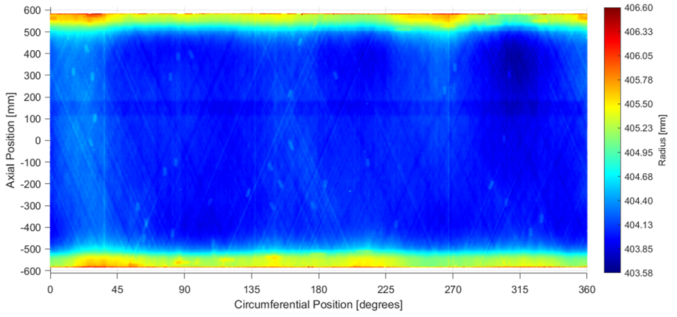

(b) Outer Surface data.

Figure 6.7: NDL-1 Measurements. [132]

The imperfection introduced in the fully numerical model is shown in Fig. 6.7 and consists of inner and outer surface data that had 11.5 million and 28 million 3D-scan points, respectively, with areal densities of 4.1 and 9.5 points per square millimeter. Both surfaces have a ring-shaped imperfection between axial positions of 125 mm and 175 mm around their circumference. This indicates that the mandrel was likely doubly machined here during finishing and transferred to the shell during manufacturing.

The results of the analysis produce a buckling load of 2150 kN, which in turn results in a nondimensional buckling load of 578. The comparison in the dimensional and nondimensional format is shown in Fig. 6.8. This value falls above the lowest nondimensional imperfection amplitude considered $w_I = 0.1$, unlike in the Baseline case where it was close to the imperfection amplitude $w_I = 0.2$. The stiffness obtained is also similar to the value from nondimensional imperfection amplitude $w_I = 0.1$.

The conversion to the nondimensional values which depend on the shell length (L), Radius (R), components of the compliance matrix (a_{ij}), and components of the bending stiffness matrix (D_{ij}) are all taken from the idealized structure: Scaled 1.2.V.1, and as such do not include the pad-ups or the variation in thickness.

Unfortunately, the calculated nondimensional buckling load of 578 for test model NDL-1, does not match the nondimensional buckling load from the CTA8.1 test which is 451. The fully numerical model does match extremely well with the subsequent experiment [132]. This suggests that there are some limitations in the replication of the buckling response with this scaling methodology. This will be discussed in the following section.

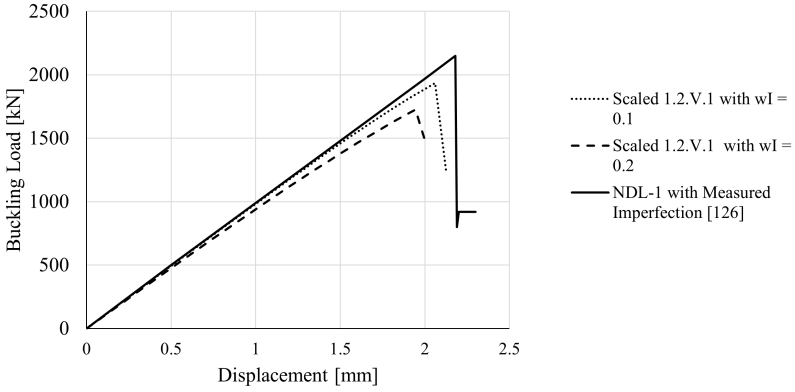

(a) Comparison of the dimensional numerical results with nondimensional imperfection amplitude $w_I = 0.1$ and $w_I = 0.2$, compared with the numerical results of NDL-1.

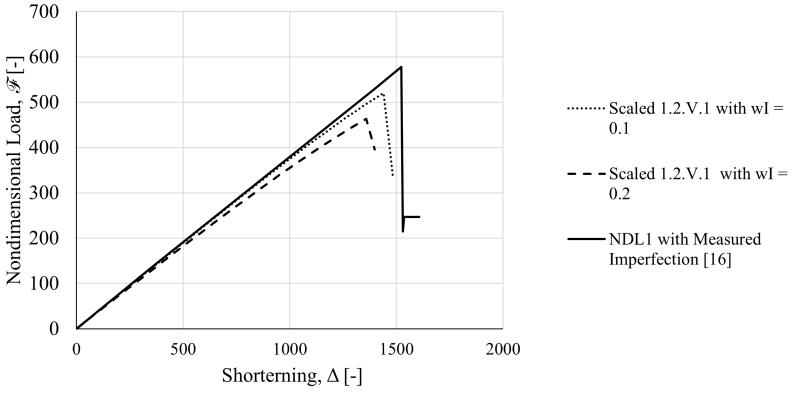

(b) Comparison of the nondimensional numerical results with nondimensional imperfection amplitude $w_I = 0.1$ and $w_I = 0.2$, compared with the numerical results of NDL-1.

Figure 6.8: Comparison numerical results of Baseline 1 with nondimensional imperfection amplitude $w_I = 0.1$ and $w_I = 0.2$, compared with the numerical results of NDL-1. [132]

6.2. COMPARISON WITH AVAILABLE TEST DATA

THE results from two published axial compression buckling tests are explored in this Section. The objective is to evaluate the scaling methodology described in Chapter 5 and to identify its limitations. Therefore, the test results are presented in both dimensional and nondimensional forms. Both tests were performed by NASA, and in both cases the structures were loaded to failure, which occurred immediately upon buckling, as expected.

The first test, conducted on the baseline structure, is referred to as CTA8.1. This structure serves as the reference, with its buckling response intended to be replicated in the scaled model. Schultz et al. [16] provided a detailed description of the test article, the experimental procedure, and the results. The idealized version of this test article was presented in Chapter 5 as Baseline 1. The test article and setup are shown in Fig. 6.9a.

The second test, performed on the scaled structure, is referred to as NDL-1. This test article was designed to replicate, as closely as possible, the buckling response of CTA8.1. The idealized version of this test article was presented in Chapter 5 as Scaled 1.2.V.1. Rudd et al. [132] provided a description of the test article, the experimental procedure, and the results. NDL-1 is shown in the load frame prior to testing in Fig. 6.9b.

(a) Baseline structure test: CTA8.1. [16]

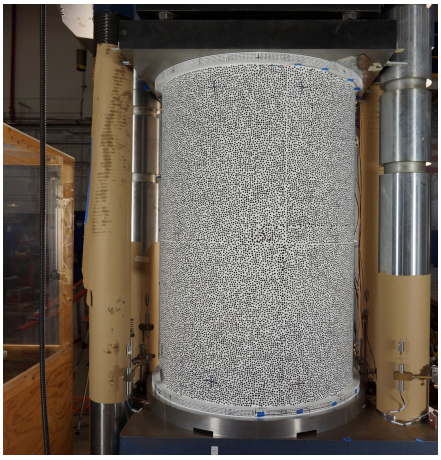

(b) Scaled structure test: NDL-1. [132]

Figure 6.9: Test setup; photos courtesy of NASA.

The buckling test facility used to test CTA8.1 at the NASA Marshall Space Flight Center (MSFC) had previously been used to test eight large-scale stiffened metallic cylindrical shells [133]. For the large scale test CTA8.1, test data were obtained from various sources. Load was measured via load cells installed in the load lines. Displacement was recorded using 28 electrical displacement transducers. To measure strains, 256 electrical-resistance strain gauges and approximately 16,000 fiber-optic strain sensor

locations were employed. In addition, eight low-speed digital image correlation (DIC) photogrammetry systems were used to capture full-field strains and displacements. During the dynamic buckling event, six high-speed DIC systems measured strains and displacements.

The buckling test facility used for NDL-1 at NASA Langley employed similar but reduced equipment. Monitoring stations were used to observe full-field displacements and strains using low-speed DIC, along with real-time load and axial displacement measurements. Test data for NDL-1 were gathered from several sources. Load was measured using a load cell. Displacement was measured by six direct current differential transducers (DCDTs) placed around the load frame. To measure strains on both the inner and outer surfaces, 12 axially oriented gauges were spaced at regular intervals. Additionally, four inner and four outer meridian gauges measured circumferential strain at the same angular positions. Finally, eight DIC systems recorded the experiment: four low-speed and four high-speed systems, with each system comprising two cameras.

For the purposes of this study, only the load and the average displacement recorded were compared to assess the quality of the scaling. To that aim, first of all the experimental buckling load is compared in Table 6.5. As established in the literature, the Knock Down Factor (KDF) initially predicted was conservative for both shells. The larger shell, CTA8.1, had a lower KDF, which is indicative of the larger influence of imperfections on the larger shells and the influence of imperfections in the core and facesheets interface.

Table 6.4: Experimental buckling load results from CTA81 [16] and NDL-1. [132]

Shell	Buckling Load [kN]	KDF real	KDF predicted with SP-8007
CTA-8.1	3811	0.87	0.61
NDL-1	2077	0.95	0.79

These results can also be observed in Fig. 6.10 in the dimensional form and in Fig. 6.11 the nondimensional form. The first observation that can be made is that although the stiffness and strength of both shells is very different in dimensional form, there is a high agreement in the nondimensional stiffness, but some differences in the nondimensional buckling load.

To a certain degree this was expected by the assumptions made by the scaling process, which, as described in Chapter 5, uses the second scaling strategy, going from a sandwich composite cylinder with composite facesheets to a composite structure with no core. This, as described in detail in Chapter 3 has a penalty regarding the lack of inclusion of transverse shear effects. In fact, in the assessment of the scaling quality depicted in Chapter 5 a variation of 8% with respect to the non-dimensional buckling load was already expected even in the perfect shell Fig. 5.30.

Nevertheless, the observed test error in the nondimensional buckling load is substantially larger than the previously predicted value of 8%, reaching a difference of 22%

instead. This is a considerable deviation from the expected value. This departure from the error margin that was projected gives rise to the possibility that there are underlying elements or variables that have not been taken into consideration that are affecting the accuracy of the findings. Therefore, it is of the important to conduct a more in-depth investigation into the possible factors that led to this disparity. Among the possible explanations are the modeling assumptions, or the fundamental difference in the manufacturing process between a sandwich composite and a composite laminate.

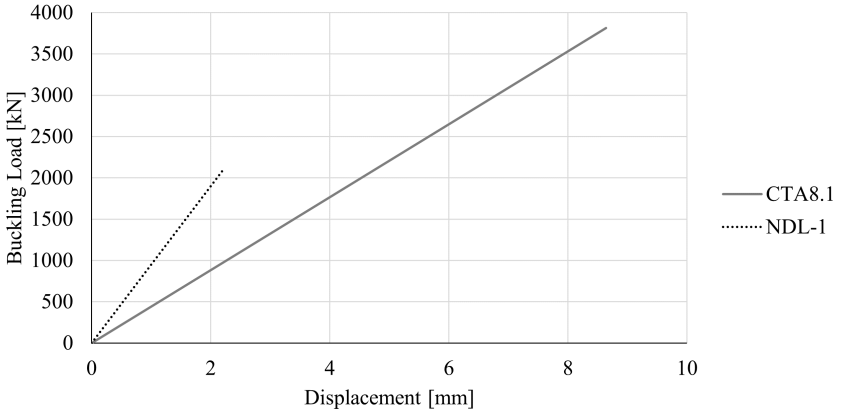

Figure 6.10: Averaged axial DIC-derived dimensional load-displacement behavior.

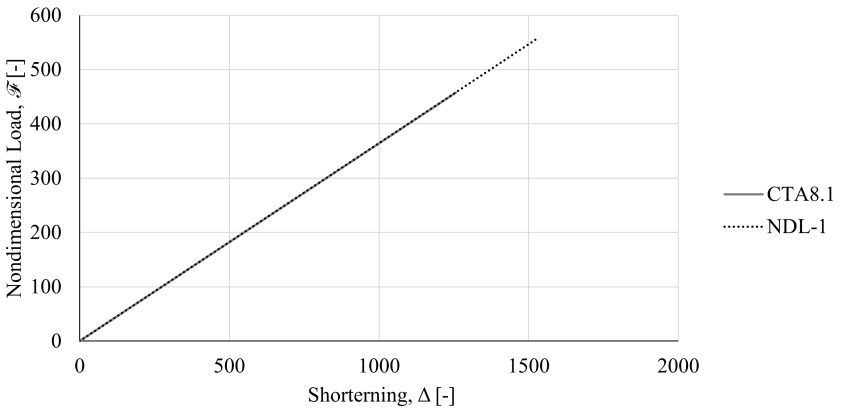

Figure 6.11: Averaged axial DIC-derived non-dimensional load-shortening behavior.

interesting comparison relates to the predicted buckling load at different levels of nondimensional imperfection amplitude. As discussed in Chapter 4, the use of a nondimensional imperfection factor (w_I) allows for a consistent comparison of imperfection sensitivity across different scales. In Table 6.5, both dimensional and nondimensional buckling loads are shown for the scaled shell (Scaled 1.2.V.1) and its test counterpart

(NDL-1), as well as for the baseline structure (Baseline 1) and its corresponding test (CTA-8.1).

The theoretical nondimensional buckling loads follow similar trends for both the baseline and scaled structures as w_I increases. However, when comparing with test results, the experimental value for NDL-1 corresponds to a nondimensional imperfection amplitude of $w_I < 0.1$, whereas for CTA-8.1 it falls within the range $0.1 \leq w_I < 0.2$. These values are consistent with the numerical responses examined in Fig. 6.5 and Fig. 6.8. This discrepancy illustrates a key limitation: although the nondimensional formulation enables meaningful comparison of imperfection amplitude effects, it does not capture the exact imperfection shape, which is critical to the real buckling response.

Table 6.5: Dimensional and Nondimensional Load Comparison.

Shell	Buckling Load [kN]	Nondimensional Buckling Load [-]
NDL-1	2077	558
Scaled 1.2.V.1 with $w_I = 0.1$ ($\omega_I = 0.13$ mm)	1887	507
Scaled 1.2.V.1 with $w_I = 0.2$ ($\omega_I = 0.26$ mm)	1732	465
Scaled 1.2.V.1 with $w_I = 0.3$ ($\omega_I = 0.39$ mm)	1593	428
Scaled 1.2.V.1 with $w_I = 0.4$ ($\omega_I = 0.52$ mm)	1468	394
Scaled 1.2.V.1 with $w_I = 0.5$ ($\omega_I = 0.66$ mm)	1357	364
CTA-8.1	3811	457
Baseline 1 with $w_I = 0.1$ ($\omega_I = 0.4$ mm)	4075	489
Baseline 1 with $w_I = 0.2$ ($\omega_I = 0.8$ mm)	3717	446
Baseline 1 with $w_I = 0.3$ ($\omega_I = 1.2$ mm)	3406	409
Baseline 1 with $w_I = 0.4$ ($\omega_I = 1.6$ mm)	3141	377
Baseline 1 with $w_I = 0.5$ ($\omega_I = 2.0$ mm)	2901	348

It is important to note that the objective of the scaling methodology was not to replicate the imperfection sensitivity curve of the baseline, but rather to study how structures with comparable relative imperfection levels behave in global buckling. Designing a scaling strategy to reproduce the same imperfect buckling load would require previous knowledge of the full imperfection profile, an impractical design approach. Instead, the methodology isolates the imperfection sensitivity trends without embedding the result into the setup.

These findings demonstrate both the utility and limitations of the current approach: while imperfection amplitude scaling provides valuable insight into sensitivity trends, it also reveals that variations in the expected imperfection, unavoidable in real-world specimens, can significantly affect the buckling load.

6.3. CONCLUSIONS

The numerical analysis performed in this chapter is contrasted with the analytical models developed in previous sections. Both the conventional shell elements (S4R) and continuum shell elements (SC8R) accurately captured the buckling behavior of cylindrical shells under axial compression, with mesh convergence results demonstrating less than 1% error. This confirms the efficacy of the analytical model, particularly in predicting the perfect shell buckling loads.

On the other hand, the assessment of the scaling methodology, which compares the full-scale structure (CTA8.1) with the scaled model (NDL-1), reveals both strengths and limitations. While the dimensional stiffness of the full-scale and scaled models differ significantly, their nondimensional stiffness shows high agreement. However, a notable discrepancy arises in the predicted nondimensional buckling load, where the observed error reaches 22%, substantially higher than the 8% error anticipated. This larger deviation suggests that certain factors were not accounted for in the scaling process, possibly due to differences in manufacturing or the inherent assumptions made in the model. Such findings indicate that further refinement of the scaling approach is necessary, particularly when transitioning from sandwich composite cylinders to laminate structures without cores.

Imperfection sensitivity emerges as a critical factor in determining the buckling behavior of cylindrical shells. Both numerical and experimental results indicate that imperfections, even in small amplitudes, significantly influence the buckling load. The comparison between the baseline structure (CTA8.1) and the scaled structure (NDL-1) underscores the difficulty in accurately predicting the effects of imperfections, especially dealing with structures of different scales. These findings suggest that imperfections must be modeled differently in the nondimensional formulation.

The experimental data, when compared to the predictions, further emphasizes the limitations of the current scaling methodology. The differences observed between the experimental results and the predictions highlight the need for more sophisticated techniques to account for imperfections, material properties, and the core-to-laminate transition in composite structures. Such refinements are essential to improving the accuracy of scaling methods and ensuring that predictions align more closely with experimental outcomes.

In conclusion, future research should prioritize the separation of imperfection sensitivity from other influencing factors, such as material differences and manufacturing variations. This would allow for a more precise evaluation of the individual contributions of these factors to the overall structural behavior. By focusing on this aspect, the precision of scaling methodologies can be improved, ultimately leading to more reliable predictions of buckling behavior in scaled cylindrical shell structures.

7

CONCLUSION

pero te digo adiós, para toda la vida,
aunque toda la vida siga pensando en ti

José Ángel Buesa

This chapter concludes the thesis by describing the key finding and contributions and by proposing future research recommendations. The chapter begins by examining the most significant findings in relation to the proposed research questions. Following this, recommendations are provided to guide further exploration into identified gaps or limitations. Together, these conclusions summarize the study's main outcomes and offer a framework for advancing research within the field.

7.1. KEY FINDINGS AND CONTRIBUTIONS

THE key findings of this research are framed around the four primary research questions that guided the study. These questions focus on the impact of transverse shear effects, imperfection sensitivity, the development of a systematic scaling methodology, and the discrepancies between analytical and numerical predictions and experimental results. In the following sections, each research question will be addressed, with an explanation of the corresponding findings and their significance.

7.1.1. SHEAR TRANSVERSE EFFECTS INFLUENCE

RQ1: To what extent do the shear transverse effects influence the buckling response in sandwich composite structures and how should it be modeled in the different scaled structures?

An advantage of extending the nondimensional governing equations to accurately model the problem is that the nondimensional parameters created can be used for other purposes beside the scaling laws. Using the nondimensional parameters, it is possible to navigate the design space of different shells and to investigate the impact of changes in the properties of the shells towards the buckling response.

More specifically, the focus is in the reduction of the buckling load due to the influence of the core transverse shear effects and the relation between the load and other factors of the shells. This is represented via the nondimensional parameter χ_1 over the transverse shear buckling load ratio ($\mathscr{F}/\mathscr{F}_0$).

It can be demonstrated that the nondimensional transverse shear parameter (χ_1) in conjunction with the Batdorf-Stein parameter (Z) influence the most the transverse shear buckling load ratio ($\mathscr{F}/\mathscr{F}_0$) [120]. Shells with a stiffer core material, represented with a higher nondimensional transverse shear parameter (χ_1), are less influenced by the core transverse shear. For the same value of χ_1, thinner shells, as represented by a higher Batdorf-Stein parameter (Z), present a higher transverse shear influence.

It can also be seen how nondimensional buckling results are applicable to different shells of different scales, which is key for the scaling methodology developed. Several specific shells (numbered 1–6) are compared, and their differences and similarities are highlighted. For instance, sandwich composite Shell 1 and Shell 2 share all the same nondimensional parameters and therefore have the same nondimensional buckling load with and without transverse shear influence. This is even if Shell 2 (radius: 1.4 m) is much larger than Shell 1 (radius: 0.4 m), Shell 2 has double the number of plies as Shell 1, and the core material, while isotropic in both shells, has different properties.

7.1.2. IMPERFECTION SENSITIVITY

RQ2: How should the imperfection sensitivity in sandwich shell structures be modeled for the scaled structures?

Modeling the imperfection sensitivity is not exclusive to sandwich cylindrical shells, since this is an intrinsic part of the shell buckling behavior. Imperfection sensitivity is widely acknowledged to be the main cause of discrepancy between the experimental data and analytical prediction.

A trigonometric imperfection is included in the derivation of the nondimensional

equations for axial buckling of sandwich composite cylindrical shells including transverse shear. A solution for the nondimensional buckling load is derived from the equilibrium and compatibility equations including an initial geometric imperfection. This model uses the bifurcation buckling modes of the shell as initial geometric imperfections. The limit buckling load $\mathscr{F}_i$ for each imperfection amplitude w_I occurs when the shell cannot support more load.

The nondimensional imperfection formulation allows to apply nondimensional results to different shells of different sizes. Even if the magnitude of the imperfection is different in the different scales, the nondimensional load displacement results can be compared.

Moreover, using the nondimensional parameters, it is possible to navigate the design space of different shells and to investigate the impact of changes in the properties of the shells on imperfection sensitivity. Overall, the analysis and results can be used to design sandwich composite cylindrical shells as well as to account for an initial imperfection factor in the scaling methodology developed.

7.1.3. ANALYSIS-BASED METHODOLOGY

RQ3: How can a systematic methodology be designed to scale down composite cylindrical shells while preserving their buckling response?

The appeal of developing a systematic analysis-based scaling methodology stems from the drawbacks of performing multiple full-scale tests. An analysis-based methodology would allow for the rapid formulation of scaled-down structures, fit for smaller laboratories. The analytical, numerical and experimental results of these scaled-down structures can then be used in the design of large-scale structures, thereby reducing the number of large-scale tests.

The difficulty in developing such an analysis-based methodology is that test results are highly dependent on geometry variations and the shell's imperfection signature. A successful methodology requires accurate modeling of the phenomena, the selection of appropriate scaling laws, and the investigation of feasibility areas. The approach taken in this thesis makes use of a nondimensional formulation of the equations, where the components of the equations become the scaling laws.

Upon establishing the nondimensional governing equations, their parameters, and solutions, the scaling procedure is then defined. For this thesis, two scaling strategies were pursued. All of them make use of the nondimensional governing equations as scaling laws, but each of them is suitable for a different case, and each has its own advantages and disadvantages.

The first strategy scales from a baseline sandwich structure to a scaled sandwich

structure. The manufacturing limitations in the thickness of the scaled structure's core limit this method. Depending on the size of the baseline structure, the scaled structure can produce thickness values that are not feasible. For example, it is difficult to replicate the nondimensional transverse shear parameter (χ_1) at low thickness values. It is also not possible to replicate the nondimensional transverse shear parameter (χ_1) with existing materials in some scale ranges. Both reasons amount to a manufacturing challenge: even if a scaled structure is possible in theory, it cannot be built, and thus the purpose of the scaling procedure is not fulfilled.

The second strategy scales from a baseline sandwich structure to a solid laminate structure. This strategy avoids the manufacturing problems described for the previous one. The challenge in this case is to compare the two different types of structures. In particular, it is challenging to compare imperfection levels.This type of strategy was used for the test specimen produced and tested by Rudd et al. [132].

7.1.4. PREDICTIONS IN DIFFERENT SCALES

RQ4: What are the discrepancies between analytical predictions and experimental observations of buckling behaviour in different scales of composite shell structures produced with the systematic methodology?

The evaluation of the systematic scaling methodology, which compares the test of a full-scale structure to a scaled model, exposes both benefits and weaknesses. Although the full-scale and scaled models have quite different dimensional stiffness, their nondimensional stiffness is the same. However, a significant disparity develops in the predicted nondimensional buckling load, where the observed error exceeds 22%, much more than the 8% error expected.

This significant deviation indicates that factors not accounted for in the analytical models may have influenced the experimental outcomes. The difference suggests that the assumptions made in the scaling methodology, particularly the transition from sandwich composite shells with facesheets to laminate composite structures, might not fully capture the complexity of the buckling behavior in the scaled model.

Additionally, the discrepancy also highlights the impact of imperfection sensitivity. Both analytical and numerical analyses incorporate imperfection factors, but the sensitivity of the experimental results to imperfections, especially in scaled models, introduces further discrepancies. Imperfections, can significantly alter the buckling load, and the scaling methodology is unable to completely replicate these effects across different scales.

Another source of discrepancy is the manufacturing limitations. For instance, differences in the thickness due to manufacturing tolerances in scaled structures versus full-scale ones introduce inaccuracies in the numerical and analytical predictions. Moreover,

in the scaled model (NDL-1), modifications were made to accommodate laboratory constraints, such as adjusting the length due to available mandrel size, even if they were not expected to have large influence.

Therefore, the main discrepancies arise from the sensitivity to imperfections, manufacturing and laboratory limitations, and, most critically, limitations in the scaling methodology when transitioning between different structural configurations (sandwich composite to laminate composite). The analytical and numerical models provide reasonable approximations but fall short in accounting for all experimental variables, especially before the design is fully known.

7.1.5. CONTRIBUTIONS

This research main contribution lies on advancing the understanding of buckling in sandwich composite cylindrical shells by expanding the nondimensional framework proposed by Nemeth [125]. The newly defined nondimensional parameters, such as the transverse shear parameter (χ_1) provide a means to study the interaction between material properties, geometric configurations, and buckling responses for sandwich composite shells of different scales.

The extended nondimensional framework was executed with a scaling application as main purpose but the insights gained from this work enable a deeper understanding of the role of transverse shear and imperfection sensitivity in determining the buckling response. This allows for the prediction and comparison of buckling behavior across different scales.

Moreover, the integration of these nondimensional parameters into a systematic scaling methodology provides a novel approach for analyzing sandwich composite cylindrical shells. From the limited experimental results available, the scaling methodology successfully replicates the nondimensional stiffness of the large model in the scaled one, demonstrating its potential as a scaling approach, even if it falls short to replicate the nondimensional buckling load.

All together, by utilizing these newly defined parameters and scaling strategies, this work delivers another tool for gaining insights in the design and analysis of both large-scale and laboratory-scaled structures.

7.2. RECOMMENDATIONS FOR FUTURE RESEARCH

WHILE the developed framework and scaling methodologies provide valuable insights into the buckling behavior of sandwich composite cylindrical shells, several limitations were encountered during the research process. One of the primary chal-

lenges is the inherent complexity in accurately capturing imperfection sensitivity in both the analytical and numerical models. The nature of imperfections in real-world structures can vary significantly, leading to discrepancies when compared with idealized models. Although the developed nondimensional framework accounts for imperfections, further refinement is necessary to better align the predictions with experimental outcomes.

Another limitation is related to the boundary conditions and manufacturing constraints in scaled-down experimental models. In practical terms, it is difficult to manufacture small-scale models that precisely replicate the material properties, stiffness, and geometry of full-scale structures. These variations, along with differences in the testing environment, contribute to the observed discrepancies between the predicted and actual buckling loads. The scaling methodology, while effective, still requires more empirical validation to address these manufacturing challenges and improve the accuracy of predictions across different scales.

Given the limitations identified, there are three avenues for future research that can build upon the findings of this thesis. First, the nondimensional framework could be extended to incorporate more detailed modeling the structure and manufacturing induced imperfections. This would enhance the accuracy of buckling load predictions.

Second, further experimental testing is essential to validate the proposed scaling methodologies more comprehensively. In particular, testing on scaled sandwich composite shells obtained with the first scaling strategy would provide deeper insights into the relationship between theoretical predictions and real-world behavior. This was not possible to do due to manufacturing limitations for the baseline structures proposed during these project, but other baseline structures could be chosen to validate the methodology.

Lastly, it would be beneficial to explore new approaches to improving the alignment between analytical, numerical, and experimental results. For instance, machine learning models could be applied to better capture the variability in imperfections. These approaches could lead to more robust predictions of buckling behavior across a broader range of composite shell structures.

BIBLIOGRAPHY

[1] M. Onoda and O. R. Young, *Satellite earth observations and their impact on society and policy*. Springer Nature, 2017.

[2] R. Parkinson, "The hidden costs of reliability and failure in launch systems," *Acta Astronautica*, vol. 44, no. 7, pp. 419–424, 1999.

[3] L. Brevault, M. Balesdent, and S. Defoort, "Preliminary study on launch vehicle design: Applications of multidisciplinary design optimization methodologies," *Concurrent Engineering*, vol. 26, no. 1, pp. 93–103, 2018.

[4] V. S. Reddy, "The spacex effect," *New Space*, vol. 6, no. 2, pp. 125–134, 2018.

[5] K. Song, A. Satyanarayana, A. Przekop, and M. R. Schultz, "Development of a numerical modeling approach for buckling analysis of sandwich composite cylindrical shells with selected results," Tech. Rep. TM-20210013939, NASA, 2021.

[6] M. W. Hilburger, "Buckling of thin-walled circular cylinders," Tech. Rep. SP-8007-2020/REV 2, NASA, 2020.

[7] V. Ding, S. Torabian, S. Adany, X. Yun, A. Pervizaj, A. T. Myers, and B. W. Schafer, "Experimental results of stability of cylindrical shells under combined bending and torsion," *Journal of Structural Engineering*, vol. 151, no. 1, p. 04024188, 2025.

[8] K. K. Yadav and S. Gerasimidis, "Imperfection insensitive thin cylindrical shells for next generation wind turbine towers," *Journal of Constructional Steel Research*, vol. 172, p. 106228, 2020.

[9] K. Song, M. R. Schultz, C. J. Kosztowny, A. Przekop, N. W. Gardner, and M. T. Rudd, "Buckling test and analysis of the 8-foot-diameter sandwich composite cylinder test article cta8. 3 as part of the shell buckling knockdown factor project: Test dates 16˜ 19 december 2019," Tech. Rep. TM-20210024768, NASA, 2022.

[10] A. Przekop, M. R. Schultz, C. J. Kosztowny, N. W. Gardner, K. Song, and M. T. Rudd, "Buckling test and analysis of the 8-foot-diameter sandwich composite cylinder test article cta8. 2 as part of the shell buckling knockdown factor project: Test dates 5-7 december 2017," Tech. Rep. TM-20210024095, NASA, 2022.

[11] D. W. Sleight, D. N. Kosareo, and S. D. Thoma, "Composite interstage structural concept down select process and results," in *SAMPE Conference*, 2012.

[12] G. Henson, *Aerospace Materials and Applications*, ch. Materials for Launch Vehicle Structures, pp. 435–504. American Institute of Aeronautics and Astronautics, 2018.

[13] A. E. Lovejoy, D. C. Jegley, M. W. Hilburger, and A. Przekop, "Lessons learned from large-scale aerospace structural testing," in *62nd AIAA/ASME/ASCE/AHS/ASC Structures, Structural Dynamics, and Materials Conference*, 2021.

[14] H. Wagner, E. Petersen, R. Khakimova, and C. Hühne, "Buckling analysis of an imperfection-insensitive hybrid composite cylinder under axial compression–numerical simulation, destructive and non-destructive experimental testing," *Composite Structures*, vol. 225, no. 111152, 2019.

[15] C. Bisagni, "Buckling tests of sandwich cylindrical shells with and without cut-outs," in *American Society for Composites 31st Technical Conference and ASTM Committee D30 Meeting*, pp. 1–10, 2016.

[16] M. R. Schultz, D. W. Sleight, N. W. Gardner, M. T. Rudd, M. W. Hilburger, T. Palm, and N. J. Oldfield, "Test and analysis of a buckling-critical large-scale sandwich composite cylinder," in *2018 AIAA/ASCE/AHS/ASC Structures, Structural Dynamics, and Materials Conference*, no. 1693, 2018.

[17] M. Hilburger, "Developing the next generation shell buckling design factors and technologies," in *53rd AIAA/ASME/ASCE/AHS/ASC Structures, Structural Dynamics and Materials Conference 20th AIAA/ASME/AHS Adaptive Structures Conference 14th AIAA*, p. 1686, 2012.

[18] A. Takano, "Statistical knockdown factors of buckling anisotropic cylinders under axial compression," *Journal of Applied Mechanics*, vol. 79, no. 5, p. 051004, 2012.

[19] M. T. Rudd, M. R. Schultz, N. W. Gardner, C. J. Kosztowny, and C. Bisagni, "Experimental validation of the buckling behavior of unreinforced and reinforced composite conical-cylindrical shells for launch-vehicles," *Composite Structures*, vol. 349, p. 118493, 2024.

[20] J. Arbocz and J. Hol, "Collapse of axially compressed cylindrical shells with random imperfections," *Thin-walled structures*, vol. 23, no. 1-4, pp. 131–158, 1995.

[21] L. Friedrich, S. Loosen, K. Liang, M. Ruess, C. Bisagni, and K. U. Schröder, "Stacking sequence influence on imperfection sensitivity of cylindrical composite shells under axial compression," *Composite Structures*, vol. 134, pp. 750–761, 2015.

[22] J. R. Vinson, *The behavior of sandwich structures of isotropic and composite materials*. CRC Press, 1999.

[23] L. Librescu and T. Hause, "Recent developments in the modeling and behavior of advanced sandwich constructions: a survey," *Composite structures*, vol. 48, no. 1-3, pp. 1–17, 2000.

[24] E. Karyadi, *Collapse behavior of imperfect sandwich cylindrical shells*. PhD thesis, Delft University of Technology, Delft, The Netherlands, 1998.

[25] H. Gu and A. Chattopadhyay, "Delamination buckling and postbuckling of composite cylindrical shells," *AIAA journal*, vol. 34, no. 6, pp. 1279–1286, 1996.

[26] N. D. Duc, "Nonlinear thermal dynamic analysis of eccentrically stiffened s-fgm circular cylindrical shells surrounded on elastic foundations using the reddy's third-order shear deformation shell theory," *European Journal of Mechanics-A/Solids*, vol. 58, pp. 10–30, 2016.

[27] T. Q. Quan and N. D. Duc, "Nonlinear vibration and dynamic response of shear deformable imperfect functionally graded double-curved shallow shells resting on elastic foundations in thermal environments," *Journal of Thermal Stresses*, vol. 39, no. 4, pp. 437–459, 2016.

[28] A. Szekrenyes, "Mechanics of shear and normal deformable doubly-curved delaminated sandwich shells with soft core," *Composite Structures*, vol. 258, p. 113196, 2021.

[29] B. Alanbay, R. C. Batra, and R. K. Kapania, "Effect of extreme in-plane and transverse stiffness ratios on frequencies and load transfer between face sheets and core of rectangular sandwich plates," *Composite Structures*, vol. 278, p. 114730, 2021.

[30] S. Abrate and M. Di Sciuva, "Equivalent single layer theories for composite and sandwich structures: A review," *Composite Structures*, vol. 179, pp. 482–494, 2017.

[31] A. Noor and W. Burton, "Assessment of shear deformation theories for multilayered composite plates," *Applied Mechanics Reviews*, vol. 42, no. 1, pp. 1–13, 1989.

[32] A. Pirrera and P. M. Weaver, "Geometrically nonlinear first-order shear deformation theory for general anisotropic shells," *AIAA Journal*, vol. 47, no. 3, pp. 767–782, 2009.

[33] H. Altenbach, V. Eremeyev, and K. Naumenko, "On the use of the first order shear deformation plate theory for the analysis of three-layer plates with thin soft core layer," *ZAMM - Journal of Applied Mathematics and Mechanics / Zeitschrift für Angewandte Mathematik und Mechanik*, vol. 95, 2015.

[34] M. Kabir and D. Poorveis, "Buckling of discretely stringer-stiffened composite cylindrical shells under combined axial compression and external pressure," *Scientia Iranica*, vol. 13, no. 2, 2006.

[35] F. M. Nasrekani and H. Eipakchi, "Analytical solution for buckling analysis of cylinders with varying thickness subjected to combined axial and radial loads," *International Journal of Pressure Vessels and Piping*, vol. 172, pp. 220–226, 2019.

[36] P. H. Cong, P. T. Long, N. Van Nhat, and N. D. Duc, "Geometrically nonlinear dynamic response of eccentrically stiffened circular cylindrical shells with negative poisson's ratio in auxetic honeycombs core layer," *International Journal of Mechanical Sciences*, vol. 152, pp. 443–453, 2019.

[37] P. Pai and M. Schulz, "Shear correction factors and an energy-consistent beam theory," *International Journal of Solids and Structures*, vol. 36, pp. 1523–1540, 1999.

[38] K. H. Lo, R. M. Christensen, and E. M. Wu, "A High-Order Theory of Plate Deformation—Part 2: Laminated Plates," *Journal of Applied Mechanics*, vol. 44, pp. 669–676, 12 1977.

[39] E. Viola, F. Tornabene, and N. Fantuzzi, "General higher-order shear deformation theories for the free vibration analysis of completely doubly-curved laminated shells and panels," *Composite Structures*, vol. 95, pp. 639–666, 2013.

[40] M. Cho, K.-O. Kim, and M.-H. Kim, "Efficient higher-order shell theory for laminated composites," *Composite Structures*, vol. 34, no. 2, pp. 197–212, 1996.

[41] A. Gorgeri, R. Vescovini, and L. Dozio, "Analysis of multiple-core sandwich cylindrical shells using a sublaminate formulation," *Composite Structures*, p. 111067, 2019.

[42] T. S. Hartwich, S. Panek, D. Wilckens, T. Wille, and D. Krause, "The influence of r/t-ratio on the imperfection sensitivity of the buckling load of thin-walled cfrp cylindrical shells," *Composite Structures*, vol. 341, p. 118216, 2024.

[43] T. Von Karman and H.-S. Tsien, "The buckling of thin cylindrical shells under axial compression," *Journal of the Aeronautical Sciences*, vol. 8, no. 8, pp. 303–312, 1941.

[44] M. Stein, "The influence of prebuckling deformations and stresses on the buckling of perfect cylinders," Tech. Rep. TR-R-190, NASA, 1964.

[45] W. T. Koiter, *On the stability of elastic equilibrium*, vol. 833. National Aeronautics and Space Administration, 1967.

[46] L. Ali, E. B. Jalal, K. Abdellatif, and E. B. Larbi, "Effect of multiple localized geometric imperfections on stability of thin axisymmetric cylindrical shells under axial compression," *International Journal of Solids and Structures*, vol. 48, no. 6, pp. 1034–1043, 2011.

[47] J. Hutchinson, "Axial buckling of pressurized imperfect cylindrical shells," *AIAA journal*, vol. 3, no. 8, pp. 1461–1466, 1965.

[48] W. T. Koiter, I. Elishakoff, Y. Li, and J. Starnes Jr, "Buckling of an axially compressed cylindrical shell of variable thickness," *International Journal of Solids and Structures*, vol. 31, no. 6, pp. 797–805, 1994.

[49] J. N. Reddy, *Energy principles and variational methods in applied mechanics*. John Wiley & Sons, 2017.

[50] H. Huang and Q. Han, "Buckling of imperfect functionally graded cylindrical shells under axial compression," *European Journal of Mechanics-A/Solids*, vol. 27, no. 6, pp. 1026–1036, 2008.

[51] C. R. Steele and Y. Y. Kim, "Modified mixed variational principle and the state-vector equation for elastic bodies and shells of revolution," *Journal of Applied Mechanics*, vol. 59, pp. 587–595, 1992.

[52] S.-J. Liao, "A kind of approximate solution technique which does not depend upon small parameters—ii. an application in fluid mechanics," *International Journal of Non-Linear Mechanics*, vol. 32, no. 5, pp. 815–822, 1997.

[53] A. Khamlichi, M. Bezzazi, and A. Limam, "Buckling of elastic cylindrical shells considering the effect of localized axisymmetric imperfections," *Thin-walled structures*, vol. 42, no. 7, pp. 1035–1047, 2004.

[54] J.-G. Teng and J. M. Rotter, "Buckling of pressurized axisymmetrically imperfect cylinders under axial loads," *Journal of engineering mechanics*, vol. 118, no. 2, pp. 229–247, 1992.

[55] L. Yang, Z. Chen, F. Chen, W. Guo, and G. Cao, "Buckling of cylindrical shells with general axisymmetric thickness imperfections under external pressure," *European Journal of Mechanics-A/Solids*, vol. 38, pp. 90–99, 2013.

[56] V. Z. Gristchak and O. A. Golovan, "Hybrid asymptotic method for the effect of local thickness defects and initial imperfections on the buckling of cylindrical shells," *Journal of Theoretical and Applied Mechanics*, vol. 41, no. 3, pp. 509–520, 2003.

[57] N. Sakakibara, S. Kyriakides, and E. Corona, "Collapse of partially corroded or worn pipe under external pressure," *International Journal of Mechanical Sciences*, vol. 50, no. 12, pp. 1586–1597, 2008.

[58] T. A. Netto, U. S. Ferraz, and A. Botto, "On the effect of corrosion defects on the collapse pressure of pipelines," *International journal of solids and structures*, vol. 44, no. 22-23, pp. 7597–7614, 2007.

[59] P. M. Weaver and R. Dickenson, "Interactive local/euler buckling of composite cylindrical shells," *Computers & structures*, vol. 81, no. 30-31, pp. 2767–2773, 2003.

[60] R. Priyadarsini, V. Kalyanaraman, and S. Srinivasan, "Numerical and experimental study of buckling of advanced fiber composite cylinders under axial compression," *International Journal of Structural Stability and Dynamics*, vol. 12, no. 04, p. 1250028, 2012.

[61] M. Alfano and C. Bisagni, "Probability-based methodology for buckling investigation of sandwich composite shells with and without cut-outs," *International Journal for Computational Methods in Engineering Science and Mechanics*, vol. 18, no. 1, pp. 77–90, 2017.

[62] L. Gangadhar and T. S. Kumar, "Finite element buckling analysis of composite cylindrical shell with cutouts subjected to axial compression," *vol*, vol. 89, pp. 45–52, 2016.

[63] H. Allahbakhsh and M. Shariati, "Buckling of cracked laminated composite cylindrical shells subjected to combined loading," *Applied Composite Materials*, vol. 20, no. 5, pp. 761–772, 2013.

[64] R. Degenhardt, A. Kling, A. Bethge, J. Orf, L. Kärger, R. Zimmermann, K. Rohwer, and A. Calvi, "Investigations on imperfection sensitivity and deduction of improved knock-down factors for unstiffened CFRP cylindrical shells," *Composite Structures*, vol. 92, no. 8, pp. 1939–1946, 2010.

[65] J. Arbocz and H. Abramovich, "The initial imperfection data bank at the Delft University of Technology: Part I," Tech. Rep. LR-290, Delft University of Technology, 1979.

[66] C. Bisagni, "Numerical analysis and experimental correlation of composite shell buckling and post-buckling," *Composites Part B: Engineering*, vol. 31, no. 8, pp. 655–667, 2000.

[67] L. Wullschleger and H. Meyer-Piening, "Buckling of geometrically imperfect cylindrical shells — definition of a buckling load," *International Journal of Non-Linear Mechanics*, vol. 37, no. 4-5, pp. 645–657, 2002.

[68] R. L. Lincoln, P. M. Weaver, A. Pirrera, and R. Groh, "Imperfection-insensitive continuous tow-sheared cylinders," *Composite structures*, vol. 260, p. 113445, 2021.

[69] M. Hilburger and J. Starnes Jr., "Effects of imperfections on the buckling response of compression-loaded composite shells," *International Journal of Non-Linear Mechanics*, vol. 37, no. 4-5, pp. 623–643, 2002.

[70] M. Hilburger, M. Nemeth, and J. Starnes Jr., "Shell buckling design criteria based on manufacturing imperfection signatures," Tech. Rep. NASA/TM-2004-212659, NASA, 2004.

[71] M. Broggi, A. Calvi, and G. Schuëller, "Reliability assessment of axially compressed composite cylindrical shells with random imperfections," *International Journal of Structural Stability and Dynamics*, vol. 11, no. 02, pp. 215–236, 2011.

[72] M. Broggi and G. Schuëller, "Efficient modeling of imperfections for buckling analysis of composite cylindrical shells," *Engineering Structures*, vol. 33, no. 5, pp. 1796–1806, 2011.

[73] C. Hühne, R. Rolfes, E. Breitbach, and J. Teßmer, "Robust design of composite cylindrical shells under axial compression — Simulation and validation," *Thin-Walled Structures*, vol. 46, no. 7-9, pp. 947–962, 2008.

[74] H. Wagner and C. Hühne, "On the imperfection sensitivity and design of buckling critical wind turbine towers," *Thin-Walled Structures*, vol. 206, p. 112577, 2025.

[75] R. Xin, V. T. Le, and N. S. Goo, "Buckling identification in composite cylindrical shells with measured imperfections using a multi-dic method and finite element analysis," *Thin-Walled Structures*, vol. 177, p. 109436, 2022.

[76] M. Schultz, D. Sleight, N. Gardner, M. Rudd, M. Hilburger, T. Palm, and N. Oldfield, "Test and analysis of a buckling-critical large-scale sandwich composite cylinder," in *2018 AIAA/ASCE/AHS/ASC Structures, Structural Dynamics, and Materials Conference*, no. AIAA 2018-1693, (Reston, Virginia, USA), American Institute of Aeronautics and Astronautics, 2018.

[77] R. Khakimova, S. Castro, D. Wilckens, K. Rohwer, and R. Degenhardt, "Buckling of axially compressed CFRP cylinders with and without additional lateral load: Experimental and numerical investigation," *Thin-Walled Structures*, vol. 119, pp. 178–189, 2017.

[78] M. Arbelo, R. Degenhardt, S. Castro, and R. Zimmermann, "Numerical characterization of imperfection sensitive composite structures," *Composite Structures*, vol. 108, no. 1, pp. 295–303, 2014.

[79] M. Hilburger and J. Starnes Jr., "Effects of imperfections of the buckling response of composite shells," *Thin-Walled Structures*, vol. 42, no. 3, pp. 369–397, 2004.

[80] M. Hilburger and J. Starnes Jr., "High-fidelity nonlinear analysis of compression-loaded composite shells," in *19th AIAA Applied Aerodynamics Conference*, no. AIAA 2001-1394, (Reston, Virigina, USA), American Institute of Aeronautics and Astronautics, 2001.

[81] H. Meyer-Piening, M. Farshad, B. Geier, and R. Zimmermann, "Buckling loads of CFRP composite cylinders under combined axial and torsion loading – experiments and computations," *Composite Structures*, vol. 53, no. 4, pp. 427–435, 2001.

[82] B. Wang, S. Zhu, P. Hao, X. Bi, K. Du, B. Chen, X. Ma, and Y. Chao, "Buckling of quasi-perfect cylindrical shell under axial compression: A combined experimental and numerical investigation," *International Journal of Solids and Structures*, vol. 130-131, pp. 232–247, 2018.

[83] S. Castro, R. Zimmermann, M. Arbelo, R. Khakimova, M. Hilburger, and R. Degenhardt, "Geometric imperfections and lower-bound methods used to calculate knock-down factors for axially compressed composite cylindrical shells," *Thin-Walled Structures*, vol. 74, pp. 118–132, 2014.

[84] M. Hilburger, "High-fidelity buckling analysis of composite cylinders using the STAGS finite element code," in *55th AIAA/ASME/ASCE/AHS/ASC Structures, Structural Dynamics, and Materials Conference*, no. AIAA 2014-0846, (Reston, Virginia, USA), American Institute of Aeronautics and Astronautics, 2014.

[85] S. White, P. Weaver, and K. Wu, "Post-buckling analyses of variable-stiffness composite cylinders in axial compression," *Composite Structures*, vol. 123, pp. 190–203, 2015.

[86] C. Schillo, D. Röstermundt, and D. Krause, "Experimental and numerical study on the influence of imperfections on the buckling load of unstiffened CFRP shells," *Composite Structures*, vol. 131, pp. 128–138, 2015.

[87] K. Wu, B. Stanford, G. Hrinda, Z. Wang, R. Martin, and H. Kim, "Structural assessment of advanced tow-steered shells," in *54th AIAA/ASME/ASCE/AHS/ASC Structures, Structural Dynamics, and Materials Conference*, no. AIAA 2013-1769, (Boston, Massachusetts, USA), American Institute of Aeronautics and Astronautics, 2013.

[88] E. Labans and C. Bisagni, "Buckling and free vibration study of variable and constant-stiffness cylindrical shells," *Composite Structures*, vol. 210, pp. 446–457, 2019.

[89] T. S. Hartwich, S. Panek, D. Wilckens, M. Bock, and D. Krause, "The influence of the manufacturing process and test boundary conditions on the buckling load of thin-walled cylindrical cfrp shells," *Composite Structures*, vol. 308, p. 116674, 2023.

[90] L. Friedrich and K.-U. Schröder, "Discrepancy between boundary conditions and load introduction of full-scale built-in and sub-scale experimental shell structures of space launcher vehicles," *Thin-Walled Structures*, vol. 98, pp. 403–415, 2016.

[91] H. Wagner, C. Hühne, and I. Elishakoff, "Probabilistic and deterministic lower-bound design benchmarks for cylindrical shells under axial compression," *Thin-Walled Structures*, vol. 146, p. 106451, 2020.

[92] M. R. Schultz, D. W. Sleight, D. E. Myers, W. A. Waters Jr, P. B. Chunchu, A. W. Lovejoy, and M. W. Hilburger, "Buckling design and imperfection sensitivity of sandwich composite launch-vehicle shell structures," 2016.

[93] G. Simitses, J. Starnes, and J. Rezaeepazhand, "Structural similitude and scaling laws for plates and shells: A review," *Advances in the Mechanics of Plates and Shells*, pp. 295–310, 2001.

[94] K. E. Jackson, *Workshop on scaling effects in composite materials and structures*, vol. 3271. National Aeronautics and Space Administration, Langley Research Center, 1994.

[95] V. M. Casado, S. Hinsch, J. G. García, and S. G. Castro, "Effect of initial geometrical imperfections on the buckling load of cylindrical sandwich shells under axial compression," in *Proceedings of the 4th International Carbon Composites Conference*, pp. 1–4, 2014.

[96] C. P. Coutinho, A. J. Baptista, and J. D. Rodrigues, "Reduced scale models based on similitude theory: A review up to 2015," *Engineering Structures*, vol. 119, pp. 81–94, 2016.

[97] A. Casaburo, G. Petrone, F. Franco, and S. De Rosa, "A review of similitude methods for structural engineering," *Applied Mechanics Reviews*, vol. 71, no. 3, 2019.

[98] C. P. Coutinho, A. J. Baptista, and J. D. Rodriges, "Modular approach to structural similitude," *International Journal of Mechanical Sciences*, vol. 135, pp. 294–312, 2018.

[99] G. Simitses and J. Rezaeepazhand, "Structural similitude for laminated structures," *Composites Engineering*, vol. 3, no. 7-8, pp. 751–765, 1993.

[100] J. Singer, J. Arbocz, and T. Weller, *Buckling Experiments, Basic Concepts, Columns, Beams and Plates*, vol. 1. John Wiley & Sons, 1998.

[101] G. J. Simitses and J. Rezaeepazhand, "Structural similitude and scaling laws for laminated beam-plates," *In: Topics in composite materials and structures; Proceedings of the Sessions*, pp. 37–45, 1992.

[102] E. Szücs, *Similitude and modelling*. Elsevier, 2012.

[103] F. Penning, "Use of dynamic scale models to determine launch vehicle characteristics," Tech. Rep. MCR-68-87, NASA, 1969.

[104] J. J. Catherine and J. Mixson, "Comparison of experimental vibration characteristics obtained from a 1/5-scale model and from a full-scale saturn sa-1," Tech. Rep. TN-D-4598, NASA, 1964.

[105] E. L. Peele, H. W. Leonard, and S. A. Leadbetter, "Lateral vibration characteristics of the 1/10-scale apollo," Tech. Rep. TN-D-5778, NASA, 1970.

[106] S. A. Leadbetter, W. B. Stephens, J. L. Sewall, J. W. Majka, and J. R. Barrett, "Vibration characteristics of 1/8-scale dynamic models of the space-shuttle solid-rocket boosters," in *46th Shock and Vibration Symposium, Royal Inn at the Wharf, San Diego, California, 21-23 October 1975: Dynamic analysis, modal test and analysis*, vol. 5, p. 67, Shock and Vibration Information Center, Naval Research Laboratory, 1976.

[107] D. Davis, M. Gronet, M. Tan, and J. Thorne, "Conceptual design and analysis of a dynamic scale model of the space station freedom," Tech. Rep. CP-4598, NASA, 1994.

[108] P. Jiang, W. Wang, and G. Zhang, "Size effects in the axial tearing of circular tubes during quasi-static and impact loadings," *International Journal of Impact Engineering*, vol. 32, no. 12, pp. 2048–2065, 2006.

[109] Y. Zhu, Y. Wang, Z. Luo, Q. Han, and D. Wang, "Similitude design for the vibration problems of plates and shells: A review," *Frontiers of Mechanical Engineering*, vol. 12, no. 2, pp. 253–264, 2017.

[110] V. Ungbhakorn and N. Wattanasakulpong, "Structural similitude and scaling laws of anti-symmetric cross-ply laminated cylindrical shells for buckling and vibration experiments," *International Journal of Structural Stability and Dynamics*, vol. 7, no. 04, pp. 609–627, 2007.

[111] J. Rezaeepazhand and G. Simitses, "Design of scaled down models for stability and vibration studies," in *35th Structures, Structural Dynamics, and Materials Conference*, p. 1572, 1993.

[112] J. Rezaeepazhand, G. Simitses, and J. Starnes Jr, "Scale models for laminated cylindrical shells subjected to axial compression," *Composite Structures*, vol. 34, no. 4, pp. 371–379, 1996.

[113] A. Tabiei, G. Simitses, A. Tabiei, and G. Simitses, "Scaled down imperfection sensitive composite cylindrical shells under axial compression and lateral pressure," in *38th Structures, Structural Dynamics, and Materials Conference*, p. 1250, 1998.

[114] M. P. Nemeth, "Buckling of long compression-loaded anisotropic plates restrained against inplane lateral and shear deformations," *Thin-Walled Structures*, vol. 42, no. 5, pp. 639–685, 2004.

[115] P. Weaver, J. Driesen, and P. Roberts, "Anisotropic effects in the compression buckling of laminated composite cylindrical shells," *Composites Science and Technology*, vol. 62, no. 1, pp. 91–105, 2002.

[116] I. Yang and C. Liu, "Buckling and bending behaviour of initially stressed specially orthotropic thick plates," *International Journal of Mechanical Sciences*, vol. 29, no. 12, pp. 779–791, 1987.

[117] S. Torkamani, H. Navazi, A. Jafari, and M. Bagheri, "Structural similitude in free vibration of orthogonally stiffened cylindrical shells," *Thin-Walled Structures*, vol. 47, no. 11, pp. 1316–1330, 2009.

[118] S. L. Canfield, J. Peddieson, and G. Garbe, "Similarity criteria and associated design procedures for scaling solar sail systems," *Journal of Spacecraft and Rockets*, vol. 48, no. 1, pp. 218–221, 2011.

[119] M. Hilburger, C. Rose, and J. Starnes, Jr, "Nonlinear analysis and scaling laws for noncircular composite structures subjected to combined loads," in *19th AIAA Applied Aerodynamics Conference*, no. 1335, 2001.

[120] I. Uriol Balbin and C. Bisagni, "Buckling of sandwich cylindrical shells with shear deformable core through nondimensional parameters," *Thin-Walled Structures*, vol. 161, p. 107393, 2021.

[121] M. Nemeth, "Nondimensional parameters and equations for buckling of anisotropic shallow shells," *Journal of Applied Mechanics*, vol. 61, no. 3, pp. 664–669, 1994.

[122] D. Zenkert, *The handbook of sandwich construction*. Engineering Materials Advisory Services, 1997.

[123] E. Cheung and R. C. Tennyson, "Buckling of composite sandwich cylinders under axial compression," in *Studies in Applied Mechanics*, vol. 19, pp. 151–181, Elsevier, 1988.

[124] J. Arbocz, C. Bisagni, A. Calvi, E. Carrera, R. Cuntze, R. Degenhardt, N. Gualtieri, H. Haller, N. Impollonia, M. Jacquesson, E. Jansen, H.-R. Meyer-Piening, H. Oery, A. Rittweger, R. Rolfes, G. Schullerer, G. Turzo, T. Weller, and J. Wijker, *Space engineering - Buckling of structures ECSS-E-HB-32-24A*. 2010.

[125] M. Nemeth, "Nondimensional parameters and equations for nonlinear and bifurcation analyses of thin anisotropic quasi-shallow shells," Tech. Rep. TP-216726, NASA, 2010.

[126] M. Schultz and M. Nemeth, "Buckling imperfection sensitivity of axially compressed orthotropic cylinders," in *51st AIAA/ASME/ASCE/AHS/ASC Structures, Structural Dynamics, and Materials Conference*, p. 2531, 2010.

[127] J. Singer, J. Arbocz, and T. Weller, *Buckling experiments: experimental methods in buckling of thin-walled structures*, vol. 2. John Wiley & Sons, Inc, 2002.

[128] I. Uriol Balbin, C. Bisagni, M. R. Schultz, and M. W. Hilburger, "Scaling methodology applied to buckling of sandwich composite cylindrical shells," *AIAA Journal*, pp. 1–10, 2020.

[129] "Shell buckling knockdown factors project," Tech. Rep. 2007, NASA, 2015.

[130] A. Przekop, M. R. Schultz, C. J. Kosztowny, K. Song, M. C. Lindell, M. W. Hilburger, and M. T. Rudd, "Design and analysis of buckling-critical large-scale sandwich composite cylindrical test articles," Tech. Rep. TM20205008667, NASA, 2020.

[131] Evonik, "Product information rohacell® wf/wf-ht." https://products.evonik.com/assets/59/95/ROHACELL_WF_and_WF_HT_January_2024_EN_Asset_2345995.pdf, 2024. Accessed: (12 September 2024).

[132] M. T. Rudd, D. J. Eberlein, W. A. Waters, N. W. Gardner, M. R. Schultz, and C. Bisagni, "Analysis and validation of a scaled, launch-vehicle-like composite cylinder under axial compression," *Composite Structures*, vol. 304, p. 116393, 2023.

[133] M. Hilburger, W. Haynie, A. Lovejoy, M. Roberts, J. Norris, W. Waters, and H. Herring, "Sub-scale and full-scale testing of buckling-critical launch vehicle shell structures," in *53rd AIAA/ASME/ASCE/AHS/ASC Structures, Structural Dynamics and Materials Conference 20th AIAA/ASME/AHS Adaptive Structures Conference 14th AIAA*, p. 1688, 2012.

ACKNOWLEDGEMENTS

The PhD Project has been a tough but rewarding journey and only because of the help and support of many people are you able to hold this book today. From offering guidance and feedback to encouragement along the way, their contributions have played an essential role in bringing this work to completion.

First of all, I would like to thank Prof. Dr. Chiara Bisagni for supervising me and to Dr. Roeland de Broeker for stepping in to be my thesis promotor. I would also like to thank the committee members for taking the time to read my thesis and for being part of my PhD defense committee.

I would also like to thank Dr. Marc Schultz of NASA Langley Research Center and Michelle Rudd of NASA Marschall who provided insight and expertise that greatly assisted the research. The discussions and constructive feedback on the topic vastly improved the work. This work would also be poorer without the contributions of Dr. Kevin van Dooren and David Eberlein, who with their master thesis improved significantly my own research.

My gratitude extends to the rest of the staff of the Aerospace Structures and Materials department for providing an enjoyable environment both in the office and at social activities. Special thanks to Laura for always being ready to help and care, well beyond her duties. I would also like to thank my fellow PhD's and Postdocs for both the technical discussions and the time we spent in and out of the office. To the members of Room 2.11 in particular: Javi, Marta and Tutu: working with you was a lifesaver in times of stress and a joy in times of celebration. Many thanks also to Prem, Calvin, and Yinglu for giving me space and time to write during the last months at the cost of their own already large workload.

The PhD Board was also an important part of my PhD time and I will always be grateful to all their members. To Bruce and Tiago specially, I learnt a lot from you and I wish for our friendship to survive the distance. During my PhD I was very lucky to participate in the International Space University. This program not only gave me a broader perspective of the space industry but it also gave me access to a wonderful community. From this experience I also take with me supportive friends: Deepika, Omar, Jin and Martijn, that kept me sane during the worst times.

I also want to thank to my friends in Delft: Ioanna, Sonia, Ale, Reynard, Roberto, Rodrigo, Lucia, Renzo, Miriam, Fernanda, Carolina, Jaime, and many more who have

come and gone from this beautiful city I call my home. They helped me fall in love with Delft and provided some balance to my days with walks, barbeques, bouldering, and drinks.

Especial thanks must go to my friends from Valencia: Mary, Rosa, and Cris, who never gave up on this thesis and believed for me when I couldn't. I am also deeply thankful to Luca for his unwavering support and encouragement during the final months of my PhD journey.

Finally, I would like to thank my family. My parents: Ines and Juan, for always being supportive of my adventures. My siblings: Maria, Belen, Juan Pablo and Cecilia, have always been there for me and this work is better thanks to you.

A

SCALED STRUCTURES

This appendix provides scaled configurations for each of the baseline structures with the two scaling strategies discussed in the main text. The tables herein aim to provide a comprehensive reference for the parameter values and range of possible structural configurations.

The setups for Scaling Strategy 1, as shown in Fig. 5.2, include variations in the facesheet angle, length, core thickness, and core material. The configurations for these setups, corresponding to the baseline parameters presented in Table 5.1, are detailed here.

Similarly, the setups for Scaling Strategy 2, as shown in Fig. 5.13, involve variations in the facesheet angle, the number of lay-up repetitions, and the length. Configurations for these setups, also corresponding to the baseline parameters in Table 5.1, are also included in this appendix.

A.1. BASELINE 2

Baseline 2, which corresponds to the test article CTA8.2 whose test is described by Prezkop et al. [10], is analyzed in this section. Scaling down this baseline structure has challenges because it has a thinner core than Baseline 2. The main properties of the shell are reported in Table A.1.

Table A.1: Baseline 2 Properties.

Facesheet lay-up	Ply Thickness [mm]	Core Thickness [mm]	Total Thickness [mm]
$[\pm 60/0]_s$	0.180 [0.0071 in]	5.08 [0.20 in]	7.62 [0.30 in]

A.1.1. STRATEGY 1

THE scaled structures properties outlined in Table A.2 provide a detailed account of the material and geometric adjustments made under Scaling Strategy 1, as well as the buckling load in its dimensional form.

Table A.2: Scaled Structures Properties for the Scaling Strategy 1 of Baseline 2.

Shell	Lay-up	Length [mm]	Core thickness [mm]	Core Material	Buckling Load [kN]
Scaled 2.1.I.1	$(15/-15)_s$	1400	1.3	Rohacell 300 WF	590
Scaled 2.1.I.2	$(75/-75)_s$	415	1.3	Rohacell 300 WF	570
Scaled 2.1.II.1	$(19/0/-19)$	1382	1.6	Rohacell 300 WF	492
Scaled 2.1.II.2	$(60/0/-60)$	758	1.5	Rohacell 300 WF	692

The quality of the scaling for each design is reported in Fig. A.1. In Table A.3, the buckling load and modes are compared for Baseline 2 and the scaled models with Strategy 1.

Table A.3: Buckling Response of Baseline 2 and its corresponding scaling strategy 1 models.

Shell	Nondimensional Buckling Load [-]	Buckling Load [kN]	m [-]	n [-]
Baseline 2	675	4428	12	5
Scaled 2.1.I.1	696	590	13	1
Scaled 2.1.I.2	672	570	9	10
Scaled 2.1.II.1	685	492	12	3
Scaled 2.1.II.2	664	692	13	1

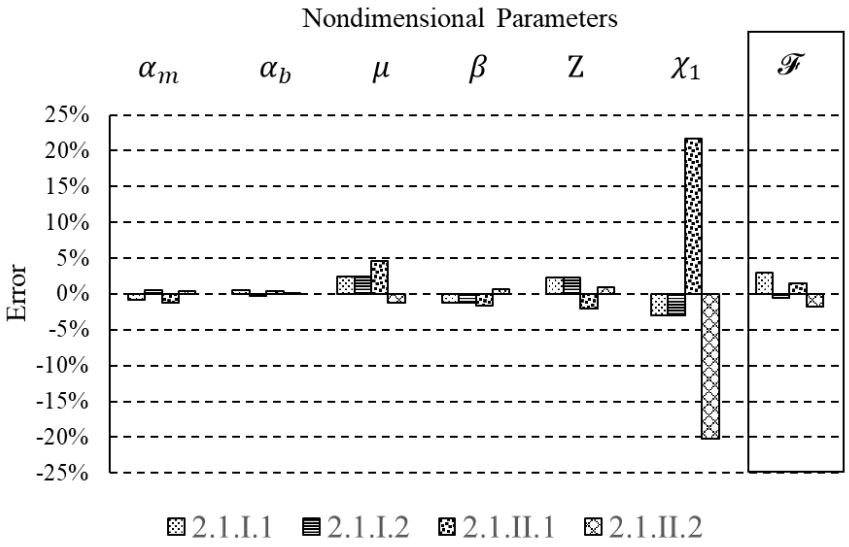

Figure A.1: Error in the Nondimensional Parameters between Baseline 2 and the Scaled Structures with Scaling Strategy 1.

A.1.2. STRATEGY 2

The scaled structures properties outlined in Table A.4 provide a detailed account of the material and geometric adjustments made under Scaling Strategy 2, as well as the buckling load in its dimensional form.

As seen in the Table A.3, these buckling load and modes are compared for the Baseline 2 and the scaled models with Strategy 2. The quality of the scaling for each design is reported in Fig. A.2.

Note that for Baseline 2, unlike in Baseline 1, the repetition number for Scaled 2.2.II.1 and Scaled 2.2.II.2 is an odd number: 7. This means that the configurations wont be exact to those of the Family V, and thus both are represented in Table A.5 and Fig. A.2.

Table A.4: Scaled structures properties for the Scaling Strategy 2 of Baseline 2.

Shell	Facesheet lay-up	Total thickness [mm]	Length [mm]	Buckling Load [kN]
Scaled 2.2.I.1	$15(/-15)_{10}$	3.51	1407	1551
Scaled 2.2.I.2	$(75/-75)_{10}$	3.51	412	1552
Scaled 2.2.II.1	$(19/0/-19)_7$	3.68	1392	1732
Scaled 2.2.II.2	$(60/0/-60)_7$	3.68	760	2791
Scaled 2.2.III.1	$([15/-15]_s)_5$	3.51	1407	1551
Scaled 2.2.III.2	$([75/-75]_s)_5$	3.51	412	1552
Scaled 2.2.IV.1	$([25/-25/9\bar{0}]_s)_4$	3.51	915	2414
Scaled 2.2.IV.2	$([73/-73/9\bar{0}]_s)_4$	3.51	415	1560
Scaled 2.2.V.1	$([19/0/-19]_s)_3$	3.15	1392	1272
Scaled 2.2.V.2	$([60/0/-60]_s)_3$	3.15	759	2048
Scaled 2.2.VI.1	$([31/0/-31/9\bar{0}]_s)_3$	3.68	972	2551
Scaled 2.2.VI.2	$([56/0/-56/9\bar{0}]_s)_3$	3.68	734	2787

Table A.5: Buckling Response of Baseline 2 and its corresponding scaling strategy 2 models.

Shell	Nondimensional Buckling Load [-]	Buckling Load [kN]	m [-]	n [-]
Baseline 2	675	4836	12	5
Scaled 2.2.II.1	710	1732	7	9
Scaled 2.2.II.2	710	2791	11	3
Scaled 2.2.III.1	748	1551	8	9
Scaled 2.2.III.2	749	1552	8	9
Scaled 2.2.IV.1	754	2414	4	9
Scaled 2.2.IV.2	747	1560	8	9
Scaled 2.2.V.1	828	1272	7	10
Scaled 2.2.V.2	830	2048	12	3
Scaled 2.2.VI.1	718	2551	2	7
Scaled 2.2.VI.2	713	2787	4	9

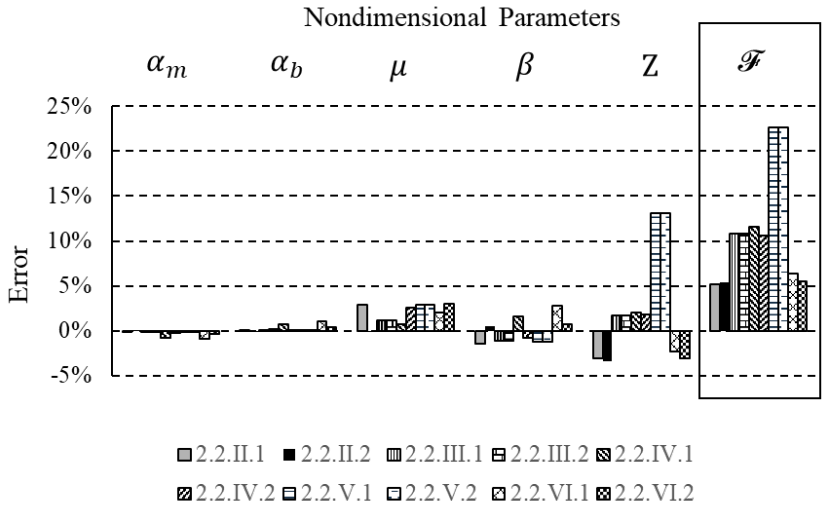

Figure A.2: Error in the Nondimensional Parameters between Baseline 2 and the Scaled Structures with Scaling Strategy 2.

A.2. BASELINE 3

The shell named Baseline 3 corresponds to the test article CTA8.3 which was described by Song et al. [9]. The main shell properties are reported in Table A.6. This is the baseline shell with the lowest total thickness evaluated, at only 6.45mm in total.

Table A.6: Baseline 3 Properties.

Facesheet lay-up	Ply Thickness [mm]	Core Thickness [mm]	Total Thickness [mm]
$[\pm 30/\bar{9}0]_s$	0.137 [0.0054 in]	5.08 [0.20 in]	6.45 [0.25 in]

A.2.1. STRATEGY 1

The scaled structures properties outlined in Table A.7 provide a detailed account of the material and geometric adjustments made under Scaling Strategy 1, as well as the buckling load in its dimensional form.

The quality of the scaling for each design is reported in Fig. A.3. In Table A.8, the buckling load and modes are compared for the Baseline 3 and the scaled models with Strategy 1.

Table A.7: Scaled Structures Properties for the Scaling Strategy 1 of Baseline 3.

Shell	Lay-up	Length [mm]	Core thickness [mm]	Core Material	Buckling Load [kN]
Scaled 3.1.I.1	$(18/-18)_s$	1208	1.2	Rohacell 300 WF	537
Scaled 3.1.I.2	$(72/-72)_s$	377	1.2	Rohacell 300 WF	536
Scaled 3.1.II.1	$(24/0/-24)$	1163	1.4	Rohacell 300 WF	442
Scaled 3.1.II.2	$(54/0/-54)$	723	1.4	Rohacell 300 WF	606

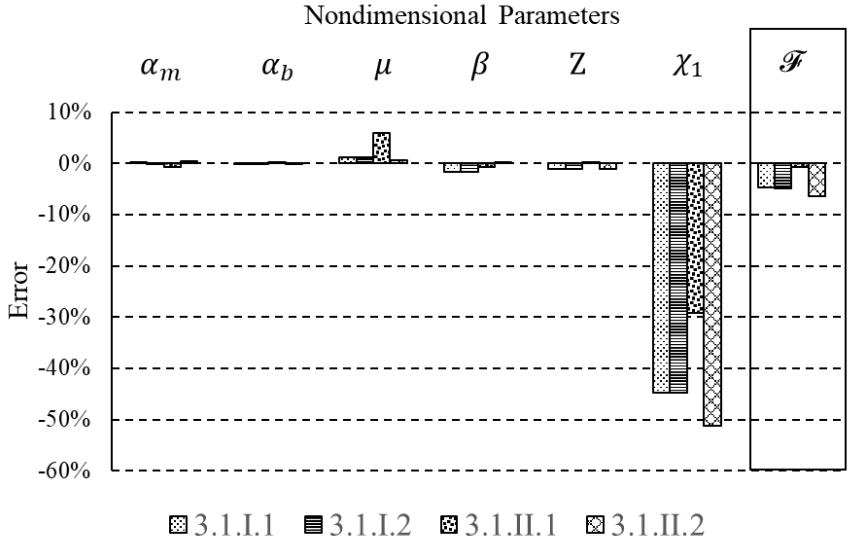

Figure A.3: Error in the Nondimensional Parameters between Baseline 3 and the Scaled Structures with Scaling Strategy 1.

Table A.8: Buckling Response of Baseline 3 and its corresponding scaling strategy 1 models.

Shell	Nondimensional Buckling Load [-]	Buckling Load [kN]	m [-]	n [-]
Baseline 3	732	2444	11	1
Scaled 3.1.I.1	697	537	11	1
Scaled 3.1.I.2	696	536	11	1
Scaled 3.1.II.1	726	442	11	1
Scaled 3.1.II.2	685	606	12	1

A.2.2. STRATEGY 2

The scaled structures properties outlined in Table A.9 provide a detailed account of the material and geometric adjustments made under Scaling Strategy 2, as well as the buckling load in its dimensional form.

Table A.9: Scaled structures properties for the Scaling Strategy 2 of Baseline 3.

Shell	Facesheet lay-up	Total thickness [mm]	Length [mm]	Buckling Load [kN]
Scaled 3.2.I.1	$(18/-18)_{10}$	3.51	1208	1524
Scaled 3.2.I.2	$(72/-72)_{10}$	3.51	377	1523
Scaled 3.2.II.1	$(24/0/-24)_6$	3.15	1170	1281
Scaled 3.2.II.2	$(54/0/-54)_6$	3.15	725	1860
Scaled 3.2.III.1	$([18/-18]_s)_5$	3.51	1208	1524
Scaled 3.2.III.2	$([72/-72]_s)_5$	3.51	377	1523
Scaled 3.2.IV.1	$([30/-30/\bar{90}]_s)_5$	3.51	764	2270
Scaled 3.2.IV.2	$([69/-69/\bar{90}]_s)_5$	3.51	383	1549
Scaled 3.2.V.1	$([24/0/-24]_s)_3$	3.15	1170	1281
Scaled 3.2.V.2	$([54/0/-54]_s)_3$	3.51	1208	1524
Scaled 3.2.VI.1	$([45/0/-45/\bar{90}]_s)_3$	3.68	754	2585

As seen in the Table A.10, these buckling load and modes are compare for the Baseline 3 and the scaled models with Strategy 2. The quality of the scaling for each design is reported in Fig. A.4.

Table A.10: Buckling Response of Baseline 3 and its corresponding scaling strategy 2 models.

Shell	Nondimensional Buckling Load [-]	Buckling Load [kN]	m [-]	n [-]
Baseline 3	732	2444	11	1
Scaled 3.2.III.1	731	1523	10	1
Scaled 3.2.III.2	730	1523	10	1
Scaled 3.2.IV.1	733	2270	10	1
Scaled 3.2.IV.2	729	1549	10	1
Scaled 3.2.V.1	810	1281	11	1
Scaled 3.2.V.2	806	1860	11	1
Scaled 3.2.VI.1	707	2585	10	1

Note than in this case for Family VI there is only one solution. The reason for this is that the closest match is the 45 angle and therefore there is no complementary solution.

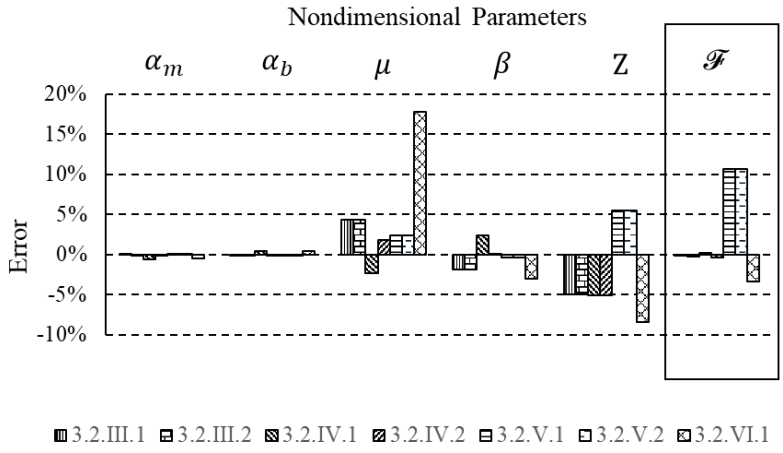

Figure A.4: Error in the Nondimensional Parameters between Baseline 3 and the Scaled Structures with Scaling Strategy 2.

A.3. BASELINE 4

Finally the shell named Baseline 4 was also studied. This shell corresponds to test article CTA8.4 [130]. This shell has the largest total thickness at a value of almost 10mm. The main shell properties are reported in Table A.11.

Table A.11: Baseline 4 Properties.

Facesheet lay-up	Ply Thickness [mm]	Core Thickness [mm]	Total Thickness [mm]
$[\pm 30/90/0]_s$	0.137 [0.0054 in]	7.62 [0.30 in]	9.82 [0.39 in]

A.3.1. STRATEGY 1

The scaled structures properties outlined in Table A.12 provide a detailed account of the material and geometric adjustments made under Scaling Strategy 1, as well as the buckling load in its dimensional form.

Table A.12: Scaled Structures Properties for the Scaling Strategy 1 of Baseline 4.

Shell	Lay-up	Length [mm]	Core thickness [mm]	Core Material	Buckling Load [kN]
Scaled 4.1.I.1	$(12/-12)_s$	1250	2.2	Rohacell 300 WF	780
Scaled 4.1.I.2	$(78/-78)_s$	354	2.2	Rohacell 300 WF	732
Scaled 4.1.II.1	$(15/0/-15)$	1242	2.5	Rohacell 300 WF	625
Scaled 4.1.II.2	$(65/0/-65)$	630	2.4	Rohacell 300 WF	978

The quality of the scaling for each design is reported in Fig. A.5. In Table A.13, the buckling load and modes are compared for the Baseline 4 and the scaled models with Strategy 1.

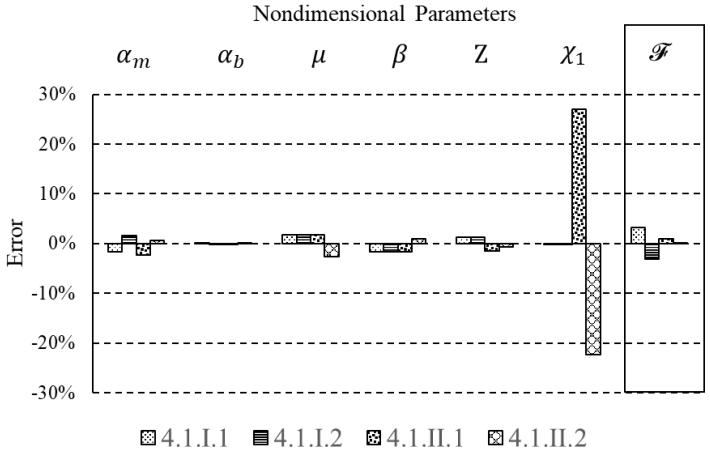

Figure A.5: Error in the Nondimensional Parameters between Baseline 4 and the Scaled Structures with Scaling Strategy 1.

Table A.13: Buckling Response.

Shell	Nondimensional Buckling Load [-]	Buckling Load [kN]	m [-]	n [-]
Baseline 4	431	5868	5	8
Scaled 4.1.I.1	445	780	5	8
Scaled 4.1.I.2	417	732	5	9
Scaled 4.1.II.1	435	625	4	8
Scaled 4.1.II.2	431	978	6	8

A.3.2. STRATEGY 2

The scaled structures properties outlined in Table A.14 provide a detailed account of the material and geometric adjustments made under Scaling Strategy 2, as well as the buckling load in its dimensional form. Note that the buckling load values are very high for many configurations, calling into question the approach in this case.

Table A.14: Scaled structures properties for the Scaling Strategy 2 of Baseline 4.

Shell	Facesheet lay-up	Total thickness [mm]	Length [mm]	Buckling Load [kN]
Scaled 4.2.I.1	$(12/-12)_{14}$	4.91	1257	2624
Scaled 4.2.I.2	$(78/-78)_{14}$	4.91	352	461
Scaled 4.2.II.1	$(15/0/-15)_{10}$	5.26	1251	3035
Scaled 4.2.II.2	$(65/0/-65)_{10}$	5.26	632	5225
Scaled 4.2.III.1	$([12/-12]_s)_7$	4.91	1257	2624
Scaled 4.2.III.2	$([78/-78]_s)_7$	4.91	352	461
Scaled 4.2.IV.1	$([21/-21/\bar{90}]_s)_6$	5.26	826	4882
Scaled 4.2.IV.2	$([76/-76/\bar{90}]_s)_6$	5.26	354	3087
Scaled 4.2.V.1	$([15/0/-15]_s)_5$	5.26	1251	3035
Scaled 4.2.V.2	$([65/0/-65]_s)_5$	5.26	632	5225
Scaled 4.2.VI.1	$([25/0/-25/\bar{90}]_s)_4$	4.91	890	4032
Scaled 4.2.VI.2	$([63/0/-63/\bar{90}]_s)_4$	4.91	602	4446

As seen in the Table A.15, these buckling load and modes are compare for the Baseline 4 and the scaled models with Strategy 2. The quality of the scaling for each design is reported in Fig. A.6.

Table A.15: Buckling Response.

Shell	Nondimensional Buckling Load [-]	Buckling Load [kN]	m [-]	n [-]
Baseline 4	431	5868	5	8
Scaled 4.2.III.1	461	2624	4	8
Scaled 4.2.III.2	461	2625	4	8
Scaled 4.2.IV.1	436	4882	4	8
Scaled 4.2.IV.2	440	3087	4	8
Scaled 4.2.V.1	431	3035	4	8
Scaled 4.2.V.2	434	5225	4	8
Scaled 4.2.VI.1	472	4032	4	8
Scaled 4.2.VI.2	458	4446	4	8

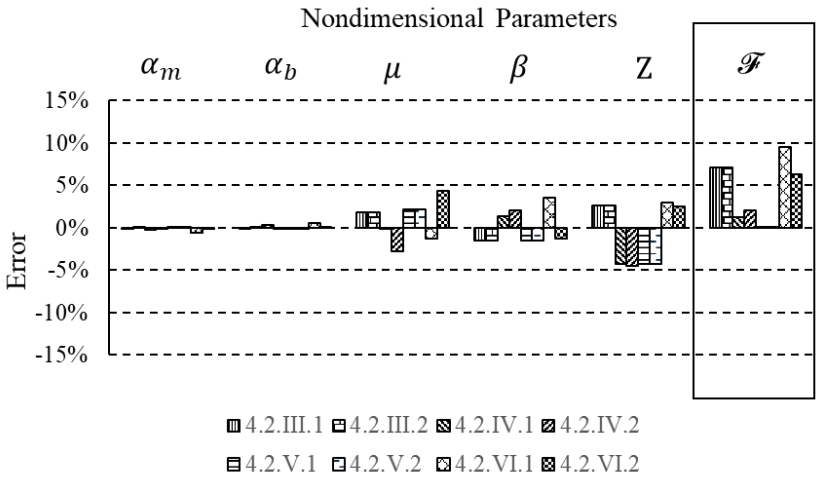

Figure A.6: Error in the Nondimensional Parameters between Baseline 4 and the Scaled Structures with Scaling Strategy 2.

CURRICULUM VITÆ

Ines URIOL BALBIN

12-03-1990 Born in Valencia, Spain.

EDUCATION

2008–2014 Aerospace Engineering
Universitat Politecnica de Valencia

2016-2025 PhD. Aerospace Engineering
Delft University of Technology

WORK EXPERIENCE

2014–2016 Passive Safety Engineer
IDIADA, Barcelona, Spain

2021–2025 Lecturer
Delft University of Technology, Delft, The Netherlands

List of Publications

Pertinent to this dissertation

- **I. Uriol Balbin** , and C. Bisagni, (2021). *Buckling of sandwich cylindrical shells with shear deformable core through nondimensional parameters*, Thin-Walled Structures, vol. 161, p. 107393
- **I. Uriol Balbin** , C. Bisagni, M. R. Schultz, and M. W. Hilburger, (2020). *Scaling Methodology Applied to Buckling of Sandwich Composite Cylindrical Shells*, AIAA Journal, vol. 58, no. 8, pp. 3680-3689.
- **I. Uriol Balbin**, C. Bisagni, M. R. Schultz, and M. W. Hilburger, (2018). *Scaling Methodology for Buckling of Sandwich Composite Cylindrical Structures*, AIAA 2018-1988, In Proceedings of 2018 AIAA/ASCE/AHS/ASC Structures, Structural Dynamics, and Materials Conference. January 2018.

Other Publications

- **I. Uriol Balbin** and M. Gavioli, (2024). *Mission MARIJN: A Case Study on Improving Undergraduate Aerospace Engineering Education.* In Proceedings of the 75th International Astronautical Congress (IAC), Milan, Italy. October 2024.
- C. Rodriguez, **I. Uriol Balbin** and B. van der Laar, (2024). *Structural Analysis of the Inflatable Deployable Booms in a Deorbiting System for Cubesats in LEO.* In Proceedings of the 75th International Astronautical Congress (IAC), Milan, Italy. October 2024.
- E. Velazquez Navarro, J. Sachithanandan, **I. Uriol Balbin**, and P. Solano-López, (2024). *Preliminary Design and Optimization of a CubeSat Demonstrator for an Origami-inspired Deployable Structure*, AIAA 2024-2255, In Proceedings of AIAA SCITECH 2024 Forum. January 2024.
- **I. Uriol Balbin**, (2023). *Is My Master Thesis Research Project Sustainable? Including Sustainability in "Research Methodologies"*. In Proceedings of the 19th International CDIO Conference, Trondheim, Norway. June 2023.
- **I. Uriol Balbin** and P. Solano-López, (2022). *Preliminary Study of An Origami-inspired Deployable Structure for a Small-Scale Demonstrator.* In Proceedings of the 73th International Astronautical Congress (IAC), Paris, France. September 2022.